Università di Pisa

Scuola di Dottorato
"Leonardo da Vinci"

PhD Programme in

Land Vehicles and Transport Systems

PhD Dissertation

Battery, Hybrid and Fuel-Cell Propulsion Systems

Giovanni Lutzemberger

SSD ING-IND/33

2011

Università di Pisa

Scuola di Dottorato
"Leonardo da Vinci"

PhD Programme in

Land Vehicles and Transport Systems

PhD Dissertation

Battery, Hybrid and Fuel-Cell Propulsion Systems

Author:
Giovanni Lutzemberger

Tutor:
Prof. Massimo Ceraolo

SSD ING-IND/33

2011

Abstract

The main purpose of the Research is theoretical and experimental evaluation of electric propulsion systems: pure electric ones, fed exclusively by electrochemical energy storage, hybrid electric, in which the power for propulsion comes from different sources, and fuel cell-based vehicles.
These studies were carried on through an extended modelling and experimental activity, related to:

- Modelling and experimental activities on electrochemical storage systems and super-capacitors, to evaluate their performance and to better individuate the optimal sizing for usage on-board electric and hybrid vehicles.
- Design and realisation of a Fuel-Cell based vehicle, starting from the design of the propulsion system, for which dedicated models in Matlab-Simulink® environment were specifically realised, coming to an extended laboratory test activity for all the components, specially for the Fuel-Cell System.
- Design of a complete line of electric and hybrid buses, based on the modelling of the propulsion system in collaboration with the manufacturer, through the usage of new object-oriented modelling techniques realised in Dymola-Modelica® environment. After evaluating different energy management strategies, an exhaustive comparison with conventional and electric pure versions has been carried on.

The PhD Thesis, after an introduction about innovative propulsion systems, describes in detail all the activities presented, trying to summarise general techniques of design and management for hybrid vehicles.

Sommario

L'attività di Ricerca svolta ha avuto come principale obiettivo l'analisi teorica e sperimentale di sistemi a propulsione innovativa: sistemi a propulsione elettrica alimentati esclusivamente a batteria, sistemi a propulsione ibrida, in cui la potenza per la propulsione proviene da sorgenti differenti, e sistemi a celle a combustibile. Questi studi sono stati condotti attraverso la definizione di modelli matematici e prove sperimentali, relative in particolare a:

- Modellazione e sperimentazione di sistemi di accumulo elettrochimico e super-condensatori, al fine di valutarne le prestazioni e le corrette procedure di dimensionamento per un utilizzo a bordo di veicoli elettrici e ibridi.
- Progettazione e realizzazione di un veicolo a celle a combustibile a idrogeno, dalla definizione del modello matematico del sistema propulsivo in ambiente Matlab-Simulink® all'esecuzione di prove sperimentali di laboratorio sulle diverse componenti, in particolare sul sistema di generazione elettrica a idrogeno.
- Progettazione del sistema propulsivo di una linea di autobus elettrici e ibridi in collaborazione con il costruttore, attraverso l'utilizzo di una tecnica di modellazione orientata agli oggetti sviluppata in ambiente Dymola-Modelica®. Una volta definite opportune strategie di gestione energetica, la versione ibrida è stata messa a confronto con la versione elettrica a batterie e quella convenzionale.

La presente Tesi di Dottorato, introdotti in linea generale i sistemi a propulsione innovativa, descrive in dettaglio le diverse attività sopra presentate con l'obiettivo di trarre tecniche generali di progettazione e gestione dei veicoli ibridi.

Acknowledgments

The author would like to thank the following people that gave special support to the Research: Prof. Massimo Ceraolo, for the fundamental support to all the activities presented, Eng. Luca Sani for the assistance about sizing of electric drives, Eng. Mirko Marracci for the implementation of the testing laboratory setup.

List of Acronyms

AUX	Auxiliary electrical load
BMS	Battery Management System
BSFC	Brake Specific Fuel Consumption
CHEV	Complex Hybrid Electric Vehicle
FCS	Fuel-Cell System
ED	Electric Drive
EGS	Electronic Generator System
EM	Electrical machine
EPC	Electronic Power Conditioner
EV	Electric Vehicle
HD	Hybridisation Degree
HEV	Hybrid Electric Vehicle
ICE	Internal Combustion Engine
ME	Mechanical Engine
NEDC	New European Driving Cycle
PHEV	Parallel Hybrid Vehicle
PMM	Power Management Module
RESS	Rechargeable Energy Storage System
SHEV	Series Hybrid Vehicle
SpHEV	Split Hybrid Vehicle
SOC	State of Charge
SORT	Standardised On-Road Test cycle

Table of contents

1. Innovative propulsion systems

1.1 Hybrid vehicles

1.1.1 Definition

Diffuse ambiguities can be observed in the technical literature about the concept of hybrid vehicle [1]. Some sources, which are also very important, define a hybrid vehicle as a vehicle which combines the use of an electric motor with a conventional ICE-based propulsion system. In the context of a global standardisation, it is preferable to adopt a more general definition (CEN EN 13447):

- A Hybrid Vehicle (HV) is a vehicle in which the propulsion energy is available from two or more types of on board energy sources, creating at least one path of energy flow between an energy storage and the wheels which is reversible and at least one path of energy flow between an energy storage and the wheels which is not reversible.
- A Hybrid Electric Vehicle (HEV) is a hybrid vehicle where at least one of the energies used for the propulsion is electric.

In accordance with the international definition the general representation of a HEV is shown in Figure 1.

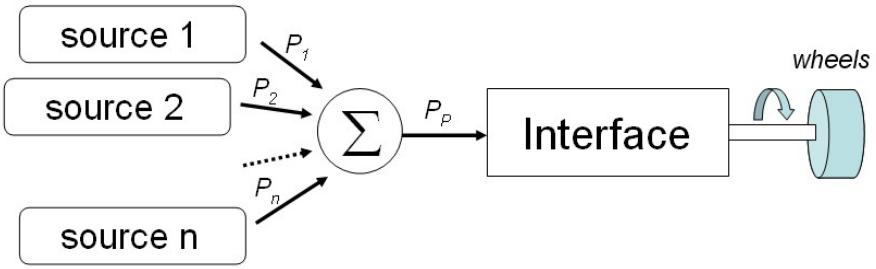

Figure 1: General scheme of HEV according with EN definition

The fundamental equation of the power balance for a hybrid vehicle, is:

$$P_p(t) = P_1(t) + P_2(t) + ... + P_n(t) \qquad \text{(Eq. 1)}$$

which demonstrates how the power required for propulsion is derived from the contribution of different sources. There are obviously degrees of freedom: the issue is related how to allocate the power between the different sources available.

In order to carry out practical considerations and to reduce the generality expressed by Figure 1, it can be better to focus attention to the vehicles that meet two special conditions:

- Two energy sources on board.
- The source that generates energy (mechanical or electric) from fuel (e.g. gasoline, natural gas or hydrogen) is generally called Primary Converter (PC). It is characterised by unidirectional energy flows (shown in the picture by using one-way arrow in the symbol P_1);
- The other is normally formed by a Rechargeable Energy Storage System (RESS), that normally delivers or stores energy. The available energy is usually much more limited than the one available from the primary source, and flows are necessarily bidirectional (shown in the picture made by two-way arrow in the symbol).

Considering the conditions reported above, which can be easily found in all cases of practical interest, the energy diagram of a general hybrid vehicle becomes the one depicted in Figure 2.

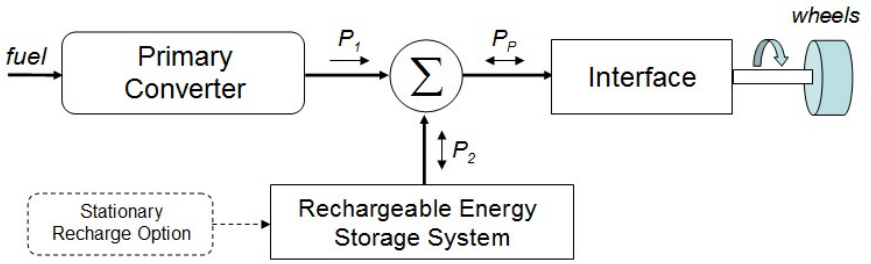

Figure 2: Diagram of power fluxes of the majority of hybrid electric vehicles

The fundamental equation of power balance is reported below:

$$P_p(t) = P_1^+(t) + P_2(t) \qquad \text{(Eq. 2)}$$

It can be noticed that in the equation the superscript "+" was adopted to highlight the power coming from the fuel converter, which can only be positive (unidirectional). The diagram of Figure 2 shows in particular how the power P_P from propulsion can be provided, within certain limits, by the combination of the primary and the secondary sources: this arbitrariness can be exploited to obtain special objectives such as reducing consumption or emissions.

The techniques and the methodologies used to pursue specific goals of optimisation, working on the sharing of power P_P between the two sources available P_1 and P_2, are reported in detail in the next paragraph.
As regarding to block Stationary Recharge Option in the diagram of Figure 2, it is related to the possibility of the Plug-in option, to recharge the RESS not only with the energy available onboard (coming from the primary source or regenerative braking), but also from the electrical grid. Therefore the RESS can be stored by the electricity generated from the grid, which is an advantageous source in terms of cost and environmental agreement, because it can be obtained by a mix of power plants which commonly have high efficiency and reduced emissions.

1.1.2 General classification

Fundamental diagrams shown in Figure 1 and Figure 2 do not specify the way to add the different power from independent sources.
Hybrid vehicles can be classified into different families depending on how this sum can be made. A simple classification, but certainly able to describe the main types, can be the following:

- Series Hybrid Electric Vehicle (SHEV): in which the sum of the power from the two sources is electrical.
- Parallel Hybrid Electric Vehicle (PHEV): where the sum of the power from the two sources is mechanical.
- Split Hybrid Electric Vehicle (SpHEV): in which the sum of the power from the two sources is obtained directly on the road.
- Complex Hybrid Electric Vehicle (CHEV): which present various combinations of previous schemes.

1.1.2.1 Series Hybrid Vehicle

The general scheme of a series hybrid vehicle is shown in Figure 3. It can be seen as a specialisation of the general scheme of Figure 2, in which the sum of the power coming from the two independent sources becomes into the electrical node. It can be notice that:

- The Primary Converter (PC) transforms the primary energy fuel into the electrical power. Obviously this type of conversion can be achieved in many different ways, through an Internal Combustion Engine (ICE) coupled to an Electric Generator (EG), or through a Fuel Cell System (FCS). In practical cases the output power is delivered to a DC-bus.
- The bus, which is the electrical node, where the combination of electric powers coming from the two different sources is obtained. Normally the bus can be a simply DC node.
- The Rechargeable Energy Storage System (RESS), typically consisting of an electrochemical battery pack, in some cases connected to the DC-bus by means of an electronic converter.
- The electro-mechanical converter that takes electrical energy from the bus and transforms it into mechanical energy, available at wheels. Normally it is constituted by an Electronic Power Conditioner (EPC) and a three-phase Electrical Machine (EM) operating as motor during traction phases, and as generator during braking.

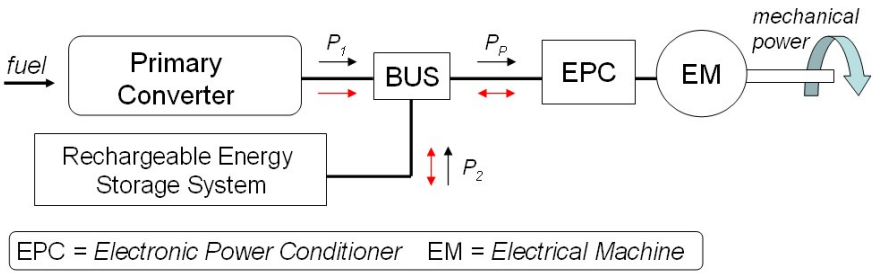

Figure 3: General scheme of a Series Hybrid Vehicle

Series hybrid drive trains offer several advantages:

- The *Primary Converter* is fully decoupled from the driven wheels. Therefore, it can be operated at high efficiency work condition, that can be further improved by optimal design and control.

- Electric motors have a near-ideal torque-speed characteristics, so they do not need multi-gear transmissions. Furthermore, instead of using one single motor and a traditional differential gear, two motors can be used, each of them powering a single wheel. The ultimate refinement would be the usage of four motors, thus making the vehicle an all-wheel-drive with out the expense and complexity of differentials and drive shafts running through the frame.
- Simple control strategies may be used as a result of the mechanical decoupling provided by the electrical transmission.

However, series hybrid electric drive trains have some disadvantages:

- The various subsystems add further weight and cost.
- The traction motor must be sized to meet maximum requirements since it is the only system propelling the vehicle.

1.1.2.2 Parallel Hybrid Vehicle

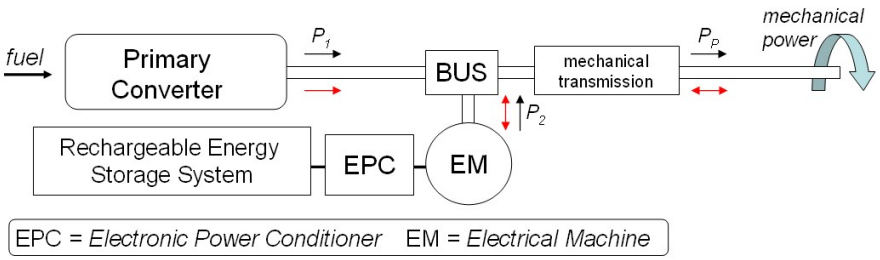

Figure 4: General scheme of a Parallel Hybrid Vehicle

The general scheme of the Parallel hybrid is shown in Figure 4. Also this scheme can be seen as a specialisation of the general scheme of Figure 2, in which the sum of power from two independent sources becomes inside the mechanical node. It can be notice:

- The Primary Converter that takes energy from a fuel and generates mechanical power.
- The bus, which is the mechanical node, where the combination of mechanical powers coming from the two different sources is obtained. It could be formed by a planetary gear.
- The Rechargeable Energy Storage System: it can be connected to an Electrical Machine (EM) controlled by an Electronic Power Conditioner (EPC).

- The mechanical transmission which transfers the mechanical energy to the wheels. It can be a simple shaft or commonly a reduction gear.

The main advantages of the Parallel hybrid drive trains are:

- The Electric Machine is not sized to meet the maximum requirements since it is combined to the other mechanical sources for propelling the vehicle.
- The different subsystems require less on-board available volumes than the series architecture.

However, the parallel hybrid drive-trains have the disadvantage that control strategies are more involved than in the series hybrid ones, due to the complexity of the architecture. Indeed the Primary Converter is not mechanically decoupled by the Electrical Machine. Therefore, it must be operated at point torques-speed related to the wheels and to the electric machine.

1.1.2.3 Split Hybrid Vehicle

The general scheme of a Split Hybrid Vehicle is shown in Figure 5. It can be seen as the parallel scheme in which the sum of the mechanical powers is made by means of the force generated by the wheels on the road.

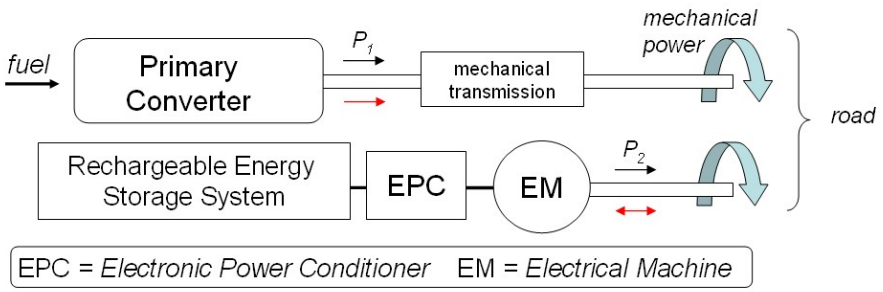

Figure 5: General scheme of a Split Hybrid Vehicle

1.1.2.4 Complex Hybrid Vehicle

In Figure 6 an example of a Complex Hybrid vehicle is shown: it consists of a combination of the series and parallel architectures. As shown in the scheme, it is clearly evident the presence of the mechanical bus (MB) and of the electric bus (EB).

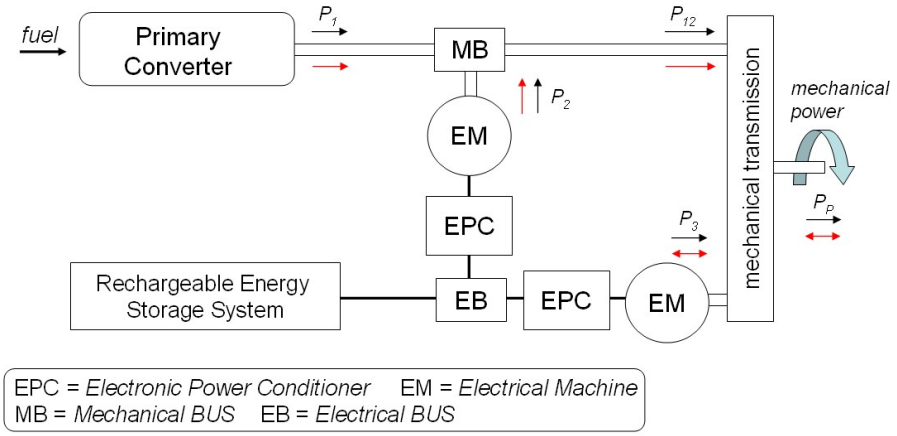

Figure 6: General scheme of a Series-Parallel Hybrid Vehicle

As it is clearly seen in the scheme, the sum of mechanical power occurs both inside the mechanical bus ($P_{12}=P_1+P_2$) and inside the mechanical transmission ($P_P=P_{12}+P_3$).

1.1.2.5 Hybridisation Degree

The hybridisation degree (HD) is a parameter commonly used to characterise the hybrid architecture. In case of a SHEV, the Hybridisation Degree is an indicator of how this configuration is different from the Pure Electric Vehicle (PEV); in case of a PHEV, how this configuration is different from the Conventional Vehicle. Indeed, as shown in Figure 3 and Figure 4, the series hybrid vehicle can be imagined as a particular kind of electric vehicle, in which an Electronic Generator System (EGS) is added to the Rechargeable Energy Storage System (RESS). Instead, the parallel hybrid vehicle can be considered as a conventional ICE-based vehicle, with the addition of an Electrical Machine connected to the Rechargeable Energy Storage System.
The Hybridisation Degree for both hybrid vehicles, series and parallel, are usually defined respectively by the following equations.

$$HDS = \frac{P_{2Max}}{P_{PMax}}\ ,\ 0 \le HDS \le 1 \qquad \text{(Eq. 3)}$$

$$HDP = \frac{P_{1Max}}{P_{PMax}},\ 0 \le HDP \le 1 \qquad \text{(Eq. 4)}$$

where:
P_{2Max} is the max power that can be delivered or adsorbed by the RESS.
P_{1Max} is the max power that can be generated by the Primary Converter.
P_{PMax} is the max power necessary for the vehicle propulsion.

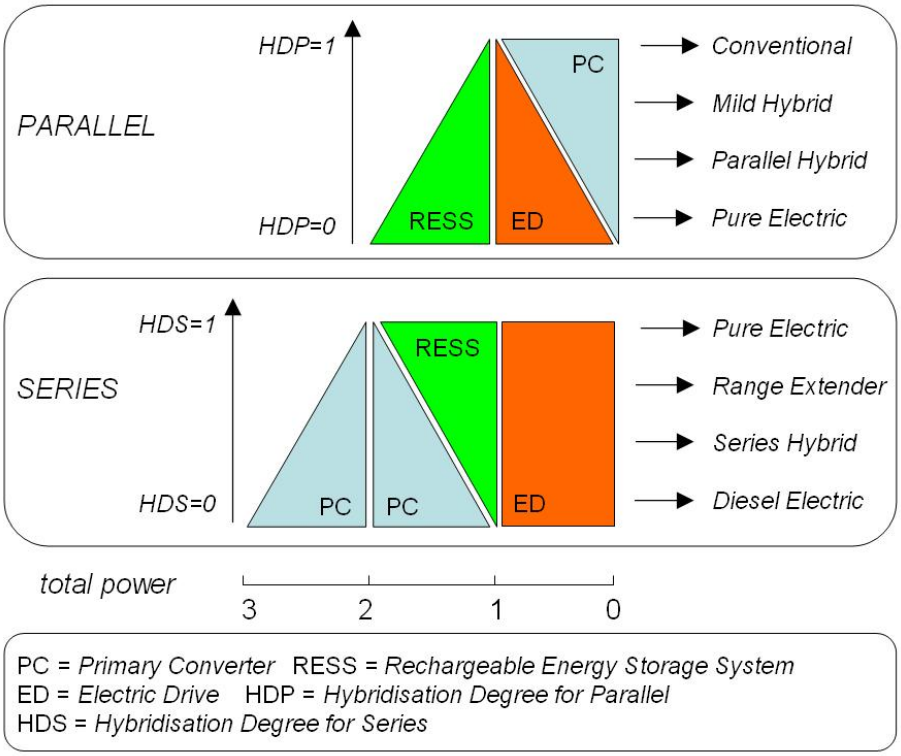

Figure 7: Hybrid classification overview considering the Hybridisation Degree definitions

With reference to the Figure 7, *HDP*=1 identifies all the conventional vehicles powered by the only mechanical primary converter. Instead *HDP*=0 or *HDS*=1 identifies the pure electric vehicle configuration.
The so called Mild-Hybrid-Vehicle (MHV), with *HDP* near 1, and Range-Extended-Vehicle (REV), with *HDS* near 1, represent two

different configurations obtained adding, respectively, a small sized RESS to the conventional vehicle, and a small sized Primary Converter to the pure electric one.
Finally, *HDS*=0 identifies the so called Diesel Electric Vehicles (DEV), that
have an electric traction system totally fed by the Primary Converter, constituted by an Electronic Generator System ICE-based.

1.1.3 Energy management strategies

This paragraph approaches the problem of the optimisation of the energy consumption onboard hybrid vehicles in a general way, considering the main issues to be solved in their conceptuality. Both parallel and series structures need to be considered: for either of them, the effect of different functions on management strategies will be discussed.

1.1.3.1 General arrangements of HEVs for the PMM

As already mentioned, hybrid vehicles can be very different in structure from each other; however, all of them share the characteristic of having two (or more) energy sources from which propulsion energy can be drawn; in hybrid electric vehicles at least one of them is electric.
The presence of different energy sources gives the possibility to share the power propulsion according to some optimisation rules, normally in terms of fuel consumption or air emissions.
The literature on this topic is very large. In particular conventional (with static and dynamic optimisation) [2], [3], [4] or innovative, such rule-based [5], neural network [6], and other [7] techniques have been proposed.
This paragraph summarises a family of techniques that have been proposed in [8], [9], [10] that are mainly based on deterministic analysis; optimisation is made instant by instant, but with integration of engineering considerations that allow to take into account the main system and load dynamics.
As already described in the previous section the simplest architectures, often taken as reference for hybridisation of the drive trains, are the Series Hybrid Electric (SHEV) and Parallel Hybrid Electric structures

(PHEV). Other general arrangements are shown in Figure 8a and in Figure 8b respectively.
In the series hybrid solution, all traction power is converted from electricity, and the sum of energy between the two power sources is made in terms of electrical quantities. In the parallel-hybrid option, the sum is made in terms of mechanical quantities, in a device referred to in Figure 8b as Mechanical bus (MB).

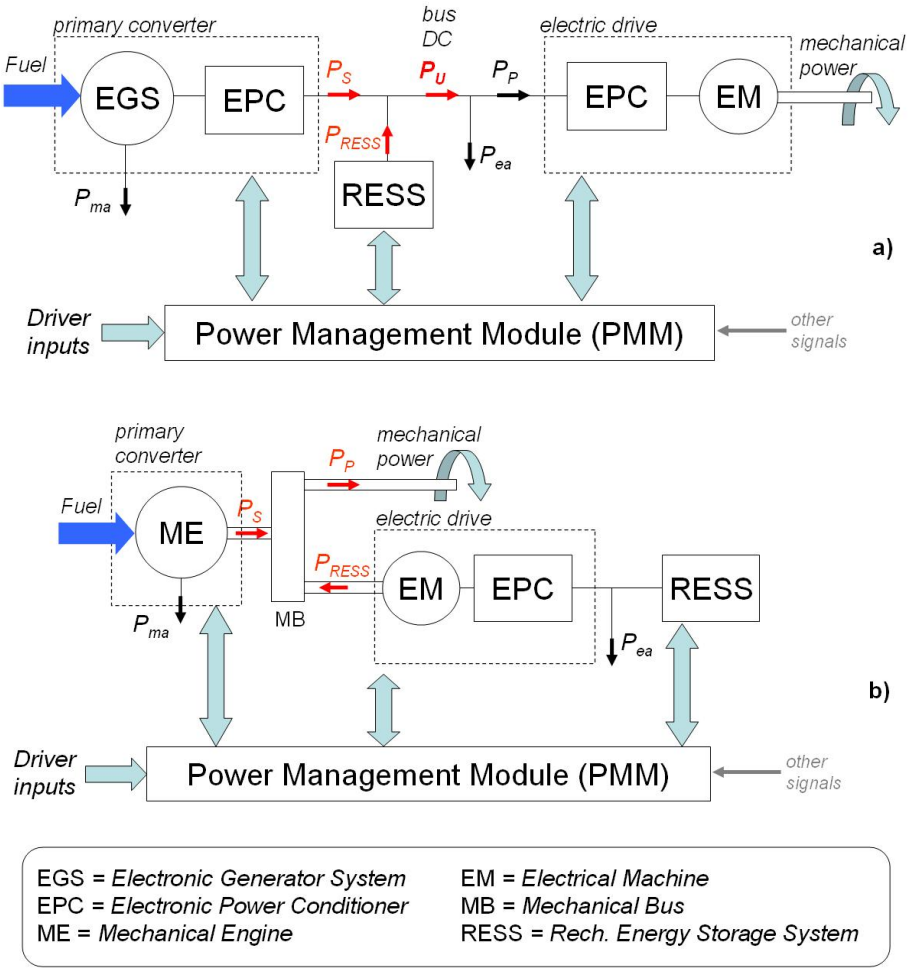

Figure 8: General arrangements of series (a) and parallel (b) drive trains

In figure, the generic component electronic generator system (EGS) is often constituted by an ICE coupled with a three-phase alternator, but can easily be otherwise: a gas turbine can be used instead of the ICE, or the whole sub-system can be of totally different nature, for example a Fuel-Cell based generation system.
Again, the device indicated in figure as mechanical Engine (ME) would be typically an ICE, but can be otherwise. In figure the main power fluxes are shown:

- P_S is the source power, that is obtained by conversion from fuel.
- P_{RESS} is the energy storage system power (taken positive when exiting the storage).
- P_{ma} and P_{ea} are the powers drawn by mechanical and electrical auxiliaries respectively (all the mechanical and electrical loads that are not devoted to propulsion, such as air conditioning, infotainment, light, …). In case of parallel structure P_{ma} is derived from the Primary Converter. In the case of Fuel-Cell based Primary Converter, P_{ma} is obviously absent.
- P_P is the power needed from propulsion.

All these powers are actually function of time. The bidirectional block arrows between the Power Management Module (PMM) and the Primary Converter, Electric Drive, RESS, are related to signal exchanges, and will be discussed in detail later.
The auxiliary powers, although very important, are normally lower than the propulsion power, and less variable over time. Therefore, they can be disregarded for basic optimisation considerations, without impact on the energy management strategies implemented. Therefore they are not considered anymore.
However, when a new specific drive train is designed, they must be taken into account, considering the exact location of mechanical and electrical power absorption, and in so far as it is known, their profile over time.
The drawings in Figure 8, in which P_{ma} and P_{ea} are disregarded, show clearly the great importance of the PMM: its fundamental role is to interpret driver's commands, and determine, according to all the available information, which part of the requested propulsion power has to be delivered by the Rechargeable Energy Storage System, and

which from the Primary Converter. In other words, how to decompose the quantity $P_P(t)$ into $P_S(t)$ and $P_{RESS}(t)$:

$$P_p(t) = P_S(t) + P_{RESS}(t) \quad \text{(Eq. 5)}$$

This degree of freedom can be used to minimise an objective function that could be fuel consumption, gaseous emissions or a combination of both. The relationship is guaranteed by the physics of the drive train; therefore only two or three quantities inside it can be explicitly determined by control actions. A possible choice is:

- $P_P(t)$ is determined to answer as close driver's commands. It may be considered the direct consequence of the trip characteristics (acceleration, speed, slope), vehicle mass, aerodynamic, mechanical drag and power losses inside the Electric Drive.
- $P_S(t)$ is determined by the PMM according to some optimisation rule (that will be discussed later).
- $P_{RESS}(t)$ is automatically determined by difference.

This choice gives the main focus to the user load P_P and the power generation from fuel; the reservoir is given somehow an accessory role.

However, nearly everything has been said can be used with minor modifications also in case of different choices (involving direct determination P_{RESS} by means of explicit control action).

The input *other signals* to the PMM is constituted by all the information useful to know all the details about the vehicle mission at that particular moment. Examples of these signals are:

- The measure of the road slope.
- Information known in advance about the trip to be made (in case of fleet vehicles, for instance, details of the typical trip can be known in advance).
- Information directly coming from the track. For instance information from GPS or Galileo positioning systems, or data from the signalling system in case the considered drive train is to be installed onboard railway trains.

The main exchange between PMM and RESS is related to the energy level, that is very important to define all the control strategies; the main exchange between PMM and Electric Drive is related to the torque request, between PMM and the Primary Converter can be

constituted by the reference source power P_S or by the ON/OFF signal, that is related to the engine switching off.

1.1.3.2 Main Issue of HEV PMM optimisation

It has been stated in the introduction that the main purpose of the PMM of electric-hybrid vehicles is to determine how to share the propulsion power between the available energy sources taking into account inputs from the driver and other possible available information.
This poses complex control problems related to:

- The choice of the correct objective function to be minimised.
- The need to have a forecast of future load based on the information available at run-time.
- The characteristics of the vehicle under consideration, in particular how big is its ability to operate in the so called Purely-Electric Drive and the presence of the plug-in capability.

In the following paragraphs these problems are presented more in detail, and possible way of solving them are presented.

1.1.3.2.1 Choosing the primary converter power and ON/OFF strategy

Whatever the nature of an hybrid vehicle is (series, parallel, complex) and whatever the dimensioning of the single components, it can be said in a general way that "useful" power that goes to the load $P_P(t)$ can be imagined to be constituted by an average value and a ripple; this way, last equation is modified as follows:

$$P_p(t) = P_{Pa}(t) + r(t) \qquad \text{(Eq. 6)}$$

Where, obviously, *avg* [r(t)]=0.
It is very reasonable to control the system in such a way that the quantity $r(t)$ is a part of $P_{RESS}(t)$ and does not penetrate into the primary converter:

$$P_{RESS}(t) = P_{RESSa}(t) + r(t) \qquad \text{(Eq. 7)}$$
$$P_S(t) = P_{Pa}(t) - P_{RESSa}(t)$$

This choice can be justified as follows:

- In case of ICE-based Primary Converter, it is important to reduce transients working condition operations, that are normally considered a significant cause of losses and pollutant emissions.
- In case of fuel-cell based primary converter (only for series-hybrid vehicles), the very high cost of the Fuel-Cell System makes very important to reduce its nominal power; this can be achieved by making them deliver only the average power requested by propulsion, and leaving the RESS to deliver the rest.

As far as $P_{RESSa}(t)$ is concerned, it may be zero, especially in case of hybrids with small batteries or in Fuel-Cell based vehicles. In other cases, the battery can be used to help the ICE to work in high efficiency regions, or can be discharged operating the drive train in pure-electric mode ($P_{RESSa}(t)=P_{Pa}(t)$); similar techniques are also used in [4], [5].

In cases in which it is decided to assume $P_{RESSa}(t)=P_{Pa}(t)$, the primary converter (especially if ICE-based) can even be switched off, to eliminate the energy spent to keep it idling; however the following issues are to be kept into account:

- In case of parallel hybrid drive-trains the scheme not always allows operating the ICE at null speed; the simplest way to do that is to introduce a clutch to disconnect the ICE from the mechanical bus (Figure 8).
- If the ICE is switched-off it has to be started again in the near future. For example, if it has cooled down it might work in the beginning at worse efficiencies, and some additional problems may be induced by any start-up due to the reduced lubricating oil circulation.
- The PMM must take into account any additional cost related to engine start-up, while considering the presence of the ON/OFF strategy [8]. Whether $P_{RESSa}(t)$ is zero or not, a way to control the energy stored in the RESS must be provided, at least for compensating the battery losses during transfer of $r(t)$.

This is done providing an estimation of this energy level (called SOC - State of Charge). This may be in several ways, normally based on an estimation of the state of charge of the battery.

Whatever the way in which SOC is evaluated, its control law normally operates in such a way that SOC is maintained below an upper limit

SOC_H, so that there is always (or at least for the large majority of time) the possibility to store in the battery the energy recovered during braking. SOC is also maintained higher than a lower limit SOC_L, to have always available energy for electrically supporting propulsion. The SOC optimal value in the range SOC_L-SOC_H can be determined according to a battery losses minimisation criterion, for instance according to the techniques specified in [43].
In general way, the approach of presented PMM structure does not depend on the particular criteria chosen to control the SOC value. It is worth mentioning that the P_{Pa} itself is a function of time, but evolving much more slowly than $P_P(t)$ and $r(t)$. For example, a typical acceleration lasts a few seconds and can be followed by a braking action that is typically even shorter. In contrast, P_{Pa} can vary in minutes' range, when a vehicle moves from an urban area, with low P_{Pa} requirements, to a suburban high-way.

1.1.3.2.2 Pollution and consumption optimisation

The on-line managing device of a hybrid vehicle in general operates not only to minimise fuel consumption but also to reduce pollution. This is made trying to minimise a function of both fuel consumption and emissions.
Except than in rather rare cases (as such [7], [11]) only fuel consumption optimisation is made, and pollution limitation is considered as a constraint of the process: as far as pollution is within predefined limits, it does not influence the optimisation process. This choice, used frequently, is justified considering that in present-day life, consumption is directly associated with a real cost, while regulations pose limits on different air pollutants, but give no money advantage to those vehicles that are able to emit much below the limits.

1.1.3.2.3 The need for load forecasting

It is well known that in the terrestrial electric power systems the power directed to the load, aggregated at least to a national level, is produced by a mix of power stations defined according to some optimisation rule, for example the research of the maximum global

system efficiency. Obviously, to find this optimum it is important to have a load forecast, since the load profile has a strong impact on possibility to share this load among different types of generation. In particular the use of pumped storage plant is also affected by considerations related to the limited energy capability of reservoir that should be kept from going empty or totally full. Although to a much smaller extent, this general problem applies to hybrid vehicles also: the load is constituted by the power necessary to accomplish the vehicle trip, and the choice of the amount of power to be drawn from the two different sources corresponds to the choice among different power stations.

In particular, since normally one of the two power sources is constituted by a Rechargeable Energy Storage System, the problem can be quite similar to the problem of sharing generation power between a fossil-fuel and pumped-storage power stations.

As in the case of terrestrial systems, the definition of the controller logic requires to know, at least approximately, the future system load, that is the future behaviour of the power demand $P_p(t)$, constituted by the power needed for covering the trip at the conditions stated by the driver.

However, normally only the average value need to be forecasted: it has been already shown that a very reasonable choice (proposed for instance in [4], [10]) for operating the system is to make the Primary Converter deliver the average load power, plus a correction term function of the RESS state of charge (SOC).

The forecast algorithm can exploit at forecasting time not only the previous values of $P_p(t)$, but also other information (road slope, traffic information…).

As a first approach the forecast $P_{Paf}(t)$ can be obtained using simple filters of the past history of $P_P(t)$:

- $P_{Paf}(t)$ is the output of a filter having as input $P_p(t)$ and as a transfer function 1/(1+sT)
- $P_{Paf}(t) = \frac{1}{T}\int_{t-T}^{t} P_p(\tau)d\tau$

In both cases a suitable value for T need to be chosen.

Rather obviously, these filter-based first-approach forecasts are acceptable when the near future is similar to the recent past, for

example when a vehicle that has been running for several minutes in an urban (or suburban) environment still runs un an urban (or suburban) environment; it brings to non-negligible errors during transitions from a type of operation into another, but these errors are rapidly recovered while driving after any transition.
The definition of the forecast algorithm is of great importance and needs to be developed as an autonomous item for theoretical and experimental research. It is deemed that advanced tools such as fuzzy logic and/or neural networks can be of help. They could be even integrated with on-line information coming from external sources such as weather forecast, information on road works, correlated with the vehicle position known by GPS or Galileo System.

1.1.3.2.4 Pure-Electric Drive and Plug-in capabilities

It is common for hybrid vehicles to have pure-electric drive capability. This term is used only for vehicles containing in the drive train the ICE: when it is switched off, the drive is made relying only on the power delivered by the Electric Drive, and energy drawn from the RESS. In this mode the vehicle is considered to have "zero emissions", since electric drives create absolutely no concern in terms of gaseous emissions.
Hybrid vehicles with pure-electric capability need to have larger energy stored in the RESS than vehicles without this capability.
Another important option that can be present onboard electric vehicles is the so-called "plug-in" capability. Plug-in hybrids are able to recharge the RESS not only using the Primary Converter, but also directly from the main supply of terrestrial electric network. This can be very cost effective [10], because of the high efficiency of the electricity generation of the terrestrial electrical system, and the taxation that is higher for traction fuels.
This carries the consequence that during hybrid operation the energy level oscillates moderately with respect to the overall capacity. This fact brings in the need to choose adequately where to position the oscillation band within the full SOC range. The following considerations can be made:

- When the drive-train is operating in hybrid mode and no pure-electric drive nor plug-in recharge is foreseen for the immediate

future, the position of the oscillation band is normally chosen to minimise system losses, that, in turn, means minimising RESS losses.

- If pure-electric drive is expected for the foreseeable future, it is important to operate so that the reservoir is ready (i.e. quite full) when the vehicle enters the part of the trip to be covered in pure-electric drive.
- If plug-in recharge is expected for the foreseeable future, it would be helpful to have the RESS nearly empty when the vehicle comes back to home, before plug-in recharge takes place.

1.1.3.2.5 A possible general PMM structure

The several problems to be solved when defining the PMM structure and logic discussed in previous paragraphs are very hard to be combined in a unique structure. Nevertheless, a general scheme that allows visualisation of important PMM sections where the above-reported operation logics are to be enclosed is reported in Figure 9a and Figure 9b, referring to series and parallel schemes respectively. It is easily seen that the two structures are very similar to each other, the only difference being that in case of series architecture the torque required by the driver is directly sent to the drive train, while in case of parallel it is the result of optimisation since the PMM has to decide which part of the required torque (and power) is to be supplied by the ICE and which by the Electric Drive. In the general scheme the main functions discussed above are enclosed:

- The interpretation of driver acceleration and braking commands to determine the wanted driver torque Td^*, that equals requested torque Te^* delivered by the electric drive only in case of series-hybrid scheme.
- The interpretation of driver's intention to enter in near future in Pure Electric drive (thus requiring high SOC in the RESS) or to make Plug-in recharge (thus requiring low SOC in RESS).
- The presence of a load forecasting unit.
- The possibility of controlling the Primary Converter by either determining the wanted power P_S^* or the ON/OFF state. The P_S^* signal in some cases may be split in two individual factors (such as

torque and angular speed) by means of a local optimisation algorithm present inside the primary converter block.

For the correct interpretation of drawings of Figure 9 it must be stressed that they are logical diagrams, not description of the real systems. In particular they define functions and borderline signals for the Power Management Module, but when the structure is translated into a real implementation it is not uncommon to have a different collection of functions.

For instance, evaluation of SOC may be performed within the RESS as shown in Figure 9 in case this is of intelligent type, i.e. containing a Battery Management System (BMS) of its own; otherwise it may be an additional function of the real PMM device, performing a different set of functions of the logical PMM defined in Figure 9.

It is important to notice that the general PMM structure presented can be useful not only for rule-based strategy implementations but also for other types of controls as those based on static or dynamic optimisation, neural networks or fuzzy logic. In fact, the actual optimisation algorithm is confined in figure in the fuel (and emission) optimisation algorithm block.

Analysis of several examples taken from scientific literature show that the relevant PMM block diagram can be matched very easily to the proposed general arrangements of Figure 9b. This is particular evident when considering the data reported in recent paper [12] that presents an overview of different control strategies for parallel hybrid vehicles.

Diagrams of Figure 9, indeed, are a general representation of how to manage all the available information coming from different sources, mainly (but not only) the driver, and how to deal with the relevant control signals.

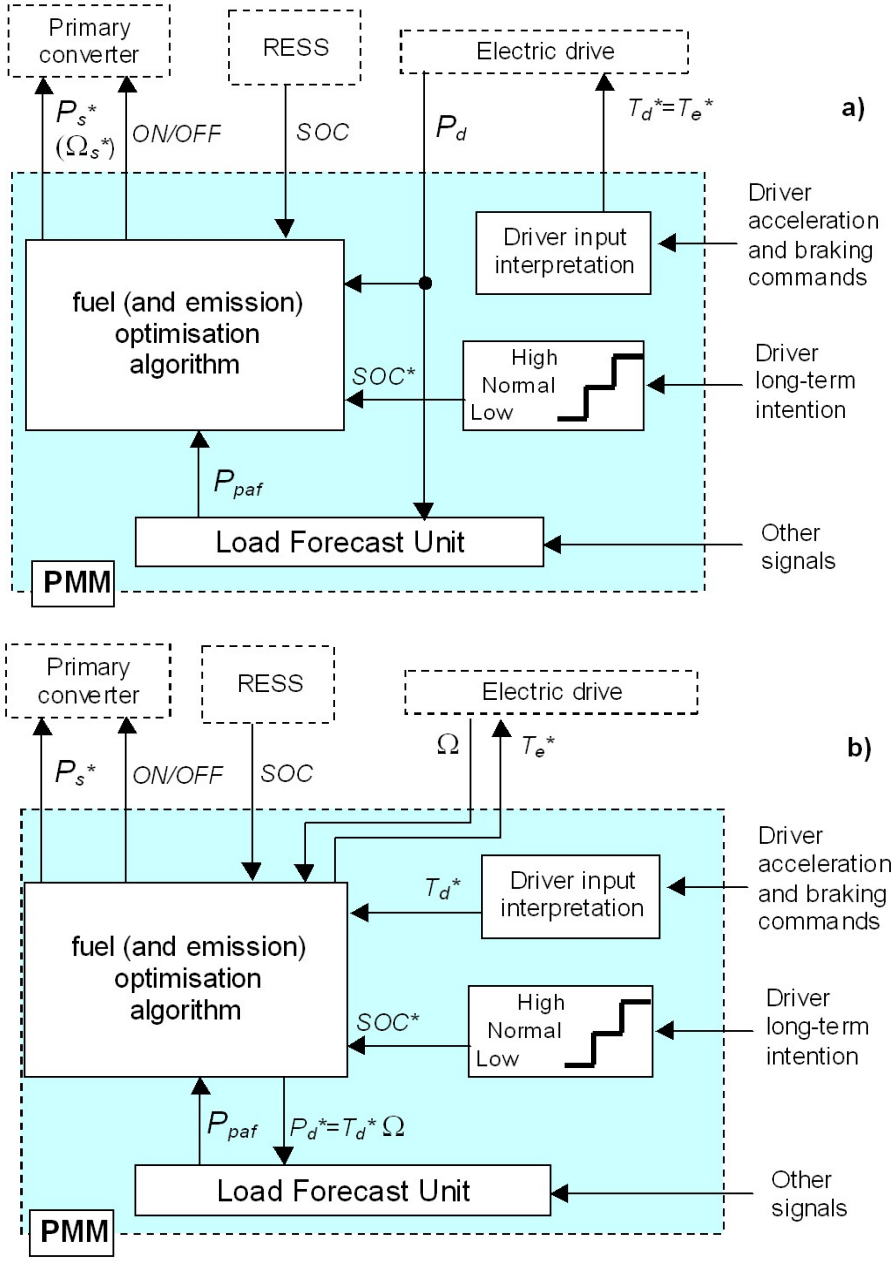

Figure 9: General arrangements showing the main PMM input/output signals of series (a) and parallel (b) hybrid drive train

1.2 Battery-fed vehicles

1.2.1 Lithium battery: general characteristics

In battery-fed vehicles, all the power required from propulsion comes from a Rechargeable Energy Storage Systems. In the last years, lithium batteries got common in consumer portable electronics, with one of the best energy densities, no memory effect, and slow losses of charge when not in use. Recently, lithium batteries have been introduced also in design of electric and hybrid vehicles: in particular, lithium ion and lithium polymer batteries are normally considered.
A lithium-ion battery is a battery type in which lithium ions move from the negative electrode to the positive electrode during discharge, and back when charging, through the non-aqueous electrolyte and separator diaphragm.
The primary functional components of a lithium-ion battery are the anode, the cathode and the electrolyte. The anode of a conventional lithium-ion cell is made from carbon, the cathode is a metal oxide, and the electrolyte is a lithium salt in an organic solvent. The most commercially popular anode material is graphite. The cathode is generally on of three material: a layered oxide (such as lithium cobalt oxide), a polyanion (such as lithium iron phosphate), or a spinel (such as lithium manganese oxide). The electrolyte is typically a mixture of organic carbonates such as ethylene carbonate or diethyl carbonate containing complexes of lithium ions. Otherwise, in lithium polymer batteries the lithium-salt electrolyte is not held in an organic solvent but in a solid polymer composite such as polyethylene oxide or polyacrylonitrile. The advantages include potentially lower cost of manufacture, adaptability to a wide variety of packaging shapes and ruggedness. Depending on material choices, the voltage, capacity, life and safety can change significantly, as visible in Table 1.

Table 1: lithium battery typology

	Voltage range (V)	**Specific Energy** (Wh/kg)	**Specific Power** (W/kg)	**Cycle life 80% DOD**
graphite/$LiNiCoO_2$	4,1-3	60-110	250-700	1000
graphite/$LiNiCoAlO_2$	4,2-2,7	100-150	400-2000	>3000
graphite/$LiNiCoMnO_2$	4,2-3	100-170	400-1000	>3000
graphite/$LiMn_2O_4$	4,3-2,2	90-150	300-500	1000
graphite/$LiFePO_4$	3,6-2	80-120	140-1100	>3000
Lithium polymer	4,2-2,7	110-180	700-2900	800-1200

Both the anode and cathode are materials into which, and from which, lithium can migrate. During *insertion* (or intercalation) lithium moves into the electrode. During the reverse process, *extraction* (or *de-intercalation*), lithium moves back out. When a lithium-based cell is discharging the lithium is extracted from the anode and inserted into the cathode. When the cell is charging, the reverse occurs. Useful work can only be extracted if electrons flow through a closed external circuit. Equations and a general scheme are reported in Figure 10.

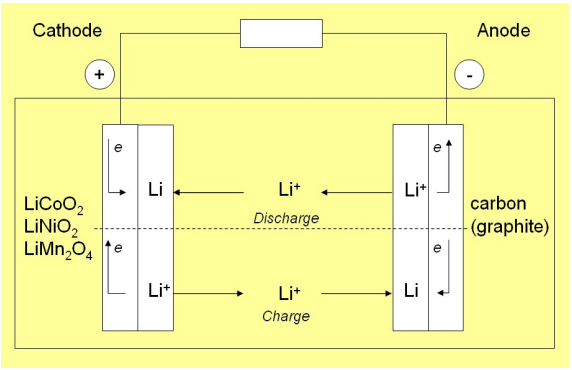

Cathode reaction

$$S + Li^+ + e^- \leftrightarrow LiS$$

Anode reaction

$$LiC_6 \leftrightarrow Li^+C_6 + e^-$$

Global reaction

$$S + LiC_6 \leftrightarrow LiS + C_6$$

$$S = LiCoO_2, LiNiO_2, LiMn_2O_4$$

Figure 10: lithium-ion cell basic behaviour

Because of the low cell voltage value, single cells are normally connected in series, to form a battery pack. Obviously series-parallel combination, to increase voltage and capacity, are normally proposed by manufacturer.

1.2.2 Characteristic parameters

A battery can be normally studied with reference to the electric charge. If output current is taken as positive, extracted charge Q_e and energy E_e can be defined on a time T interval.

$$Q_e = \int_T i(t)dt \qquad E_e = \int_T v(t)i(t)dt \qquad \text{(Eq. 8)}$$

If a discharge phase is considered, the capacity C is the delivered charge under specified conditions. Normally it is determined at constant current I_b, up to a minimum voltage value V_{fs}. The global energy is given by the product of the capacity C and the medium voltage V_m. It is possible to experimentally evaluate that the quantity of extracted charge depends by the maximum discharge current and by the temperature. The dependence of the temperature is lower for lithium batteries than for other battery typologies.

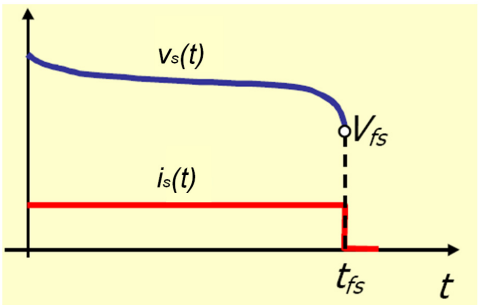

Figure 11: Discharge process at constant current

$$C = \int_0^{t_{fs}} i_s(t)dt = I_b t_{fs} \qquad \text{(Eq. 9)}$$

$$E_e = \int_0^{t_{fs}} v_s(t)i_s(t)dt = I_b t_{fs} \frac{\int_0^{t_{fs}} v_s(t)dt}{t_{fs}} = CV_m$$

C = capacity of the battery (Ah)
E_e = delivered energy (J)
i_s = discharge current (A); in this case, a constant current I_b process was considered
v_s = final discharge voltage (V)
t_{fs} = final discharge time (s)
V_m = medium voltage (V)
V_{fs} = final voltage (V)

To evaluate the level of charge of battery it is normally used a parameter called *DOD* (*depth of discharge*): it is derived from the ratio between the extracted capacity at a definite current i_s, and the nominal capacity at the same current. More commonly used is the *SOC* (*state of charge*), given by the ratio between the residual charge at a definite current and the nominal capacity, at the same current.

$$DOD = \frac{Q_e(i_s)}{C(i_s)} \qquad \text{(Eq. 10)}$$

$$SOC = \frac{Q_r(i_s)}{C(i_s)} = \frac{C(i_s) - Q_e(i_s)}{C(i_s)} = 1 - DOD \qquad \text{(Eq. 11)}$$

If a charge/discharge cycle is considered, it is possible to notice that the quantity of charge that can be extracted from the battery during discharge is a fraction of the quantity of charge introduced during charging phase. Charge efficiency η_Q can be defined as the ratio between the quantity of charge introduced in the interval *0* - t_{fc} and extracted in the interval t_{is} - t_{fs}. In analog way, also the energy efficiency η_E can be defined. Because of the voltage during charge is higher than voltage during discharge, in case of constant discharge current is, always, $\eta_E < \eta_Q$.

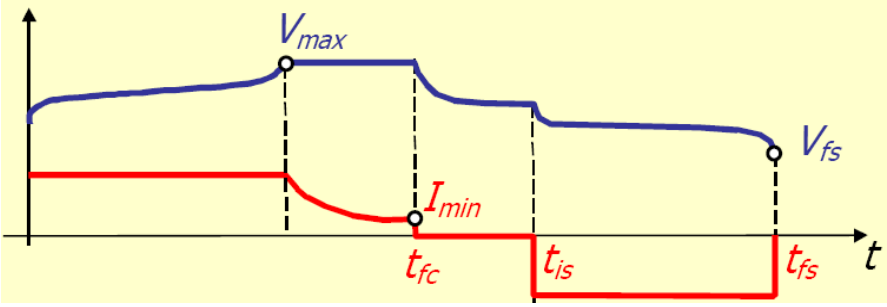

Figure 12: Current and voltage profile during charge/discharge cycles

$$\eta_Q = \left|\frac{Q_s}{Q_c}\right| = \frac{\int_{t_{is}}^{t_{fs}} |i_s(t)|dt}{\int_0^{t_{fc}} |i_c(t)|dt} \qquad \eta_E = \left|\frac{E_s}{E_c}\right| = \frac{\int_{t_{is}}^{t_{fs}} |v_s(t)i_s(t)|dt}{\int_0^{t_{fc}} |v_c(t)i_c(t)|dt} \qquad \text{(Eq. 12)}$$

Q_s = delivered charge (C)
Q_c = absorbed charge (C)
i_s = discharge current (A)
t_{is} = initial discharge time (s)
t_{fs} = final discharge time (s)
i_c = discharge current (A)
t_{fc} = final charge time (s)

E_s = delivered energy (J)
E_c = absorbed energy (J)
v_s = voltage during discharge (V)
v_c = voltage during charge (V)

1.2.3 Battery Management System

To avoid damages, lithium batteries need to be constantly monitored during working conditions: temperature must be taken under control, and voltage and current must be within limits indicated by the manufacturer. Normally the battery is monitored by the action of a Battery Management System (BMS), an electronic device that manages the cells or the battery pack. A BMS may monitor the state of the battery as represented by various item, such as voltage (total voltage or voltages of individual cells), temperature, state of charge (SOC) or depth of discharge (DOD), current. Additionally, a BMS may protect its battery preventing it from operating outside its safe operating area, such as over-current, over-voltage, under-voltage, over-temperature: the BMS may prevent operation outside the battery's safe by including an internal switch which is opened if the battery is operated outside its safe area. Otherwise, it can only reports an alarm, with indication to the device to reduce or even terminate the usage of the battery. Finally, in order to maximise the battery's capacity, and to prevent localised under-charging or over-charging, the BMS may actively ensure that all the cells that compose the battery are kept at the same state of charge (SOC), through balancing. It may do so by wasting energy from the most charged cells (passive equalisation), such as by connecting them to a load, shuffling energy from the most charged cells to the least charged ones (active equalisation).
The communication of all the above data to an external device can be guaranteed using communication links such as CAN Bus, serial or

wireless communications. Normally, the manufacturer supplies also a software that allows to visualise all the parameters on a standard personal computer. In Figure 13, a typical BMS monitor software, in which is possible to visualise the voltages of all the cells, temperatures, current and total voltage, in addition to an extended series of alarms.

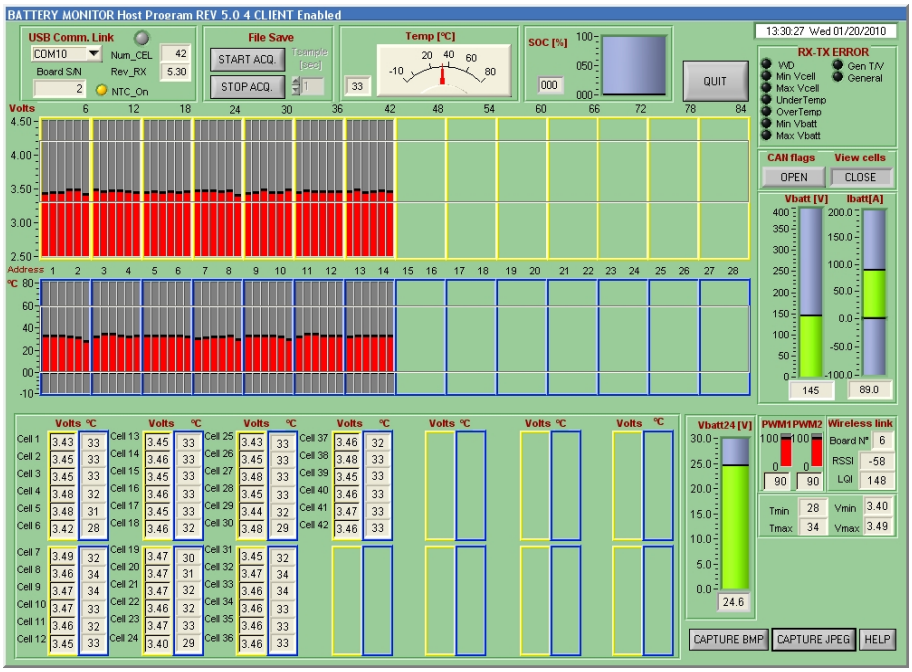

Figure 13: Battery Monitor Host Program[1]

[1] MIRMU srl

1.3 Fuel-Cell vehicles

1.3.1 Fuel-Cell: general characteristics

A Fuel-Cell System is an electrochemical device, that converts a source fuel into an electric current. It generates electricity inside a cell through reactions between a fuel and an oxidant, triggered in the presence of an electrolyte. Fuel cells can operate continuously as long as the necessary reactant and oxidant flows are maintained.
There are a lot of different Fuel Cell types, respect to the electrodes and the electrolyte used, and the temperature during the reaction.

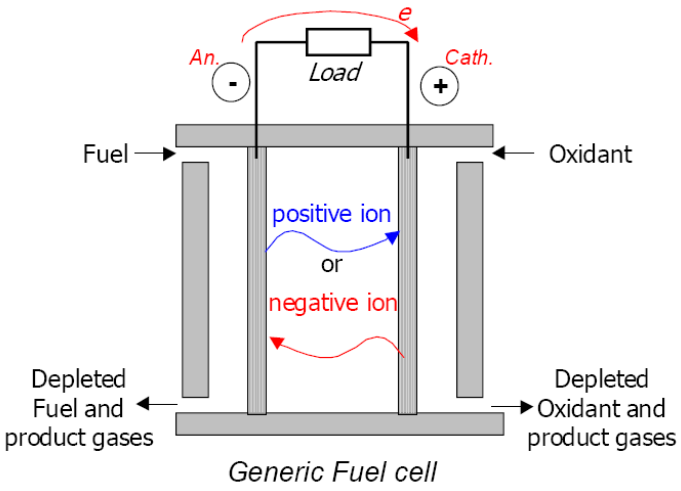

Figure 14: Generic Fuel-Cell scheme

How reported in next table, it is possible to notice there are types of Fuel Cells using acid (PAFC) or alkaline (AFC) electrolyte. In addition, those using solid polymer electrolyte (PEFC). In other types, MCFC (molten carbonate) and SOFC (solid oxide), reactions become at very high temperature.

Table 2: Fuel-Cell typology

Fuel-Cell type	Mobile ion	Net output	Temperature (°C)
Phosphoric acid PAFC	H^+	H_2O	150-220
Alkaline AFC	OH^-	H_2O	70-250
Proton exchange membrane PEMFC	H^+	H_2O	70-80
Molten carbonate MCFC	CO_3^{2-}	H_2O , CO_2	600-650
Solid oxide SOFC	O^{2-}	H_2O , CO_2	800-1000

The voltage of each single cell is strongly dependent by the electrolyte considered. In the next figure, it can be seen how the voltage measured for different types is include inside the interval 0,7-1 V.

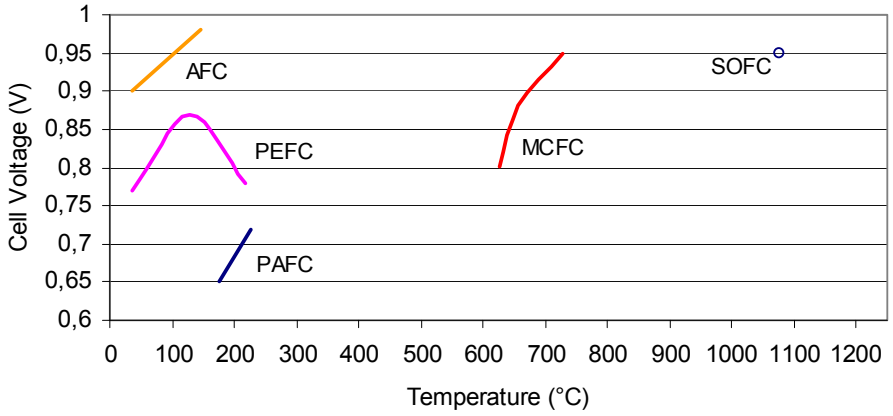

Figure 15: Characteristic Fuel-Cell temperature

1.3.2 Polymer Electrolyte Fuel-Cell (PEMFC)

The main characteristics of the proton exchange membrane fuel cell (PEMFC), can be summarised below:

- Hydrogen is channelled through field flow plates to the anode on one side of the fuel cell, while oxidant (oxygen or air) is channelled to the cathode on the other side of the cell.
- At the anode, a platinum catalyst causes the hydrogen to split into positive hydrogen ions (protons) and negatively charged electrons.
- The polymer electrolyte membrane (PEM) allows only the positively charged ions to pass through it to the cathode. The negatively charged electrons must travel along an external circuit to the cathode, creating an electrical current.
- At the cathode, the electrons and positively charged hydrogen ions combine with oxygen to form water, which flows out of the cell.

The electrode-bipolar plates are usually made of metal, nickel or carbon nano-tubes, and are coated with a catalyst (like platinum or palladium). The electrolyte is constituted by a polymeric material called *Nafion*, a sulfonated tetrafluoroethylene based fluoropolymer-copolymer, used for its excellent thermal and mechanical stability. To guarantee the adequate ionic permeability of the membrane, it is fundamental to maintain the correct level of hydration of the membrane. The main characteristic of the PEMFC is related to the very low working temperature, between 70°C and 80°C.

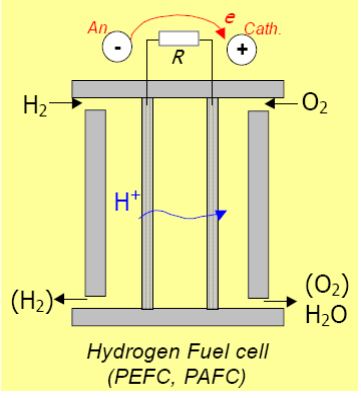

Anode reaction

$$H_2 \rightarrow 2H^+ + 2e^-$$

Cathode reaction

$$\frac{1}{2}O_2 + 2H^+ + 2e^- \rightarrow H_2O$$

Global reaction

$$H_2 + \frac{1}{2}O_2 \rightarrow H_2O$$

Figure 16: PEM Fuel-Cell scheme

Main advantageous are related to the compactness, toughness and lightness of these systems, able to be installed on-board vehicles.

1.3.3 Physical structure and assembly

In one generic cell, opportune channels are necessary to move reactants near to the electrodes, to maintain the chemical reaction.

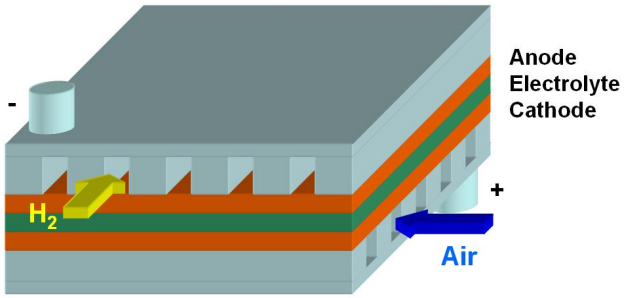

Figure 17: Fuel-Cell structure

Because of the low cell voltage value, the single cells are connected in series, to form a Stack. Normally bipolar plates are used to connect each single cell to the other. On these bipolar plates, channels are realised to allow the flow of the gases, hydrogen and oxygen.

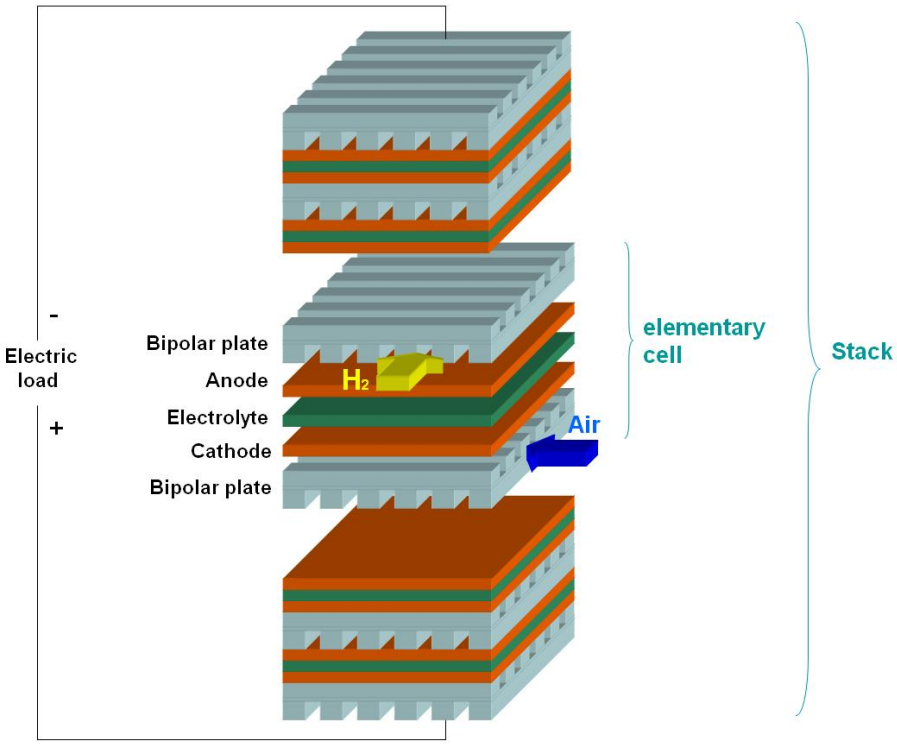

Figure 18: Fuel-Cell Stack

In figures reported below taken from [13] two different architectures for the gas flow channels can be observed: *External manifolding* based on cross-flow channels, or *Internal manifolding*, based on more complex design to allocate inside the plate a cooling circuit. Further details can be founded in [13].

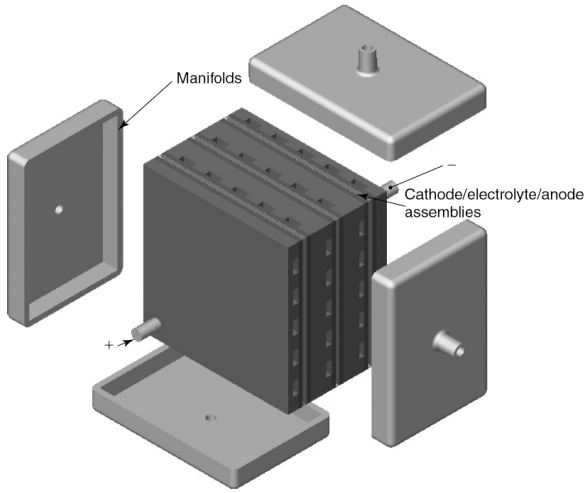

Figure 19: External manifolding

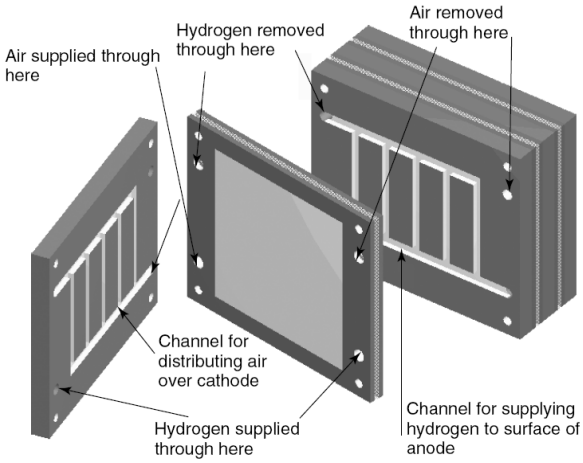

Figure 20: Internal manifolding

The Fuel-Cell System Stack must be assisted by several auxiliary devices: it must be notice the presence of a pressure reducer from the tank (the hydrogen is normally compressed at least 350 bar or more inside cylinders) to the ejector. Furthermore, there is also an air circuit composed by an air-filter and a blower. Finally a cooling circuit is normally used, to maintain the Stack at the correct temperature: for

small system, it can be of air type. For medium and high power system, it can be of water type with external radiator. The recirculation reported in figure for the hydrogen is not used by all the PEMFC type: fuel cells in which this function is absent, are generally called of *dead-end type*.

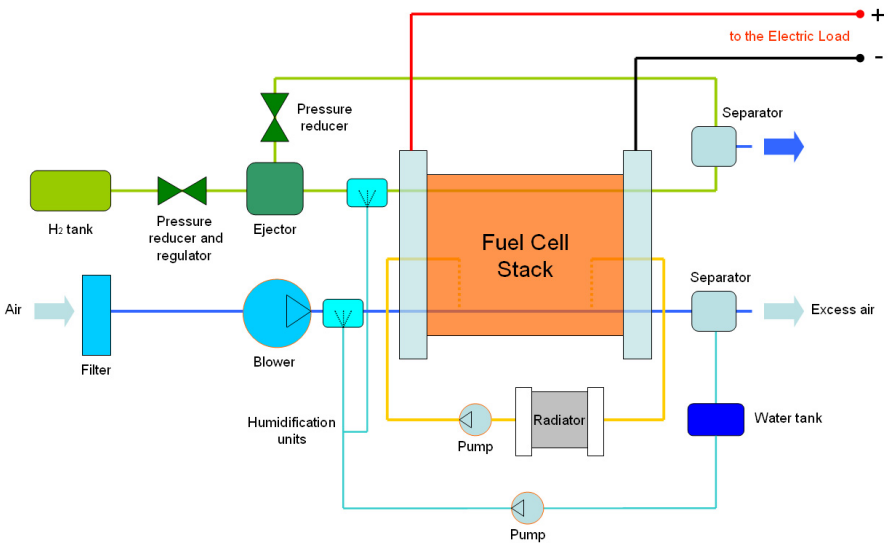

Figure 21: Fuel Cell System, balance of plant

1.3.4 Management of the membrane humidification

As mentioned in the previous paragraph, to maintain the correct ionic permeability the humidification level of the membrane needs to be observed. Water is produced inside the cathode. Normally some procedures can be employed to humidify the reactants, air and oxygen. In addition, it is important to avoid that water may back diffuse from the cathode to the anode, if the cathode side holds more water. However, in some cases water will be dragged from the anode to the cathode sides by protons moving through the electrolyte. Finally, water can be further removed by evaporation into the air circulating over the cathode. All these possibilities are summarised in the scheme below, taken from [13].

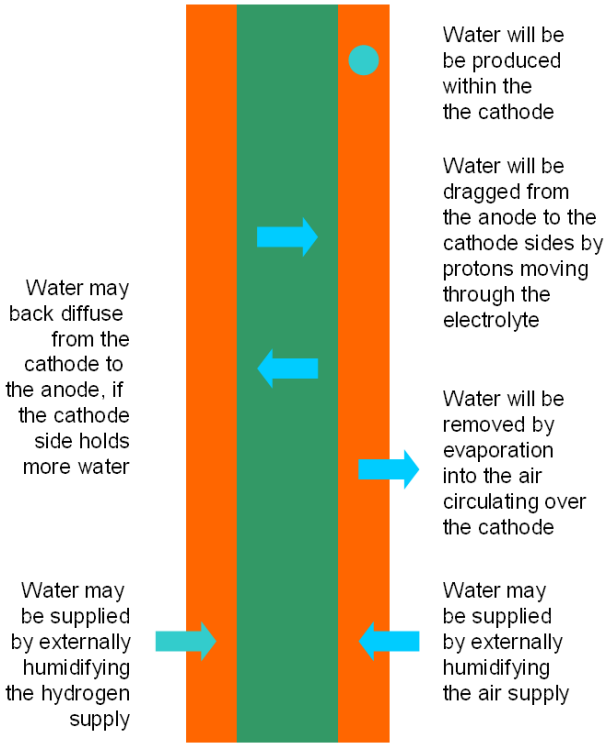

Figure 22: Membrane humidification

1.3.5 Characteristic parameters

This paragraph shows the expression of the OCV (Open Circuit Voltage). Because of some electrochemical aspects, the real voltage can significantly be different. In addition, expression of the efficiency for the cell are reported.

1.3.5.1 Ideal and practical voltage

The possibility for a reaction to become instantaneously is given by the Gibbs Energy indicator, reported below:

$$G = H - TS \qquad \text{(Eq. 13)}$$

G = Gibbs Energy (J/mol)
H = Enthalpy (J/mol)
S = Entropy (J/mol)
T = Temperature (K)

If the variation of the Gibbs Energy indicator is lower than zero, the reaction becomes spontaneously. If the indicator is equal to zero, neither the forward nor the reverse reaction prevails. If the indicator is higher than zero, external energy must be supply. The work produced by the reaction can be of the mechanical type L_m or not mechanical type L_{nm}. For a reversible reaction it can be notice that:

$$\Delta G = -L_{nm} \qquad \text{(Eq. 14)}$$

The electrical work can be defined as the work done on a charged particle by an electric field.

$$-\Delta G = L_e = \int E dq \qquad \text{(Eq. 15)}$$

G = Gibbs Energy (J/mol)
E = Voltage (V)
dq = charge of the particle (C/mol)

For a chemical reaction, the previous expression can be also expressed in:

$$-\Delta G = L_e = nFE_0 \qquad \text{(Eq. 16)}$$

Le = electrical work (J/mol)
n = number of electrons involved during the reaction
F = Faraday constant (C/mol): the quantity of charge inside a mole of electrons, equal to 96485 C
E_0 = Open circuit voltage (V)
ΔG = Gibbs Energy (J/mol)

For the PAFC or PEFC, the reaction already seen is presented below:

$$\mathrm{H_2} + \frac{1}{2}\mathrm{O_2} \rightarrow \mathrm{H_2O} \qquad \text{(Eq. 17)}$$

Because of $\Delta G < 0$, the reaction becomes spontaneously. From the expression already presented, considering the number of electrons involved in the reaction, expression of OCV can be obtained.

$$E_0 = \frac{-\Delta G}{2F} \qquad \text{(Eq. 18)}$$

How it can be seen, OCV is a function of the Gibbs Energy, indeed of the temperature of the chemical reaction. Considering the expression already seen related to the Gibbs Energy (considering ΔH and ΔS constant):

$$\Delta G = \Delta(H - TS) = \Delta H - T\Delta S$$

$$\left(\frac{\partial E_0}{\partial T}\right)_p = \frac{\Delta S}{2F} \qquad \text{(Eq. 19)}$$

From the last expression, a linear dependence between OCV and temperature can be observed. The two different trends in figure are related to the liquid state or gas state considered for the water (product of the reaction).

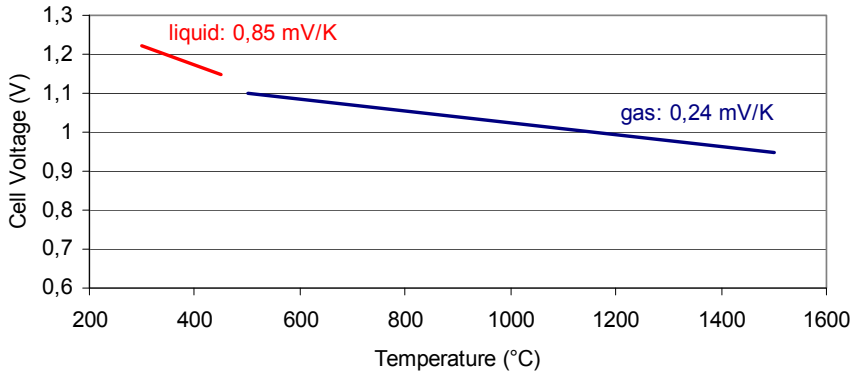

Figure 23: Open Circuit Voltage vs temperature

How can be observed, in the field of normal temperature for a *PEM-FC* (340-360 K), OCV is about 1,2 V. The other significant effect to be analysed is related to the pressure and concentration of the reactant gaseous, and described by the Nerst equation reported below. The E_0 term is corrected by the adding of a logarithmic correction term, in which is evaluated the effect of the activity for different substances (in chemical thermodynamics, activity is a measure of the effective concentration of a species in a mixture).

$$E = E_0 + \frac{RT}{2F}\ln\left(\frac{a_{H_2}\cdot a_{O_2}^{0.5}}{a_{H_2O}}\right) = E_0 + \frac{RT}{2F}\ln\left(\frac{\frac{P_{H_2}}{P^0}\cdot\left(\frac{P_{O_2}}{P^0}\right)^{0.5}}{\frac{P_{H_2O}}{P^0}}\right) \qquad \text{(Eq. 20)}$$

E_0 = Open Circuit Voltage OCV (V) at reference pressure of 100 kPa
a_i = Activity, equal to the ratio of effective and reference pressure (100 kPa)
R = Gas constant, equal to a 8,314 J/(K mol)
F = Faraday constant (C/mol)
T = temperature (K)

The real voltage is lower than the OCV previously evaluated (1,2 V for temperature lower than 100°C). The real trend for the cell voltage is reported in the figure below, in function of the current density drawn by the device.

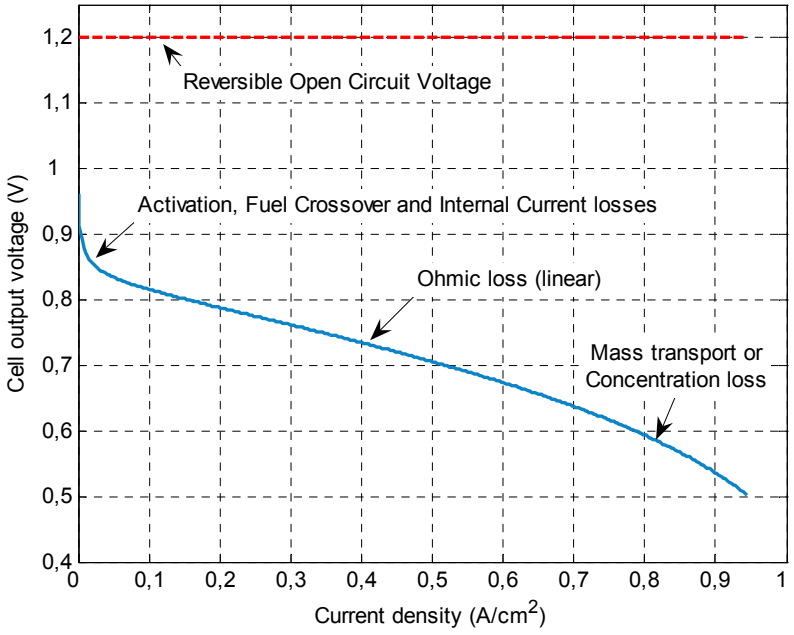

Figure 24: Voltage vs current density

The shape of the curve is influenced by four different characteristic phenomena:

- Activation losses, in the first part of the curve, caused by the slowness of the reaction near to the electrodes. Activation losses can be reduced increasing the temperature of the cell, the pressure or the concentration of the reactants. Otherwise, using more efficient catalyst layers.
- Fuel cross-over, when fuel goes from anode to the cathode without performing the ionisation process.
- Internal currents, when not only ions but a modest quantity of electrons are moved through the electrolyte.
- Ohmic losses, in the middle of the curve, realised by resistance of the electrolyte to the crossing of the electrons. This kind of loss can be considered proportional to the current density.
- Mass transport or concentration loss, in the final part of the curve, because of reduction of reactants pressure during the chemical reaction.

All phenomena can be summarised by following expression:

$$V = E - \Delta V_{act} - \Delta V_{ohm} - \Delta V_{trans}$$

$$V = E - A\ln\left(\frac{i + i_n}{i_0}\right) - ir - me^{ni} \qquad \text{(Eq. 21)}$$

E = ideal Open Circuit Voltage (V)
V = Cell voltage (V)
i = cell current density (A/cm²)

$\Delta Vact$ = Activation losses, Fuel crossover, Internal currents

A = Tafel (V)
i_0 = exchange current density (A/cm²)
i_n = fuel cross-over and internal current density (A/cm²)

$\Delta Vohm$ = Ohmic losses

r = specific resistance inside surface (Ω·cm²)

$\Delta Vtrans$ = Mass transport

m = experimental constant (V)
n = experimental constant (cm²/A)

1.3.5.2 Efficiency

This paragraph shows the evaluation of efficiency for the PEMFC. The thermodynamic efficiency can be calculated by the formula:

$$L_u = Q_1 - Q_2$$

$$\eta = \frac{L_u}{Q_1} = \frac{Q_1 - Q_2}{Q_1} = 1 - \frac{Q_2}{Q_1} \qquad \text{(Eq. 22)}$$

L = Work
Q = Heat transferred inside/outside the system
η = Efficiency

For the cycles composed by reversible reactions, the expression of the efficiency can be considered as function of temperatures of the two different sources. These are commonly called high-efficiency cycles. The most famous, composed by two isothermal and two adiabatic reactions, is the Carnot cycle. The efficiency expression is reported below.

$$\eta_C = \frac{L_u}{Q_1} = \frac{T_1 - T_2}{T_1} = 1 - \frac{T_2}{T_1} \qquad \text{(Eq. 23)}$$

For a PEMFC efficiency is evaluated as the ratio between the electrical energy produced and the heat generated through the conventional combustion process of the fuel. This quantity is expressed by the enthalpy of the reaction. Expression of the efficiency are reported below:

$$\eta_{0,PCI} = \frac{vi}{\Delta H_{(g)} \frac{i}{nF}} = \frac{v}{1{,}25} \qquad \text{(Eq. 24)}$$

$$\eta_{0,PCS} = \frac{vi}{\Delta H_{(l)} \frac{i}{nF}} = \frac{v}{1{,}48}$$

v = cell voltage (V)
i = current density (A/cm²)
$\Delta H(g)$ = enthalpy of reaction, gas state, -242 J/mol
$\Delta H(l)$ = enthalpy of reaction, water state, -286 J/mol
F = Faraday constant, 6485 C/mol
n = number of electrons exchanged during the reaction (equal to 2)
i/nF = number of moles in the unit of time (mol/s)

The maximum efficiency for a Fuel Cell can be obtained when the electrical energy is equal to the variation of the Gibbs Energy: A total conversion of chemical energy into electrical energy can be reached, and the evaluation of the efficiency is given by the ratio between Gibbs energy and enthalpy.

$$\eta_{LIM,PCI} = \frac{\Delta G \frac{i}{nF}}{\Delta H_{(g)} \frac{i}{nF}} = \frac{Ei}{\Delta H_{(g)} \frac{i}{nF}} = \frac{\Delta G}{\Delta H_{(g)}} \qquad \text{(Eq. 25)}$$

$$\eta_{LIM,PCS} = \frac{\Delta G \frac{i}{nF}}{\Delta H_{(l)} \frac{i}{nF}} = \frac{Ei}{\Delta H_{(l)} \frac{i}{nF}} = \frac{\Delta G}{\Delta H_{(l)}}$$

v = cell voltage (V)
i = current density (A/cm²)
E = Open Circuit Voltage (V)
ΔG = Gibbs energy (J/mol)
$\Delta H(g)$ = enthalpy of reaction, gas state, -242 J/mol
$\Delta H(l)$ = enthalpy of reaction, water state, -286 J/mol
F = Faraday constant, equal to 96485 C/mol
n = number of electrons exchanged during the reaction (equal to 2)
i/nF = number of moles in the unit of time (mol/s)

How can be clearly seen by last two expressions, efficiency can reach the maximum value when the current density is equal to zero. After that, the relationship between the Carnot limit and the maximum Fuel Cell efficiency with temperature is reported. From the expression of the Gibbs Energy, and considering ΔS and ΔH independent from the temperature, it is possible to notice the linear relationship.

$$\left(\frac{\partial \Delta G}{\partial T}\right)_p \cong \Delta S \qquad \text{(Eq. 26)}$$

How reported in figure, for a Fuel Cell the maximum efficiency can be higher than Carnot limit up to 700°C.

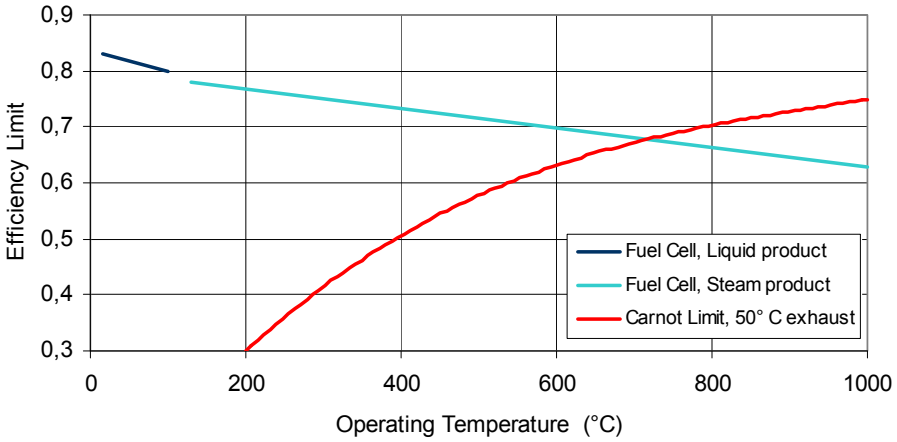

Figure 25: Efficiency limits

About the efficiency evaluation, it must be taken into account the fuel cross-over, for which all the fuel cannot participate to the reaction. Normally a new term η_c can be defined, characterised as an "utilisation" coefficient μ_c for the fuel, equal to 0,95.

$$\eta_C = \mu_c \eta_0 \qquad \text{(Eq.27)}$$

Additionally, also the power adsorbed by the auxiliary devices, formed by the blower, or water pump must be taken into account. It is possible to define a new η coefficient.

$$\eta = \mu_c \frac{vi - P_{aux}}{\Delta H_{(g)} \frac{i}{nF}} = \mu_c \frac{vi - P_{aux}}{\frac{vi}{\eta_0}} = \eta_c \frac{vi - P_{aux}}{vi} \qquad \text{(Eq. 28)}$$

The presence of P_{aux} modify the shape of the curve, reported below with the other efficiency coefficient analysed.

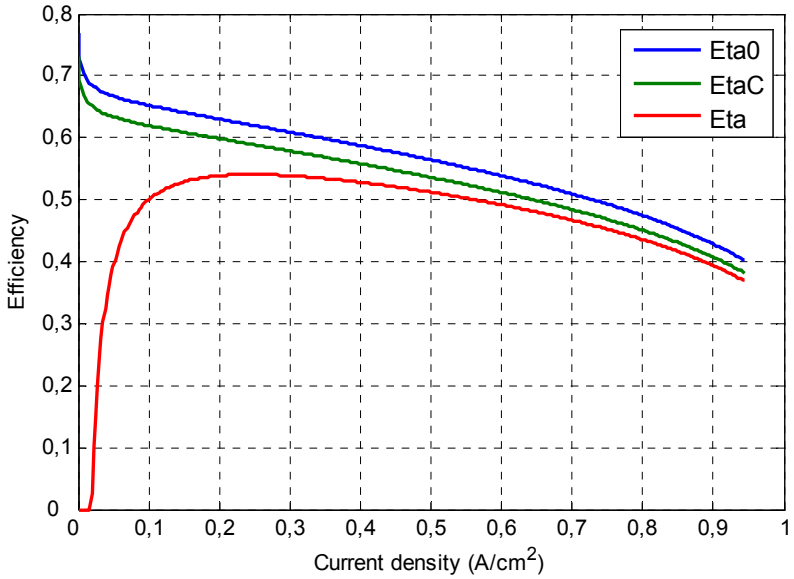

Figure 26: Efficiency curves

In the last figure, the ratio between generated power and maximum generated power is reported. How can be noticed, the point corresponding to the maximum power is different from the point corresponding to the maximum efficiency. Considering the high cost of the Fuel Cell technology, it seems to be better not sizing the system on the maximum efficiency zone, using a Stack more powerful respect to the request of the load: normally, only the maximum power requested from the load must be taken into account. In addition, efficiency is always higher that 45% in a large zone.

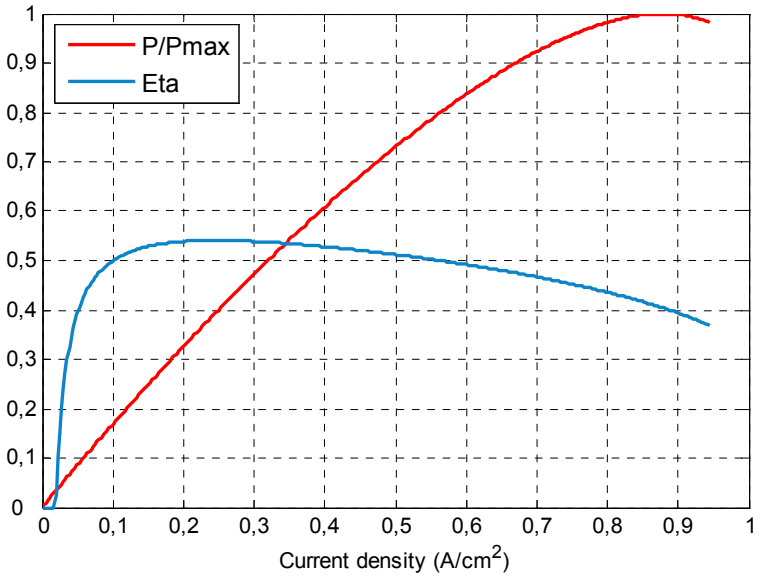

Figure 27: Characteristic power and efficiency curves

1.3.5.3 Typical data

Some typical parameters can be used to evaluate the characteristics and performance of the Fuel Cell System. In particular, it must be chosen the point of work on the characteristic plot voltage/current. Normally, values as 0,65-0,7 V/cell and 0,7-0,8 A/cm² can be chosen, near to the maximum power generated. Nominal temperature is about 70-80°C. Other characteristic values are the specific power and the power density and obviously the cost. All data are reported in table.

Table 3: PEM-FC general characteristics

	PEM-FC system
Nominal cell voltage (V)	0,65-0,7
Current nominal density (A/cm²)	0,7-0,8
Nominal temperature (°C)	70-80
Efficiency at 0,25 Pmax	0,45-0,55
Power density (W/L)	200-400
Specific power (W/kg)	200-250
CO tolerance (ppm)	15-30
Step time 0,1-0,9 Pmax (s)	3
Life (h)	1000
Cost (€/kW)	5000

2. Modelling and experimental activity on electrochemical storage systems and super-capacitors

Models of the Rechargeable Energy Storage System (RESS) are extremely important, both at the vehicle design phase, to simulate the vehicle behaviour, and on-board a vehicle during its operation, to estimate mainly future battery performance and battery state-of-charge (SOC).
At the same time, it is important to develop also experimental activities on lithium batteries, characterised by high energy and power density, and clearly power-oriented devices like super-capacitors.
Next paragraphs show, after the description of the modelling activities for lithium batteries, a comparison between the two different technologies, lithium batteries and super-capacitors, with reference to the existing devices. About high power batteries, also an extended test-activity oriented to performance verification and cycle life evaluation will be presented.

2.1 Experimental models for lithium batteries

2.1.1 A general approach to battery modelling

Lithium batteries employ different cathode material chemistries, the important ones being $LiNi_xCo_yAl_zO_2$ (NCA), $LiNi_xMn_yCo_zO_2$ (NMC), $LiMO_x$-, manganese-spinel based cathodes or olivine-type cathode materials (especially $LiFePO_4$). Characteristics of one family of lithium batteries substantially differ from the others. As shown before, the $LiFePO_4$ battery has a reduced operating voltage range (V_{cell} = 2V-3,6V) and a flat open circuit voltage (OCV) – state of charge (SOC) relationship, which are not so for other lithium batteries. Moreover, $LiFePO_4$ shows a significant deviation between the OCV measured after previous charge and that measured after previous discharge – a phenomenon called *hysteresis*.
Unfortunately, there is a clear lack of suitable mathematical model which accurately predicts its behaviour. It has been attempted to create an experimentally-determined model for a lithium battery, based on experimental tests on high power lithium NMC batteries. There is

reasonable confidence, that the same model would also be adequate for high-energy batteries as well.
There are two different approaches which are followed to study the behaviour of an electro-chemical battery:

- the use of electro-chemical analysis of the inner behaviour of the battery. There are a lot of papers in literature which follow this approach, such as those reported in [14], [15].
- the use of equivalent electric networks. This approach, as well has been used by several authors in the past: in literature [16]-[28] there can be found a list of some important papers relating to battery modelling, using equivalent electric networks.

Although both approaches are common, the first approach is predominantly used by battery manufacturers and battery chemistry researchers and is not very useful for electrical engineers and system integrators who need easy-to-use models which are expressed in terms of quantities they are used accustomed to, such as voltages and currents.
Consequently, it seems to be better to follow the second approach, which is easier to use, for modelling electric and hybrid vehicle batteries.
A general representation of the electric equivalent circuit of an electrochemical accumulator is shown in Figure 28.

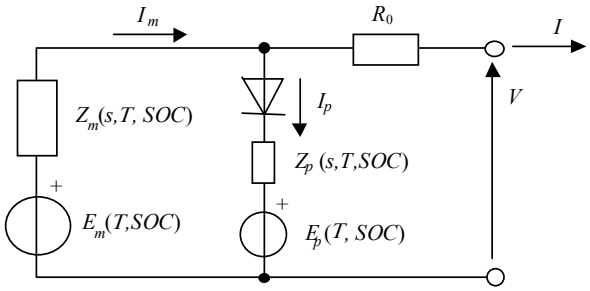

Figure 28: Battery electric equivalent taking into account a parasitic reaction

In this figure:

- the branch, containing the battery electromotive force E_m, represents the main, reversible reaction of the battery: the charge stored in the battery during the charge process is the time integral

of the current I_m entering that branch. This branch is modelled as an electromotive-force, and a function of the battery SOC and the electrolyte temperature (assumed to be uniform) T.

- the branch containing the battery electromotive force E_p, represents the parasitic reactions inside the battery which are not associated with charge accumulation inside the battery. For example, in lead-acid batteries, the parasitic reaction is constituted by the water electrolysis that occurs at the end of the charge process.
- the impedances are represented as functions of the laplacian transform variable s, since in this way a single $Z(s)$ can be representative of any network of resistor and/or capacitor and/or inductor components. For instance, the network containing two resistors in parallel with two capacitors reported in Figure 30, constitutes an expansion of the laplacian impedance $Z(s)$.

In large regions of battery operation, the parasitic reaction effects can be neglected. For instance, in the case of lithium batteries it can be neglected during the discharge process and during the initial stages of charging [20]. For this reason, the simplified model of the kind shown in Figure 29 can be used.

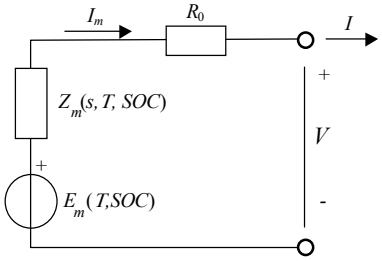

Figure 29: Simplified battery electric equivalent (neglecting the parasitic reactions)

The model shown in Figure 29 can be used for batteries that show a very high coulombic efficiency: the parasitic reactions have little influence on the battery behaviour.
If the battery, for a given SOC and temperature, has a linear behaviour, the branch impedance is a function of the Laplace variable s only.

In several battery types, including the lithium batteries, however, more complex modelling is necessary.
In case of modelling Z_m as a function of Laplace variable *s,* very often the dependence of $Z_m(s)$ is explicitly rendered using networks of parameters depending only on SOC and temperature (θ). As an example, in [20] the main branch of a Lead-acid battery model is expressed in terms of resistors and capacitors, as shown in Figure 30.

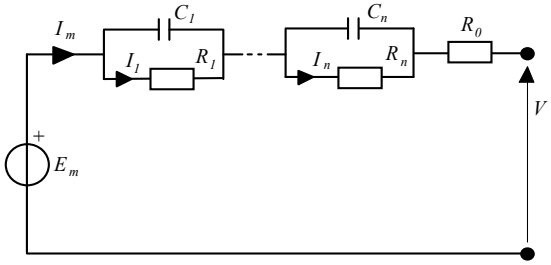

Figure 30: An R-C network to simulate the $Z_m(s)$ behaviour

The components in the circuits presented in the previous section are not constant: they normally depend upon the battery SOC and battery inner temperature. The latter, in the model proposed, has necessarily to be unique for the whole battery, since the equivalent circuits depend on a unique value of the temperature; consequently, in practical cases in which the temperature is not uniform inside the battery, this value is taken as the average or an equivalent value of temperature inside the battery.
This unique temperature can be computed with sufficient precision using the thermal equation of a single homogeneous mass exchanging heat with the surrounding air:

$$C_T \frac{d\theta}{dt} = -\frac{\theta - \theta_a}{R_T} + P_s \qquad \text{(Eq. 29)}$$

or, equivalently:

$$\theta(s) = \frac{P_s R_T + \theta_a}{1 + R_T C_T s} \qquad \text{(Eq. 30)}$$

C_T = battery thermal capacitance (J/K)
θ = is the electrolyte temperature (K)
R_T = is thermal resistance between the battery and its environment (K/W)
θ_a = temperature of the environment air surrounding the battery (K)
s = Laplace transform variable

A practical way to define the battery State of Charge (SOC) is to start from the quantity called "extracted charge" defined as:

$$Q_e(t) = \int_0^t I_m(\tau)d\tau \qquad \text{(Eq. 31)}$$

(it is assumed that the battery is completely full at t=0).

Then, the definition of SOC is:

$$SOC = 1 - \frac{Q_e}{C_{SOC}} \qquad \text{(Eq. 32)}$$

where C_{SOC} is the capacity of the battery considered.

A problem in the complete definition of SOC comes from the fact that the charge that can be extracted from a given battery depends upon several quantities; considering a constant current discharging it depends on:

- battery temperature (or, somehow equivalently, ambient temperature).
- value of the discharge current.
- end-of-discharge voltage.

The end of discharge voltage can be defined, once the system in which the battery is inserted is defined. In case of an Electric Vehicle (EV) or a Hybrid Electric Vehicle (HEV), for instance, the battery interfaces with a Power Electronic Device that can be controlled in such a way that no power is withdrawn from the battery if the voltage falls below a given threshold. This threshold can then be assumed as the end-of-discharge voltage.

The dependence of the capacity on the discharge current is very different from one battery typology to another. Just to give an idea, if, as usually, C_1 and C_{10} indicate the battery capacities when they are discharged in 1h and 10h respectively, the ratio C_{10}/C_1 is typically around 2 for lead-acid batteries and just 1,1 for Nickel-Cadmium and Lithium-polymer batteries. Therefore, for the SOC to be defined correctly, it is important to specify the discharge time along with the C_{SOC}. This will be done in the following for the lithium battery considered.

The strong dependence of the SOC on the battery temperature requires the numerical value of SOC to be normally associated with the temperature which that SOC refers to.

2.1.2 Experimental determination of a Lithium battery model

This paragraph shows an approach to solving the problem of mathematical modelling of the lithium battery by determining it experimentally. The approach presented is generic and can be applied to any type of lithium battery. However, for validation of results, NMC lithium batteries were used. Preliminary analysis of the experimental results have shown the coulombic efficiency of the considered battery to be as high as 99,1%. This suggests that, at least at a first approximation, the parasitic branch of the equivalent model of Figure 28 can be neglected, and an equivalent model of the type shown in Figure 29 or Figure 30 can be used.
It is to be stressed that the unavoidable presence of parasitic reactions (or, equivalently of coulombic efficiencies below unity), even in cases which do not create visible effects on a single charge/discharge cycle in a single cell, surely can, over long periods of time, create uneven charge distribution among cells in series, that must be corrected to avoid serious battery problems. Once it was adopted the general structure of Figure 30, the next step is to determine the number of *RC* blocks to be used, and the expression of their dependence over SOC and temperature.
For the sake of simplicity, the choice of using a single *R*-*C* block has been made, and therefore the electric circuit representation of the mathematical model is that shown in Figure 31.

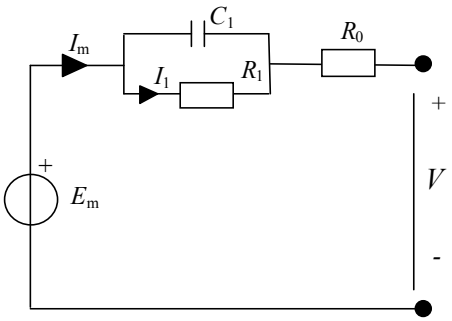

Figure 31: Circuital representation of the proposed model

The mathematical model of the battery is symbolised by this circuital representation, coupled with the expressions of capacitance and electrical circuit components as a function of temperature and SOC:

$C=C(\mathrm{SOC},\theta,\mathbf{p})$ (Eq. 33)

$R_0= R_0(\mathrm{SOC},\theta,\mathbf{p})$

$R_1=R_1(\mathrm{SOC},\theta,\mathbf{p})$ $C_1=C_1(\mathrm{SOC},\theta,\mathbf{p})$

$E_m= E_m(\mathrm{SOC},\theta,\mathbf{p})$

where $\mathbf{p}=(p_1, p_2, ...p_k)$ is the vector of constant parameters describing the actual behaviour of the considered battery model and specimen.

The model is completed by the expressions associating battery operation with inner temperature and those corelating discharge processes with SOC. In general, the determination of the structure of functions can be made by means of comparison between the actual and modelled behaviour in a selected number of tests, determining functions and parameters, and then evaluation of model performance in cases different from those that have determined it. For instance, in tests, the battery current and ambient temperature can be taken as input, and battery voltage, inner temperature, and extracted charge as output (Figure 32) output. In general, the process of model synthesis and parameter evaluations requires minimising an error function such as:

$$err(X_a(t), X_m(t,\mathbf{p})) = \min \quad \text{(Eq. 34)}$$

where X_a =(V_a,θ_a) and X_m =(V_m,θ_m) are actual and model quantities respectively, and the error function *err* can be of many kinds, such as, for instance:

$$err(x(t), y(t)) = \sqrt{\frac{1}{T}\int_{t_1}^{t_1+T}(x(t)-y(t))^2\,dt} \qquad \text{(Eq. 35)}$$

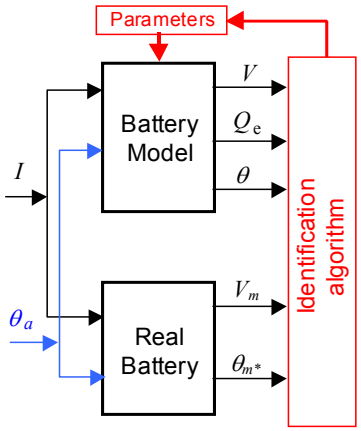

Figure 32: The process of model and parameter identification (inner temperature is estimated from the case temperature)

The next step is to experimentally determine the model parameters. The battery is first charged (positive current), then subjected to partial-discharge – rest phase cycles. At the end of each rest phase the voltage is independent of the previous battery current, and is a good indication of battery OCV and SOC. The experiment determined the impulse-response of the battery, providing a mechanism to evaluate the parameters for the battery model (result of the experiment shown in Figure 33). From the knowledge of the current drawn from the battery at each step and the value of the corresponding rest voltage, a correlation curve between OCV and SOC shown in Figure 34 can be derived.

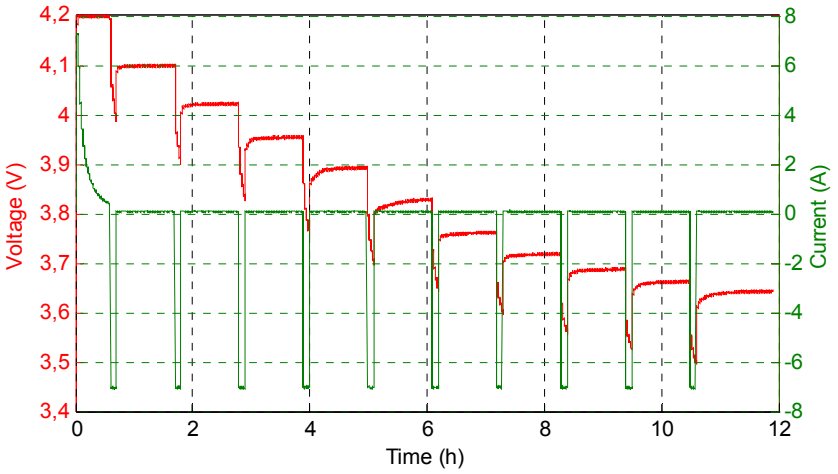

Figure 33: Experimental test to evaluate OCV-SOC correlation

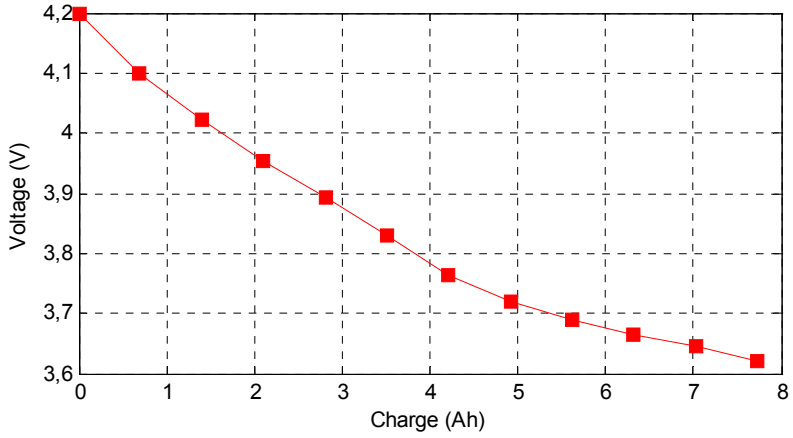

Figure 34: OCV-SOC correlation for a lithium battery, from results of Figure 33

Moreover, different typologies of lithium-batteries could present a flat zone in the middle part of the curve, that could create some difficulties during SOC evaluation, because of necessity to have an extremely precious measure of the voltage, to avoid significant errors during evaluation of the extracted capacity.

The basic structure and criteria proposed is expected to be adequate for several lithium batteries. Experimental tests from the same

manufacturer have been evaluated, considering in particular a 7,2 Ah ultra-high power battery. The experiments were all conducted at the same controlled ambient temperature of 20°C, and consequently, in this case, the parameter dependence on temperature was not taken into account. Starting from the experimental test based on partial step discharges, as shown in Figure 33, the process of parameter identification described above can be followed, obtaining the following expressions:

$C_1 = 82419(SOC)^3 - 119776(SOC)^2 + 50522(SOC) + 7415,9$

$R_0 = 0,0082(SOC)^3 - 0,0113(SOC)^2 + 0,003(SOC) + 0,0114$

$R_1 = 0,036(SOC)^3 + 0,0551(SOC)^2 - 0,0251(SOC) + 0,0103$

$E_m = -0,1558(SOC)^3 + 0,625(SOC)^2 + 0,0776(SOC) + 3,643$

These polynomial expressions, which are functions of SOC were derived for the particular battery under test to calibrate the model. The adequacy of the experimental model was evaluated by feeding the same current profile of the experimental test of Figure 33 and comparing the response of the voltages. This is shown in Figure 35.

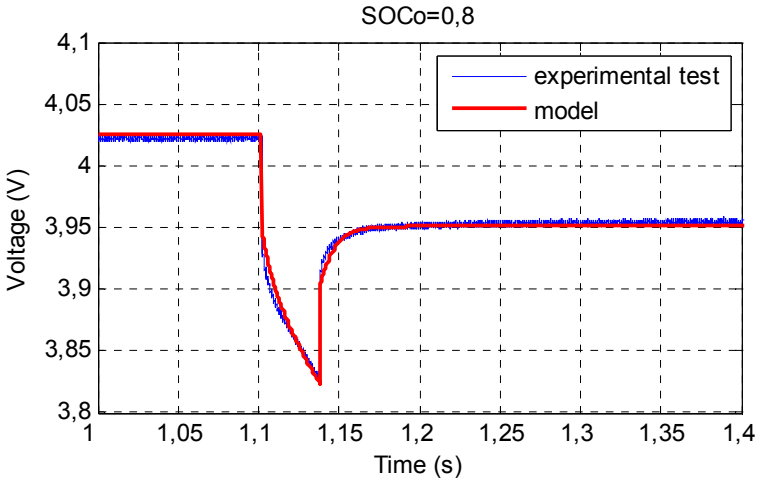

Figure 35: Comparison between the model and experimental test response starting from different initial SOC, from test of Figure 33

After the calibration, the validation of the model was performed using a more realistic test described in [29], by taking the current profile of a series-hybrid vehicle following a New European Driving Cycle (NEDC) as input and comparing the voltage responses, as shown in Figure 36. The modelled voltage closely followed the one in the experiment, clearly ratifying the adequacy of the experimentally derived model.

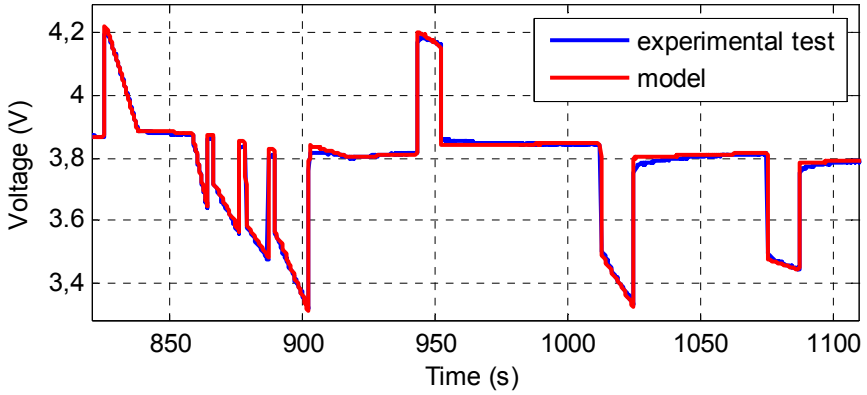

Figure 36: comparison between model and experimental test, NEDC cycle, extra-urban part

2.2 Hardware and devices under test

This section shows the hardware used for the experimental tests, and the two different devices used (lithium ion battery and super-capacitor), described below. For the last experimental tests, only one lithium single cell has been used.

2.2.1 Hardware

- *Charging System*
  The charging system is driven by a 1500 W power supply[2]. The device allows to charge the equipment under test keeping both voltage or current constant and is fully remote controlled via GPIB standard interface.

[2] Toellner TOE 8872

- *Discharging System*
  The discharging system is driven by a 6000 W electronic load[3]. The device allows to discharge the equipment under test in constant I-Mode, constant U-Mode, constant P-Mode or constant G-Mode and is fully remote controlled via GPIB standard interface.
- *Measurement System*
  Total voltage and current are measured by two 6½ digit multimeters[4] directly and using a shunt (for high currents) or a LEM current transducers (for small currents) respectively. Each battery cell voltage is measured and controlled also by a 16-bit multifunction National Instruments acquisition board. Ambient and device temperatures are measured and controlled using two RTD (PT100) transducers connected to multimeters.

In Figure 37 a photograph of a portion of the hardware experimental setup described above is reported.

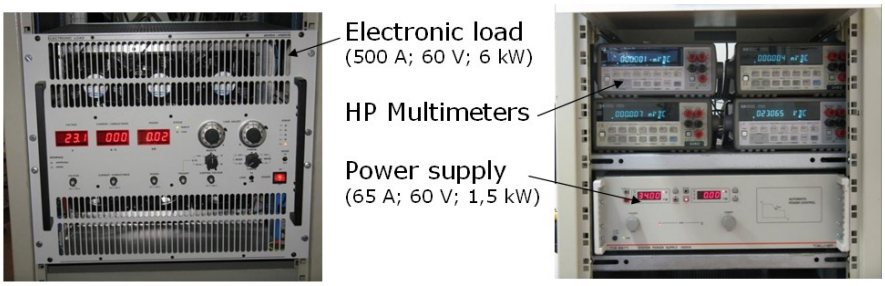

Figure 37: Hardware experimental setup

- *Test Cycle Control* - The test cycle control is implemented using National Instruments Labview® graphical programming software. The system fully control charging, discharging and measurement systems using GPIB standard interface and digital I/O of a data acquisition card (DAQ).

[3] Zentro-Elektrik EL 6000
[4] Hewlett Packard 34401A

2.2.2 Devices under test

2.2.2.1 Super-capacitor

The super-capacitor considered in the tests is a 20 F 15 V system[5] whose declared data is:

Table 4: super-capacitor, general characteristics

R_{dc} (mΩ)	I_{sc} (A)	E_{max} (Wh/kg)	P_{max} (W/kg)	m (kg)
32	730	2,72	13587	0,230

Where:

- R_{dc} is the Equivalent Series resistance computed as the ratio between the voltage variation ΔV and the current step ΔI that has caused it, after 5 s from the actual current step.
- I_{sc} is the maximum peak current during a short-circuit starting from fully charged capacitor.
- E_{max} is the maximum specific energy stored in the device, measured as $\frac{1}{2}C\Delta$I.
- P_{max} is the conventional peak specific power, measured as $V_{max}^2/(4mR)$ where R is the conventional inner resistance, measured at a frequency of 1 kHz. Rather obvious it is the maximum instantaneous power the capacitor would be able to deliver, when fully charged, if it behaved exactly as an ideal capacitor in series with the 1-kHz resistance.
- mass m includes inner equalisation system.

All these parameters can be well understood using the very simplified equivalent super-capacitor circuit shown in Figure 38: the maximum deliverable power here is $V^2/(4R)$.

[5] Maxwell BPAK0020-P015-B01 [30]

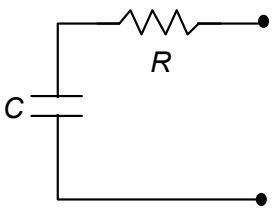

Figure 38: A very simplified model of the super-capacitor

2.2.2.2 Battery

The battery under test, to be fairly compared with a super-capacitor, has been chosen to be one of the lithium batteries capable of the highest power on the market[6]. It is a battery composed by eight cells in series, and a nominal, two-hour capacity of 7,2 Ah. Performance data for this battery are available for full discharges up to I/C_n equal to 15 A/Ah, while pulse discharges may be performed up to 20 A/Ah. From manufacturer's graphical documentation [31] the following significant numerical data can be inferred:

Table 5: lithium battery, manufacturer's documentation

Discharge regime I/C_n (A/Ah)	0,5	1	5	10	15
Delivered charge %	102	98	97	96	96
Average voltage (V)	3,85	3,80	3,70	3,60	3,50

All the data reported confirm the definite vocation of this battery for high powers, since very little charge penalty occurs.
In the final tests, related to experimental road tests and cycle life evaluation, the battery used is composed by only one single cell, of the same typology of the cells already used (7,2 Ah). According to this manufacturer's data, therefore, a single cell, whose mass is 0,226 kg, should be able to deliver (at I/C_n equal to 15 A/Ah, for about 230 s) around 1673 W/kg, (or 1460 W/kg if a overhead of 13% for case and

[6] Kokam SLPB 45205130P [31]

BMS is taken into account) that is difficult to compare with the value of 13587 W/kg of the considered super-capacitor, much higher, but available for only a split second.

2.3 Comparison of SC and high-power batteries for use in hybrid vehicles

Rechargeable Energy Storage Systems (RESS) for hybrid vehicles are required to deliver or absorb electric power in short intervals of time, typically a few seconds or tens of seconds; therefore they need to have different characteristics from batteries for pure-electric vehicles, that are discharged in tens of minutes or hours. This fact is commonly described saying that hybrid-electric storage systems are power oriented, while pure-electric vehicle batteries are energy oriented.

The most important systems to on-board store energy in hybrid vehicles are the so-called super-capacitors and power-oriented electrochemical batteries. The common judgment on these two devices is that super-capacitors are more power oriented, while batteries are more energy oriented; because of this in some cases composite (or *hybrid*) systems containing both devices are proposed even though this raises markedly the propulsion system complexity. However it must be said that recently "very-high power" lithium batteries, i.e. batteries able to deliver for a few seconds very high powers (per kg of battery), have hit the market. This technology improves the competitiveness of lithium batteries versus super-capacitor systems, and may be able to supply all the power and energy the vehicle needs, thus avoiding the need hybrid energy storage systems.

This preliminary analysis on the two systems considered makes shows that it is of interest to make a direct comparison of the two systems by means of specific lab tests. These have been carried out and will be discussed in the following paragraphs.

To make a fair comparison of different storage systems for hybrid vehicles, they must be subjected to the same stress; in particular, their specific power must be assessed using the same discharge duration. This contrasts with the common practice of considering the specific power of SC systems as *matched impedance* power, that the SC can sustain for only a fraction of a second, and considering instead the

battery specific power as the power to be continuously delivered for a given time, typically 30 or 60 s.
Moreover the charge/discharge efficiency of the two systems must be taken in due account, since it strongly influences the whole vehicle efficiency: with reference to the *matched impedance* already mentioned for the super-capacitors, it must be said that when this power is delivered, the discharge efficiency of the capacitor is 50%, by large unacceptable for the majority of applications.

2.3.1 Stress definition

The tests used in the comparisons are based on the *discharge time* that, coherently with the typical usage of a storage system onboard a vehicle, is between a few seconds and a few minutes. This is very important because, how reported in the previous section, figures often used such as matched impedance power for super-capacitors (that, as already noted can be sustained only for a fraction of a second) or battery nominal power (often determined for discharges of around a minute) cannot be effectively compared to each other. In this paper the following stress types are used:

- *Specific power test*
  It is constituted by a full I-U charge followed by full constant I discharge at different regimes.
- *Efficiency test*
  It is constituted by repeated charge-discharge cycles.

When testing super-capacitors, discharge started at maximum capacitor voltage (fully charged capacitor) and terminated when the terminal voltage was half the initial value; with this technique, normally suggested by super-capacitor manufacturers, the energy delivered should be (especially at small currents) around 0,75 times the energy initially stored inside. When testing batteries, discharge ended when the minimum voltage of 2,7 V/cell was reached, considering the lowest voltage cell, to avoid battery damage.
To evaluate specific powers, the charging current was set at the same value used for discharging for SCs (symmetric charging), while for battery discharge regime was held constantly to 3 A/Ah, the maximum

allowed by the battery manufacturer, corresponding to a specific power of 330 W/kg (for batteries I-U charge was used).
To easily compare cycle efficiencies, additional tests were made using for SC charging a I-U profile having as current set-point a fixed value defined to have an average charge of 330 W/kg (asymmetric charging). This was done whenever asymmetrical charging lead to a lower charging than discharging current.

2.3.2 Tests

2.3.2.1 Super-capacitor tests

The considered super-capacitor has been subjected to constant-current discharge tests using current chosen so to have roughly the following discharge times: 5 s, 10 s, 20 s, 40 s: these times are significant of every-day vehicle usage, for example during urban-drive accelerations. Figure 39 shows, as an example, two cycles of the test result obtained when discharge current was 3,7 A, corresponding to an expected discharge duration of around 40 s. Ambient temperature during test was 20°C. The power delivered or adsorbed by the device is reported in Figure 40, where current of 5 A has been used.

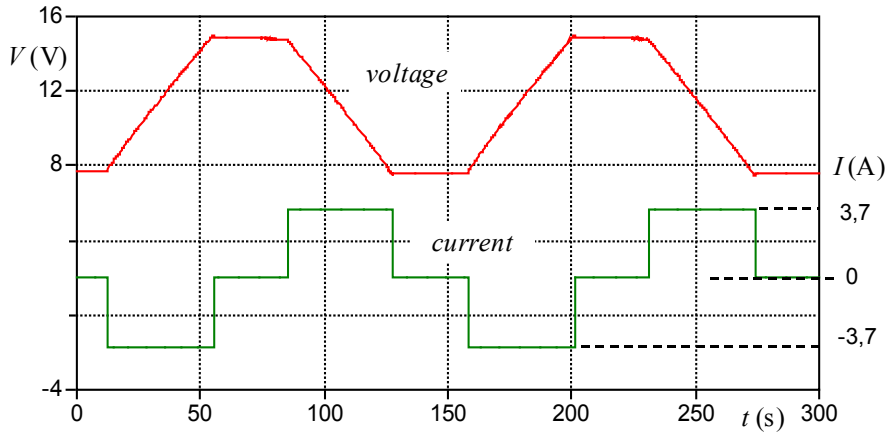

Figure 39: Super-capacitor charge-discharge cycles using a charge/discharge current of 3,7 A – voltage and current

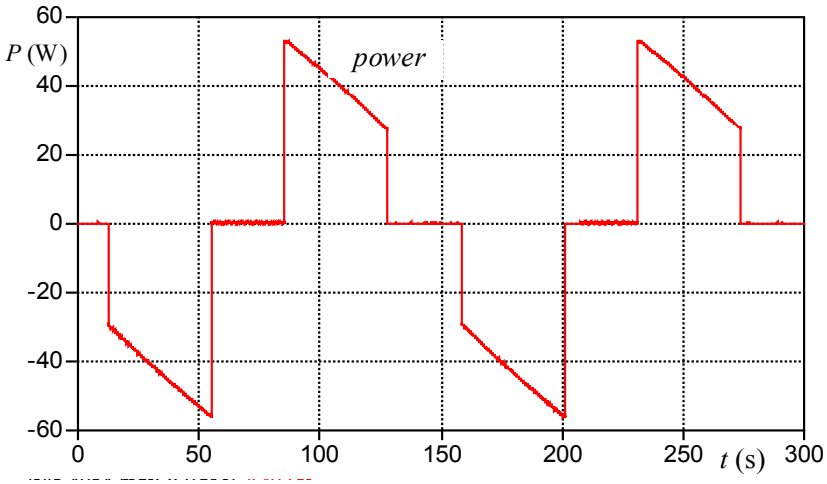

Figure 40: Super-capacitor charge-discharge cycles using a discharge current of 5 A – power delivered

To ease comparison with Lithium batteries, in case of short discharge durations, also tests with asymmetric currents were performed, limiting charge currents to a value comparable to that obtainable using batteries, and I-U charge. For instance, Figure 41 shows current and voltage for asymmetric test referring to a discharge of around 10 s.

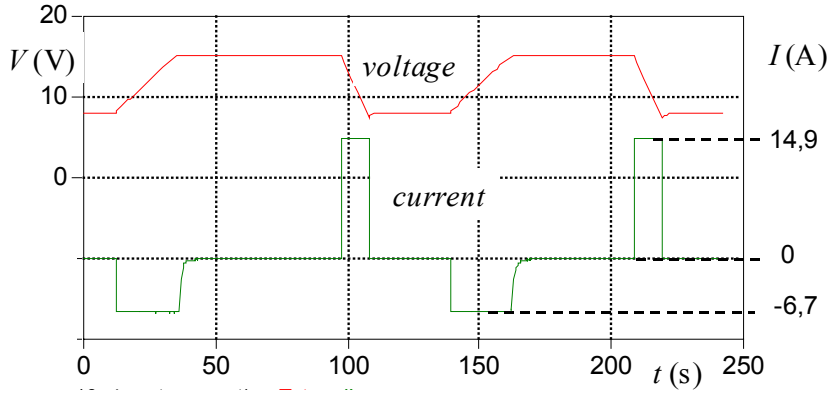

Figure 41: Super-capacitor cycles using I_U charge and discharge current of 14,9 A – voltage and current

2.3.2.2 Battery tests

The considered battery has been subjected to constant current discharge tests. In this case the discharge current values cannot be chosen in the same way used for super-capacitors, since safety limits exist on the maximum current deliverable by the battery.
Taking into account manufacturer's data tests were made at the highest range available for the battery: full tests at I/C_n of 5 A/Ah and 10 A/Ah, and short duration tests at highest currents, up to the maximum allowable pulse current, equal to 20 A/Ah (144 A)[7].
Since in these tests attention was mainly devoted to discharge phase, charging was made in a way that could mainly fully charge the battery: indeed a I-U charge has been chosen; nevertheless, since the I for the constant current part of the charge was as high as 3 A/Ah, the results are to a somewhat extent useful also for efficiency evaluations. Figure shows, as an example, two cycles of the test results obtained when discharge current was 10 A/Ah (72 A). From the corresponding power delivered by the device it is possible to infer that the battery, at this regime, is able to deliver an average power of 1kW/kg, for durations of about 510 s.

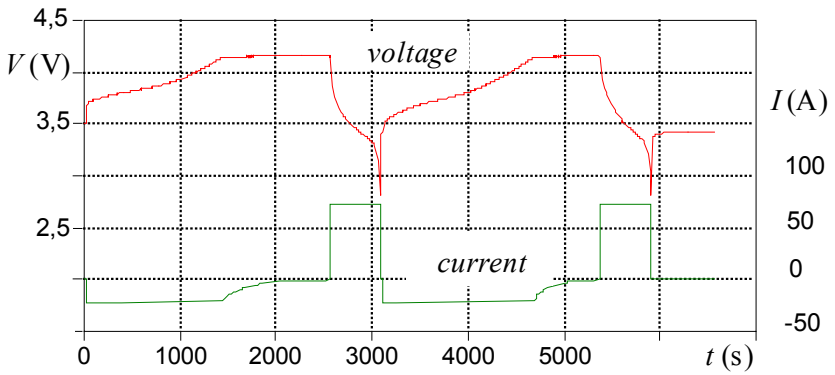

Figure 42: Battery charge-discharge cycles
using a discharge current of 10 A/Ah – voltage and current

[7] Values of current are normally expressed in terms of capacity (multiple of C_n). Because of the dimensional incompatibility, a current factor I/C_n (A/Ah) has been introduced. However, being very little known, both notations will be maintained in the following paragraphs.

2.3.3 Results

One of the main results obtained is constituted by the specific discharge powers that are summarized in Table 6. The different discharge durations were obtained discharging at fixed currents and measuring the corresponding times to reach the end-of test condition that is constituted by a combination of factors, whatever comes first.
In tests of Table 6, minimum voltage (section *stress definition*) has determined the end of discharge, except for battery tests with duration smaller than 500 s, where time duration was explicitly imposed: they implied discharge regimes over $10C_n$ that must be used only for limited time discharge, to adhere to manufacturer's requirements to avoid battery damage. The $15C_n$ discharge was limited to 240 s, while $20C_n$ discharges were limited to variable times from 5 to 60 s. As far as the charge is concerned, the SC was charged using the same current used for the discharge; the battery, on the contrary, was charged at $3C_n$, to avoid battery damage with stronger currents.

Table 6: Specific powers for the two devices (considered mass refers to modules, including cases)

discharge duration (s)	Super-capacitor		Lithium battery	
	charge	discharge	charge	discharge
5	1550	1417	330	2100
10	752	717	330	2070
20	371	361	330	2030
40	185	175	330	1980
60	122	116	330	1910
240	30	25	330	1450
500	-	-	330	976
1000	-	-	330	518

The results reported in Table 6 may be discussed as follows:

- the super-capacitor is advantaged from having nearly symmetrical charge and discharge powers while the limitation introduced to charging to I_{ch}/C_n = 3 A/Ah is a major lithium battery disadvantage.

- when only discharge power is considered the battery has a definite vantage on all the considered range, with the advantage being one order of magnitude at useful times of 40 s.
- the table does not take into account cycle lives; qualitatively, it must be said that the super-capacitor cycle life is much higher than that of batteries, but for rapid discharges the charge delivered by the battery is a small fraction of the charge totally stored, that may increase the cycle life considerably.

In typical vehicle usage the charge capability of a storage device is at least as important as the discharge capability; therefore in case a lithium battery is to be used and it is to be dimensioned onto the charging specific power, it should be oversized in discharge.
All the data reported in Table 6 can be reported inside Ragone plots, that show the dependency between specific power and specific energy for the two devices, considering different time of discharge. How reported in figure, it can be notice that the competitiveness of high power lithium batteries with respect to super-capacitors seems very high when only discharge is considered. If the usual limitation during charge is introduced, the competitiveness of Lithium batteries is greatly reduced, but still evident starting from 30 s discharge time: finally, whenever vehicle stress considered implies discharge in the order of one minute, SCs alone cannot compete.

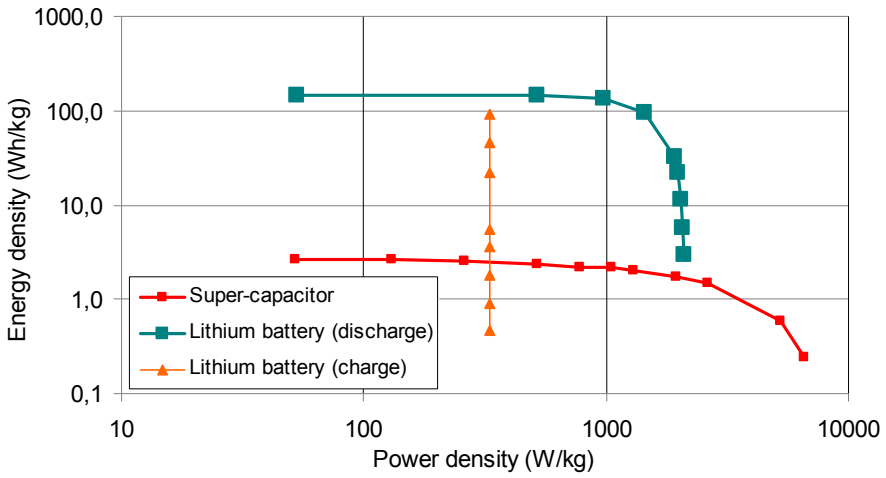

Figure 43: Ragone plots for the two different devices

Experimental tests have also been carried out to evaluate charge/discharge efficiencies. They were made in both symmetric and asymmetric charges, whose meaning is specified in section Stress Definition.

Table 7: Measured charge/discharge efficiencies (%) (considered mass refers to modules, including cases)

	Super-capacitor		**Lithium battery**
discharge duration (s)	symmetric charging	asymmetric charging	
5	79,3	84,7	87,6
10	87,4	89,5	84,8
20	91,8	94,5	83,7
40	94,7	97,5	83,0
60	96,5	-	82,5
240	99,0	-	87
500	-	-	90
1000	-	-	94

Because of its great importance in the management of lithium battery, Figure 44 shows the battery case temperature, as compared to the ambient temperature. It is noticeable that this current is very stressful for the battery, causing the temperature to reach the very maximum limit of 60°C (indicated in figure) when the current is shut-off at the end of second discharge period: the current is shut-off by reaching nearly simultaneously the minimum cell voltage, and maximum temperature; after zeroing the current the battery temperature continues to rise for a while before starting to decline.

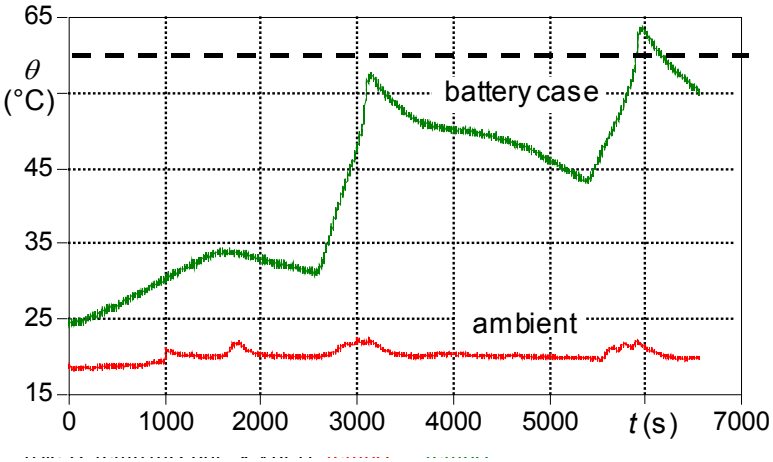

Figure 44: Battery charge-discharge cycles using a discharge current I/ C_n=10 A/Ah – temperatures

Fortunately, so long discharges are very rare onboard hybrid vehicles and, indeed, Figure 44 shows they must be avoided. This figure corresponds to the row referring to a discharge duration of 500 s. Figure 45 and Figure 46, on the contrary, show the same temperature for the 20 s and 40 s cases of Table 6, that are much more significant for hybrid vehicle usage.

Here the temperature rise, much smaller, is well compatible with typical vehicle usage.

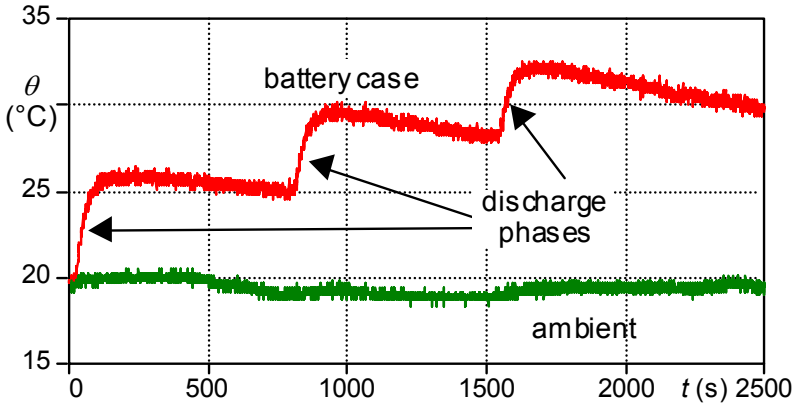

Figure 45: Battery charge-discharge cycles, with 20 s discharge time – temperatures (I/ C_n=20 A/Ah)

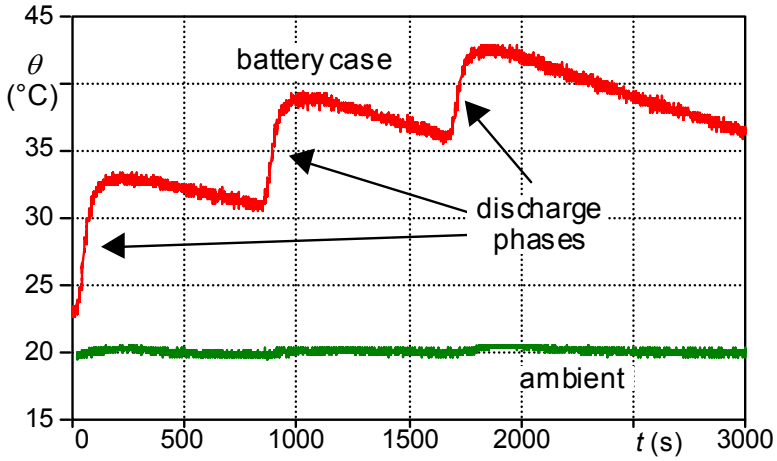

Figure 46: Battery charge-discharge cycles, with 40 s discharge time – temperatures (I/ C_n=20 A/Ah)

Since when the battery temperature stays well below 60° C the inner heat generation can be considered independent of the battery temperature itself, the temperature plots of Figure 45 and Figure 46 can be used to envisage the case temperature at other ambient temperatures, maintaining constant the gap between battery case and ambient temperatures.

Although a detailed analysis of present-day and forecasted market costs is beyond the scope of this analysis, a cost estimate can be made considering that:

- around 3,0 c€/F is the cost often quoted for today's SC cells (including overheads for monitoring and equalization systems).
- the considered battery is sold at around 1 €/nominal Wh that implies, considering an overhead of 20% due to Battery Management System a figure of 1,2 €/nominal Wh; nominal Wh is obtained multiplying the nominal Ah per the nominal voltage (3,7 V/cell).

Using this data it may be easily seen for instance (interpolating data from tables) that at 30 s discharge the SC cost per watt available in discharge is around 6 times the corresponding battery cost (40 vs 6 c€/W); the cost per watt available to charge is roughly the same for the two devices (40 c€/W). If longer discharges are considered the cost advantage of the battery becomes more marked.

2.4 High-power lithium batteries experimental road tests

How reported in the previous paragraphs, the main problem of using lithium batteries at high powers and currents is during charging, that occurs when the vehicle makes regenerative braking. Indeed, often manufacturers impose limits on the charging current that imply charging powers much smaller than discharging ones, therefore limiting the effectiveness of the whole storage system. It is, however, questionable whether for the very short durations of a braking the same current limits apply that are imposed for full recharge from battery empty. The paper investigates mainly this issue, based on the assumption that the stress induced into the battery by charging and discharging currents are related to the temperature rise. This assumption is then validated by means of cycle-life experimental evaluation. How assumed in the previous chapter, this part of the activity was realised through the usage of one single cell, whose characteristics are reported in the previous section.

2.4.1 Stress definition

The stress to which the considered storage device is to be subjected should reproduce, in a schematic idealised way, the stresses that are encountered in hybrid vehicle drive trains. However, since they are composed by idealised parts (constant current charges/discharges and pauses), the results are useful for other applications as well.
In the previous paragraph, *full charge cycling* cycles were conducted, in which the battery, in comparison with the SCs, is fully charged and fully discharged. This cycle gives information about the battery capability to absorb and deliver power in abstract, but it is not significant of actual hybrid vehicle battery stresses, in which shallow, high current, charges and discharges occur.
The cycle to be used is a consequence of the objective of the lab tests, and therefore the following different cycles have been defined:

- *Repeated partial charge (type 1)*
  cycle in which charge/discharge cycles are such that they can be repeated many times, without overcoming the battery over-temperature limits. This cycle implies shallow discharges and is

more significant of actual battery operation onboard hybrid vehicles.

- *Driving-cycle simulating battery (type 2)*
  cycle, in which the current to which the battery is subject is typical of hybrid vehicle usage operating in a NEDC driving cycle (New European Driving Cycle). This cycle gives additional information about real-life battery usage while, being much more complex, interpretation of the results are not easily transferred to other applications.

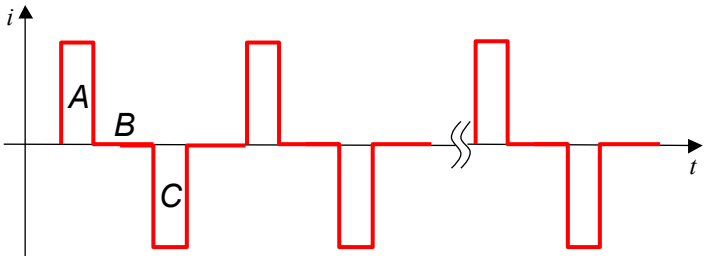

Figure 47: A partial repeated charge-discharge cycle

The repeated partial charge cycle is reported in Figure 47: it is constituted by constant-charge, constant-discharge and rest phases, with the following constraints:

- duration and current amplitude of charge phases ***A*** and discharge phases ***C*** are the same (so the cycle is charge-balanced). Values are chosen to maintain the lithium cell within the window voltage admitted (4,2-2,8 V).
- the phase ***B*** has a fixed duration of 20 s to simulate a typical vehicle battery rest.
- for each current amplitude and duration of phases ***A*** and ***C*** the battery temperature was measured.

This way the maximum charge/discharge current compatible with limits of voltage and thermal conditions is evaluated.
Finally tests of type 2 were introduced. It is well known that the NEDC cycle is composed by the four repetitions of the urban part, plus a suburban part [35]. The suburban part has normally a maximum speed of 120 km/h, but for low-powered vehicles, a version limited to 80 km/h may be used.

To define a battery current cycle based on low-powered NEDC, a series-hybrid drive train was considered, of the type shown in Figure 48. Based on a common battery management strategy [32], [33], also described in next chapter relating to the Fuel Cell hybrid vehicle, in which the primary converter delivers the average power requested by the power train, while the battery delivers (or absorbs) the ripple around that average, this drive train was simulated and the corresponding battery current evaluated.

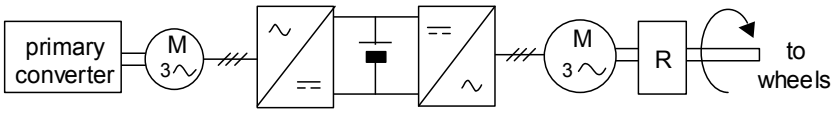

Figure 48: Simple SHEV drive train scheme

The resulting current is shown in, where the speed profile is shown as well; to make the plots clearer, only two (instead of four) urban parts of the cycle are displayed.

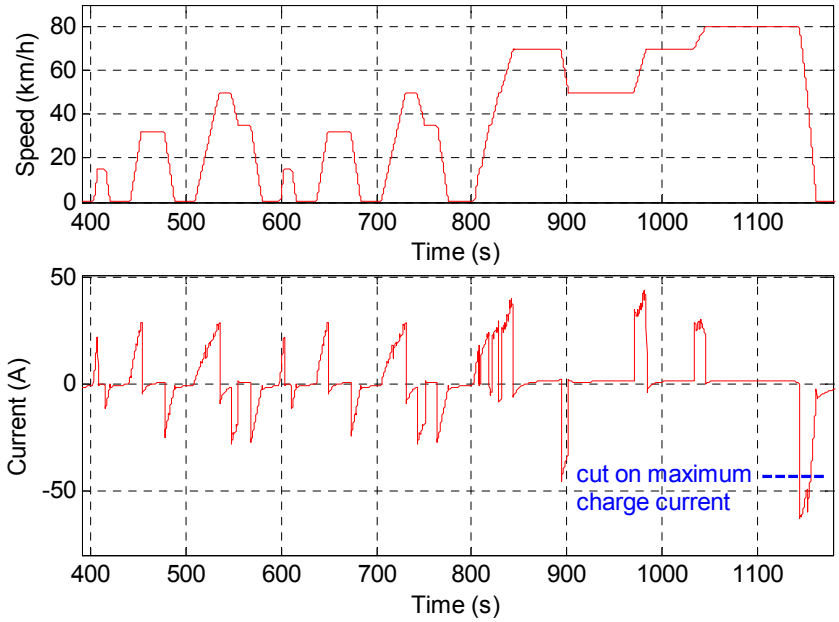

Figure 49: part of NEDC cycle for low-powered vehicles and corresponding battery current, simulated

Since it has been seen that the maximum battery stress occurs during the last vehicle braking action, it is seems reasonable to give up part of the energy that could be recovered during the last brake, limiting the maximum charge to a value that allows the battery to be dimensioned with a symmetrical profile, with equal maximum charge and discharge current. This to at least mitigate the battery difficulties with which charge currents.
As far as the actual maximum value of the peak currents, considering the results from type 2 tests, a value of I/C_n equal to 6 A/Ah is reasonable and has been chosen.

Type 2 tests were performed not only to evaluate battery performance, but also to estimate the battery cycle life, when subjected to this stress, i.e. to the typical hybrid vehicle stress.

2.4.2 Tests and main results

Therefore tests of type 1 were performed as well, testing the battery at an ambient temperature of 23°C. A sample result related to a current of $6C_n$ is reported in Figure 50, while the global set of results can be summarised as in Table 8. Although is clear from the in figure that the evolution of the refrigerating chamber temperature influences the battery case temperature, the difference becomes indeed constant after few charge-discharge cycles. The maximum case over-temperature registered, for charge-discharge current of $8C_n$ and duration of 60 s, was about 7°C.

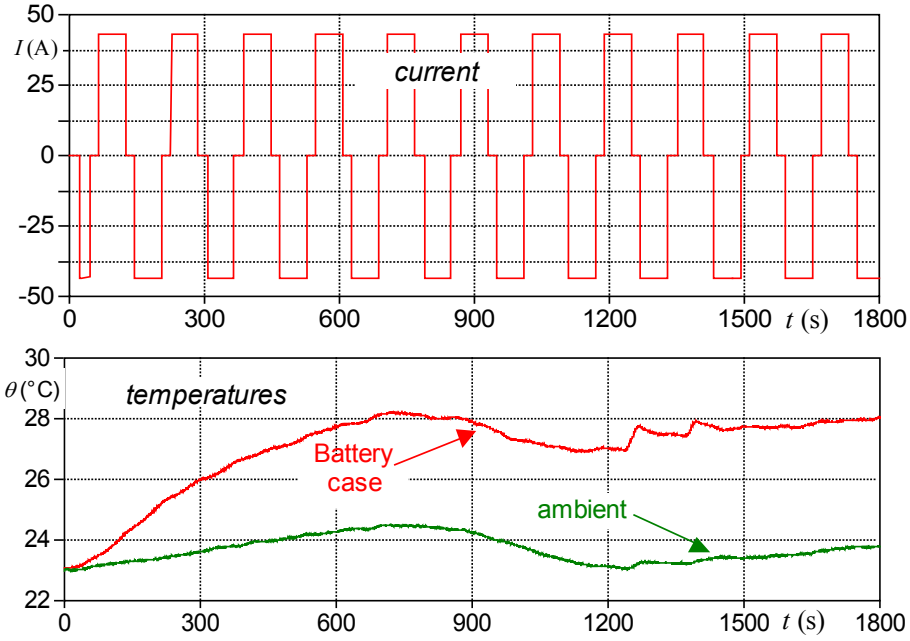

Figure 50: Battery current and temperatures during a sample test of type 2

Table 8: Current, pulse duration and case over-temperature starting from ambient (23°C) in type 2 tests

I/C_n (A/Ah)	Pulse Duration (s)	measured stable case over-temperature (°C)
3	30	1,19
3	60	1,73
6	30	3,71
6	60	4,74
8	30	5,64
8	60	6,91
9	30	6,57

The main limitation for this kind of test is due to the maximum or minimum permissible lithium cell voltages, equal respectively to 4,2 V and 2,8 V: when the battery is near the full charge condition, pulse charges must be interrupted not to overcome the maximum allowable voltage. The opposite occurs when it is near to the full discharge

condition. It must however be said, as visible in Figure 51, that the battery finds automatically the right state of charge not to overcome the maximum or minimum limit, because cuts in charge or discharge currents make the cycle unbalanced. When I/C_n was more than 9 A/Ah, the battery voltage stabilises at a level that makes the voltage cycle between minimum and maximum allowances, so this charge-discharge condition represents the maximum possible stress for the battery during tests of type 1.

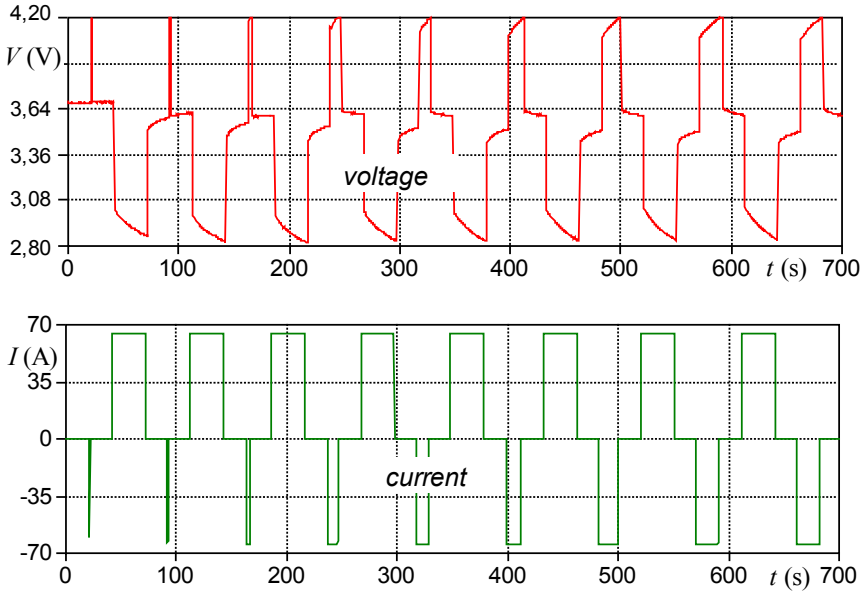

Figure 51: Voltage and current during test of type 1 related to a current of $9C_n$. Cuts on current during first charge phases are clearly shown

The performance under idealised shallow charge/discharge is much nearer to the actual vehicle usage, and shows better performance: shallow charge/discharge cycles should be possible at much higher currents than allows for full charge process, with a very modest increase of the temperature.

Finally tests of type 2 were performed. The result obtained is shown in Figure 52, where measured battery current, battery and ambient temperatures are shown. The current was shaped in such a way that

positive and negative peaks were equal, in A, to six times the nominal (one-hour) battery capacity.
It is clearly seen from these plots that this current stress does not cause important over-temperature in the battery, even though rare current peaks reach $6C_n$, not only during discharge (positive currents) but also in during charge (negative currents).

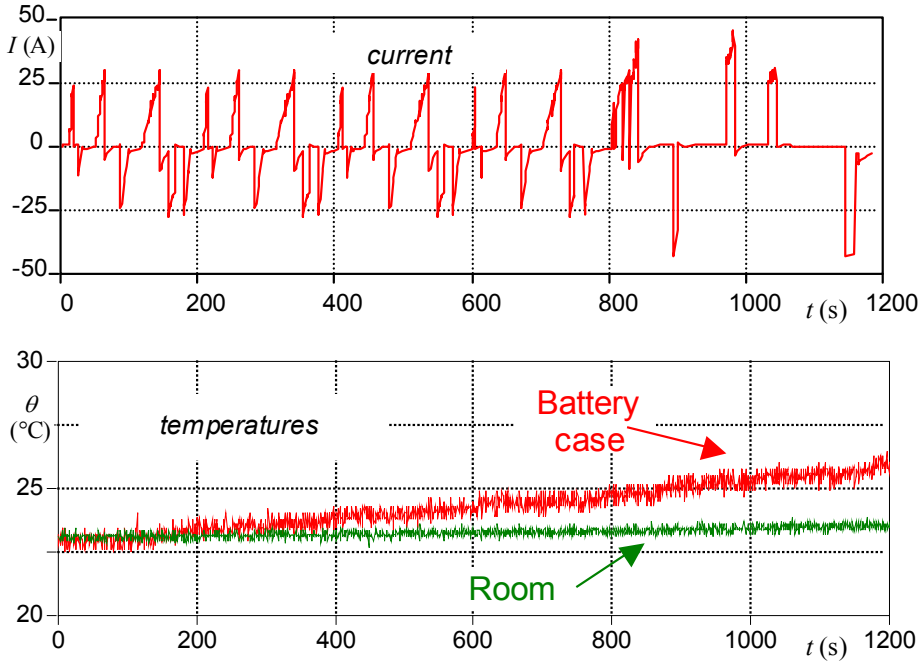

Figure 52: Battery current and temperatures during a sample test of type 2

It may be questioned that a current stress, reaching $6C_n$, much more than what considered acceptable by the manufacturer, is too stressful for the battery and could, therefore imply a short cycle life. Therefore, a cycle life test was carried out as discussed in the next section.

2.4.3 Cycle life evaluation

In the cycle life test the battery has been subjected to many (reduced-power) NEDC cycles, with periodic check of battery capacity, according to the pattern shown in Figure 53, where several NEDC cycles are reported (roughly two per hour). The tests are arranged so that:

- After each NEDC cycle, a no-operation phase of 600 s is imposed, to verify the open circuit voltage and update to the previous state the quantity of charge inside the device. After that, a charging phase is imposed: the charge current have the purpose of slightly recharging the battery to compensate for the charge lost during discharge. The correspondence between open circuit voltage and state-of-charge is discussed in [34];
- after 136 NEDC cycles, corresponding to about 1400 km, a complete charge-discharge cycle is imposed, to verify the effective capacity of the device under stress.

After about 1000 cycles, equivalent to 10000 km, the reduction in terms of capacity is about 1,8% of the initial measured value, nearly of 10,8 Ah. It means, linearly extrapolating data, that the end of life for the device under stress could be estimated to be around 10000 NEDC cycles or 10^5 km.

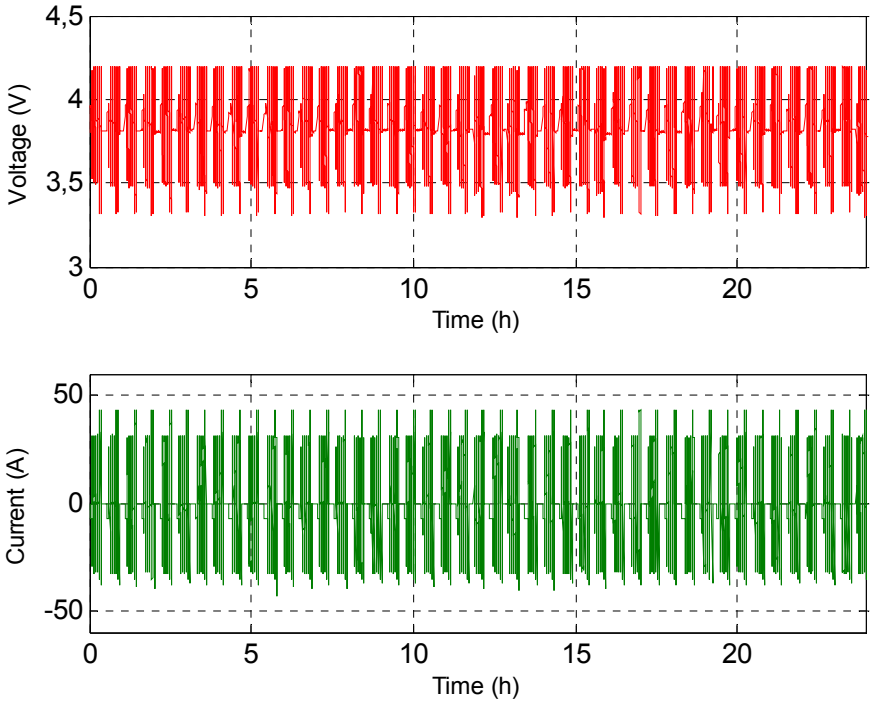

Figure 53: Voltages (top) and currents (bottom) for the cycle-life test

3. Design and realisation of a Fuel-Cell based vehicle

Electric and hybrid vehicles are considered to be an important option to reduce pollution and greenhouse effect in the environment. It is also well known that battery-fed electric vehicles have the important drawback of having small ranges and very large refilling times. A solution that mitigates these typical drawbacks, is constituted by the usage of propulsion systems in which the energy is produced onboard by a hydrogen fuel-cell based electricity generator: these systems share the vocation of battery electric vehicles of being for urban and suburban use, but at the same time offer more range and smaller refilling times, and therefore are able to perform intercity missions. Normally the propulsion system contains a Rechargeable Energy Storage System (RESS), that is able to store energy that can be later be delivered and used for propulsion. This chapter presents the some issues related to modelling of hydrogen Fuel-Cell based propulsion system; the activity was developed inside the Filiera H_2 Project, having the main objective to realise a fuel cell based mini-van. The standard version of the Piaggio Porter has been chosen as reference vehicle.

3.1 Propulsion system design

3.1.1 General architecture

The propulsion system architecture used is of the series-hybrid type (Figure 54): the presence of a Rechargeable Energy Storage System (RESS) is very effective when the vehicle is used in urban environments, since it allows regenerative braking and helps reducing the power size of the FCS. In series hybrid propulsion systems all the needed traction power is first converted into electricity, and the sum of energy between the two power sources that all hybrids have, is made in terms of electric quantities in an electric node, commonly a DC bus.

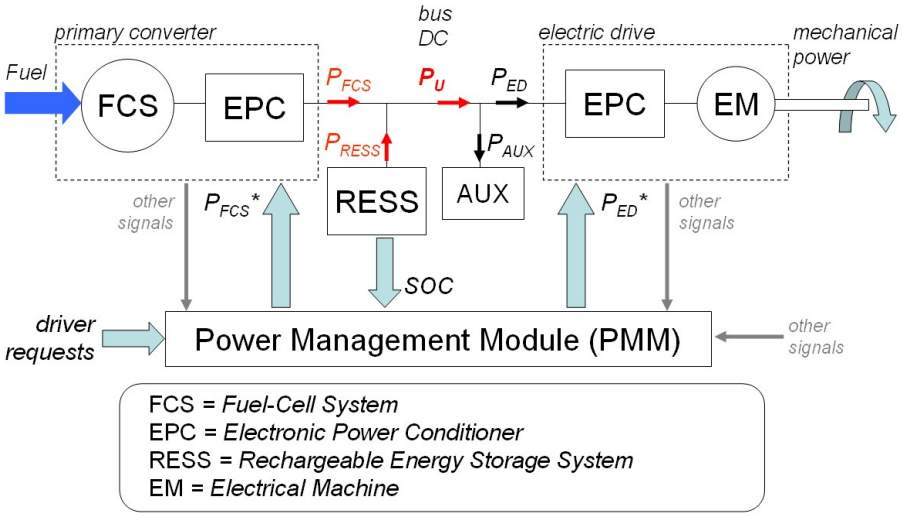

Figure 54: General arrangement of a series hybrid vehicle drive train

3.1.2 Modelling activity

3.1.2.1 General architecture

In Figure 55 graphical appearance of the upper-most layer of the simulator is shown. The Series-Hybrid propulsion structure is clearly visible: the DC bus bar, that connects generation with storage and propulsion, is in great evidence.

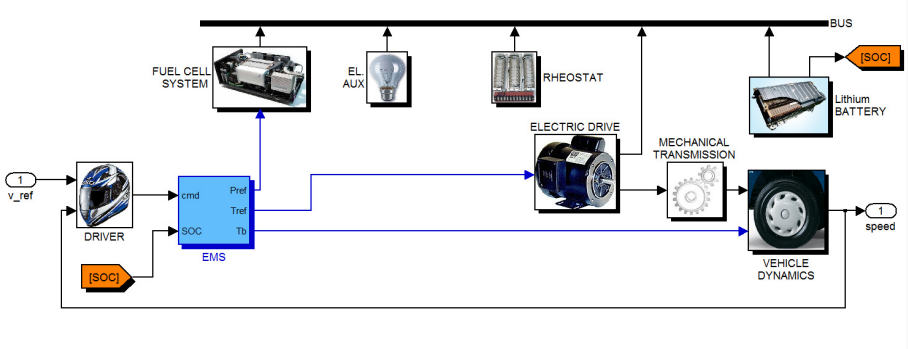

Figure 55: Simulink® block diagram of hydrogen Fuel-Cell based series-hybrid vehicle model

In particular the subsystems linked to DC bus bar are the following ones, also clearly visible in Figure 54:

- The Fuel Cell System (FCS) that generates electricity available at DC bus bar.
- The Rechargeable Energy Storage System (RESS) that can be formed by different kinds of devices such as electrochemical batteries, super-capacitors. In this case a lithium battery was considered.
- Auxiliary loads (AUX) that can be lights, the control system, the air-conditioner.
- The Electric Drive (ED), whose purpose is to provide propulsion and regenerative power (and torque), normally constituted by an electric motor and a power controller.
- The Braking Rheostat is to be used when the user implicitly requires regenerative braking, but batteries are full (see later *Interpretation of driver commands*).
- The traction system contains also the mechanical transmission and the vehicle dynamics blocks.

Central in the model is the role of the Power Management Module (PMM) that has the purpose to determine the optimal way to satisfy to driver commands while utilizing the two propulsion sources of the vehicles.

The program operates in the so-called forward approach; therefore:

- A block cycle provides a mission profile to driver.
- The Driver block emulates the behaviour of a real driver that converts a speed reference to commands for the power management module.
- the PMM determines reference signals to FCS, Electric Drive, Braking Resistor and, possibly (not shown in figure), the RESS, while receiving information from the driver, the storage SOC, and other minor signals not shown in the figure.

3.1.2.2 Interpretation of driver commands

As far as the driver commands are concerned, they are normally constituted by the position of accelerator and brake pedals.

Some regenerative braking may occur during accelerator release. This will allow light brake actions without moving foot from accelerator

pedal; moreover it simulates the ordinary behaviour of conventional, Internal Combustion Engine vehicles, that supplies braking torque when releasing accelerator. When stronger braking is needed, the user uses the brake pedal; normally the braking capability of the electric drive-train is insufficient to all braking actions, and must be integrated with conventional, mechanical braking. Since regenerative braking must take priority because of efficiency reasons, braking is electrical up to the technical limit, then mechanical braking is added.
In actual vehicles this share of two braking actions may be not easy to realize; a possible solution is to construct the pedal in such a way that for a significant amount of its initial travel the mechanical braking is zero: this way, the first part of brake travel can be used for electric braking only, while the latter causes both braking actions, the electric of which being the maximum allowable by the electric drive hardware.

3.1.2.3 Modelling subsystems

All subsystems were modelled weighing the accuracy and complexity for the purpose considered. In particular, since the fastest transients useful to globally size the hybrid drive train have constant times in the order of 100 ms, much faster phenomena, such as combustion dynamics or valve switching inside electronic converters, were considered to be algebraic.

3.1.2.3.1 Fuel-Cell System

The Fuel-Cell System is the main source for the vehicle energy propulsion. It consists of a hydrogen fuel cell stack with all its auxiliary devices, needed to supply hydrogen to anode and air to cathode, humidify, cool, etc. An electronic converter is connected between stack and DC bus-bar to adjust the voltage level of the stack with the one of bus, and to keep the latter constant. The core of a Fuel-Cell system is the Fuel-Cell itself.
A Fuel-Cell is a component that generates electricity when fed by an adequate flow of chemical reactants at adequate pressures. When (as usual with road vehicles) Proton Exchange Membrane Fuel-Cells are considered, reactants are hydrogen and oxygen, the latter being taken from the air. An extended description is reported in chapter 1.

For given pressures and flows of oxygen and hydrogen the voltage/current relationships of PEM FCs are of the type shown in Figure 56 for different cell temperatures. Obviously enough, the current the cell can carry is the shown current density times its cross-section.
As well known, often several cells are put together, typically electrically in series. Therefore, even when neglecting differences in temperature within a single cell, temperature differences between different cells may be relevant. Also pressure drops are important.

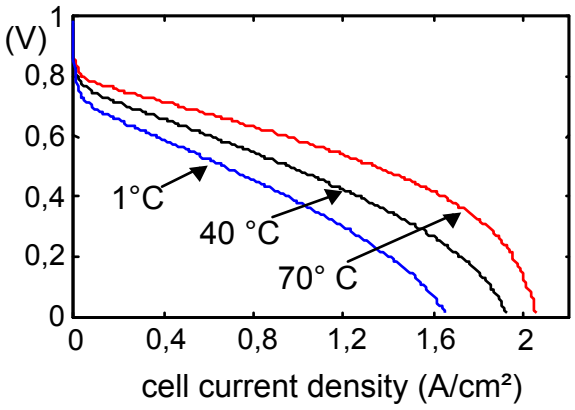

Figure 56: Examples of polarization curve (for given reactant pressures and flows)

When the detailed study of the stack or cell behavior is involved, spatial differences must be taken into account [36]. However, for simplicity reasons, the stack can be considered, how for the large majority of FC vehicle simulation programs [37], [38], as a single equivalent having a unique temperature and unique oxygen and hydrogen flows and input pressures.
This approach was followed in this kind of software. The dependence of cell behavior on reactant pressures and cell temperature are taken from [40], and adapted to the actual cell considered.
A modern PEM generation system has a rather flat, efficiency curve such as that shown in Figure 57, referring to the cell used in this paper operating at nominal temperature, together with the *theoretical cell efficiency*, that does not consider powers absorbed by the stack auxiliaries, and the global *system efficiency*.

One of the biggest advantages of the use of this kind of generation system is indeed the very high efficiency, and the large span in currents (and powers) for which larger than 50% efficiencies are available. The cell specific power is also shown in figure, normalized to its maximum value. It can be simply obtained by multiplying the current density times the cell voltage. It is useful for engineering purposes, because it clearly shows the *maximum useful density*, a limit over which it is useless to go (both power and efficiency reduce).

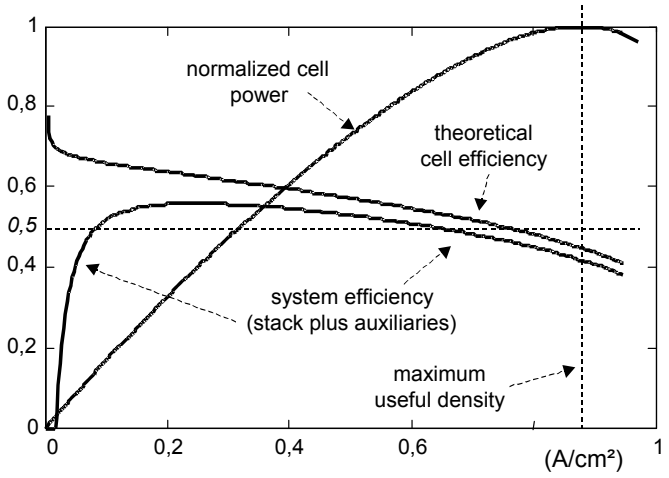

Figure 57: Example of PEM FC efficiencies

The reference FC power set by the PMM is converted into a current reference (based on mapped current-power relationships) which is further converted in a reference for the mass flow of reactants (H_2 and air) and cooling fluid to keep the stack temperature within its operating range.
Since, according to common practice and experimental results [39], [40] at given reactant pressures and stack temperature the stack voltage-current curve has been assumed constant, the dynamical behavior of the stack depends exclusively on the dynamics of partial pressures and temperature, which, in turn, depends on the behavior of stack auxiliary devices. Therefore a dynamic modeling of auxiliary devices has been assumed whenever appropriated. In particular:

- the air supply system consists of an electrically powered blower and a humidification unit, of which the former has a dynamical behavior, the latter one was assumed to be algebraic;
- the Hydrogen power supply was supposed to consists of a fuel tank, followed by a pressure regulator, and some hydrogen circulating means (typically based on a circulating ejector) and a humidification unit. Here the only dynamics considered is the regulator dynamics, assumed to be of first order type;
- the cooling system contains an electrically operated circulation pump, a radiator, an electric fan. The two electric motors have a dynamic behavior that needs being kept into account into the simulator.

3.1.2.3.2 Electronic Converters

The electronic power converters adjust the electrical power in different forms acting on the voltage and the current, by means of semiconductor devices. In a series-hybrid electric vehicle several electronic converters can be installed, for example in the FCS or RESS to interface the DC bus-bar with the Fuel-Cell generator and storage device (battery, super-capacitor) respectively, within auxiliary device electric drives.
Converters have been considered as having an algebraic behavior, and therefore they were considered as being always in steady state: if the converter that inter-faces the DC bus-bar with FCS has the purpose of maintaining the DC bus-bar voltage constant, the latter is assumed to be actually constant, whenever the converter is within its capability (output current and input voltage). Its losses were taken into account, by means of algebraic equations relating losses with the converter operating mode.
An interesting set of equations able to determine converter losses both when operating in six-step-wave and in Pulse Width Modulation is proposed in [41] and was adopted in the model. In short, this approach considers on-state and switching losses for individual valves and diodes, and sums them up to obtain the global loss.
It is possible to relate the average losses directly to static characteristics that can be approximated with polynomial functions.

3.1.2.3.3 Electric Drive

The Electric Drive is composed by an electronic converter, an electrical machine, and their control system. The electronic converter is treated not differently of the others, as explained above.
The electric machine was considered as generating an electromagnetic torque being an algebraic function of voltage and frequency at its terminals. The torque is then used to determine vehicle movement by means of the dynamics equations.
Machine losses are based on equations relating the ma-chine operating point and copper and iron losses.

3.1.2.3.4 Rechargeable Energy Storage System

In general the Rechargeable Energy Storage System can contain any electrochemical battery, super-capacitor stacks and/or flywheels. In this paper a Lithium battery was considered for its good performance in terms of power density and energy density.
The lithium battery, in a general way, can be modeled as showed in chapter 2 considering a voltage source generator in series to a R-C parallel circuit ([42], where this model is successfully used for lead-acid batteries). Parasitic reactions have been neglected, since the coulombic battery efficiency, that takes into account the balance in terms of outing and entering charges, is considered practically unity such as confirmed by experimental test [43].

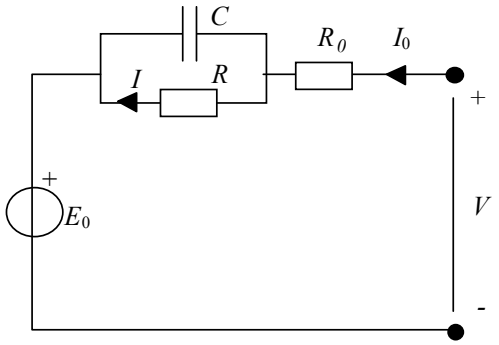

Figure 58: Equivalent dynamical model of a Lithium battery

The battery Voltage can be easily determined by means of the equation:

$$V = E_0 - V_c - R_0 I_0 \qquad \text{(Eq. 36)}$$

where, with reference Figure 58:
E_0 is the *Open Circuit Voltage,* V_c is the capacitance voltage related to the current I as follows:

$$\frac{dV_c}{dt} = \frac{1}{C}\left(I_0 - \frac{V_c}{R}\right) \qquad \text{(Eq. 37)}$$

All circuit parameters (E_0, R_0, R and $\tau = RC$) are function of the battery State Of Charge (*SOC*) and electrolyte temperature and they were determined by means of experimental tests.

3.1.2.3.5 Transmission and vehicle dynamics

Electric drives allow much greater flexibility in terms of angular speed than the conventional propulsion system based on Internal combustion engines; therefore normally the transmission from the machine shaft to wheels contains just a fixed gear ratio. The transmission may be then modeled as follows:

$$T_w = r \cdot T_{em} \cdot \eta \ , \ \Omega_{em} = r \cdot \Omega_w \qquad \text{(Eq. 38)}$$

where T_w, Ω_w and T_{em}, Ω_{em} are respectively the wheel and electric machine quantities, r is the gear ratio and η is the efficiency. Torques are positive during traction, negative during braking; the efficiency η is lower or bigger than 1 in traction or regenerative braking respectively.
The mechanical equation that describes the longitudinal vehicle kinematic behavior is:

$$M(1+\varepsilon)\frac{dv(t)}{dt} = F_t - F_r \qquad \text{(Eq. 39)}$$

where M is the total vehicle mass, F_t and F_r are traction and resistance forces at wheel respectively; v is the longitudinal vehicle speed. The variable ε takes into account all traction system rotating masses and can be evaluated as follows:

$$\varepsilon = \frac{J_{eq}}{R^2 M} = \frac{\sum_{i=1}^{n}\left(\frac{J_i}{\tau_i^2}\right)}{R^2 M} \qquad \text{(Eq. 40)}$$

where J_i is the moment of inertia of the i-th component and τ_i is the ratio of i-th gear respect to wheel, n is the number of components, R is the wheel radius, and M is the total vehicle mass.
The force F_r is the sum of different components such as aero-dynamical drag, resistant force due to bearings and wheel-road contact, force due and to gravity in case of non-null slope. In general the following equation applies:

$$F_r = A + B \cdot v^2 \qquad \text{(Eq. 41)}$$

where coefficient A takes into account the track slope and the roll resistance and B considers the aerodynamic drag.

3.1.3 Energy management strategy

To analyze possible vehicle energy management strategies, the scheme shown in Figure 54 is taken as reference. In this paragraph all the general considerations reported in chapter 1, related to the energy management strategies for hybrid vehicles, will be extended and reported to the examined case of the FC based vehicle.
The fundamental role of the PMM is to interpret driver's commands, and accordingly determine which part of the requested *useful* power would be delivered by the FCS and which by the RESS. In other words, to determine how to decompose the quantity $P_U(t)$, formed by $P_{ED}(t)$ and $P_{AUX}(t)$, into $P_{EGS}(t)$ and $P_{RESS}(t)$:

$$P_U(t) = P_{ED}(t) + P_{AUX}(t) = P_{EGS}(t) + P_{RESS}(t) \qquad \text{(Eq. 42)}$$

This degree of freedom could be used to:

- Define the optimal SOC range in which the RESS has to be operated, to have maximum efficiency during small charge-discharge cycles.
- Define the optimal point of work for the FCS, corresponding to the minimum fuel consumption.

On the other hand, experimental results already presented in [43] show that efficiency profile is quite flat for lithium ion battery, reported in Figure 59. Indeed, the general optimisation problem becomes a sub-optimisation problem for the only primary converter.

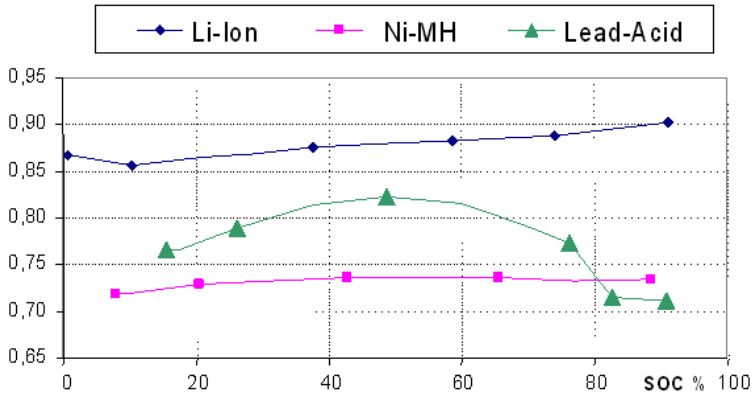

Figure 59: Efficiency vs SOC during small charge-discharge cycles

The last equation is also guaranteed by the physics of drive train. A possible control strategy could be:

- $P_{ED}(t)$ is determined to answer the driver's commands as closely as possible. It could be considered a direct consequence of trip characteristics, vehicle mass and power losses in the ED.
- $P_{AUX}(t)$ is determined by the evaluation of auxiliary loads.
- $P_{FCS}(t)$ is determined by PMM according to some optimization rule (that will be discussed later).
- $P_{RESS}(t)$ is automatically determined by difference.

The user load P_U draws the main focus in this control strategy, while the power generation from fuel, P_{EGS}, is given a supporting role. This control strategy (described in detail in [44]) is very often used in a hybrid vehicle, and presented in chapter 1.
The *useful* power that goes into the load $P_U(t)$ could be imagined to be constituted by an average value and a ripple. The last equation is thus modified as follows:

$$P_U(t) = P_{Ua}(t) + r(t) \qquad \text{(Eq. 43)}$$

where, obviously, $avg(r(t))=0$. It is possible to control the system such that the quantity $r(t)$ is delivered by P_{RESS} (t), and does not form part of the primary converter:

$$P_{RESS}(t) = P_{RESSa}(t) + r(t)\,,\ \therefore P_{FCS}(t) = P_{Ua}(t) - P_{RESSa}(t) \qquad \text{(Eq. 44)}$$

This choice can be justified, because the high cost of Fuel-Cell stacks makes very important to reduce their nominal power; this can be achieved by making them deliver only the average power requested by propulsion, and leaving the RESS deliver the rest. As far as $P_{RESSa}(t)$ is concerned, it might be considered zero, especially in case of hybrids with small batteries, or in absence of long-time discharge phases.

However, a way to control the energy stored in the RESS must be provided, at least for compensating the battery losses during transfer of *r(t)*. This is done providing an estimation of the energy stored (based upon the battery *SOC*), and introducing in the control some algorithm to keep this quantity under control. For instance, a safe operating area may be defined, having *SOCs* between 25% and 90%, and the value of P_{RESSa} is chosen for maintaining *SOC* within these limits.

The strategy presented above requires the consideration (even approximate) of the future system load, i.e. the future behaviour of the power demand $P_U(t)$, which is a function of the driver's request for torque and the vehicle duty cycle. The approximate level of power needed by the vehicle in future could be obtained by multiplying the past history of $P_U(t)$ with a simple filter:

- $P_{Ua}(t)$ is the output of a filter having as input $P_U(t)$ and as a transfer function $1/(1+s\tau)$.
- $P_{Ua}(t) = \frac{1}{T}\int_{t-T}^{t} P_U(\tau)\,d\tau$

In both cases a suitable value for τ needs to be chosen. More details on possible hybrid vehicle energy management strategies can be found in [44].

3.2 Simulation results

This simulation model has been used by the authors to size a small VAN that normally operates in urban areas, mainly used for goods transportation. In this paper only a first tentative of the power-train design is presented, since optimization is still in progress.

The propulsion system sizing has been defined in respect to the following performance specifications with the full load.

1. Horizontal drive:
   - *a) max speed: 80 km/h*
   - *b) acceleration 0 – 80 km/h: within 60 s*
   - *c) max speed range: 150 km*
2. Slope 25%:
   - *a) max speed: 20 km/h*
   - *b) start-up acceleration: 0.3 m/s^2*

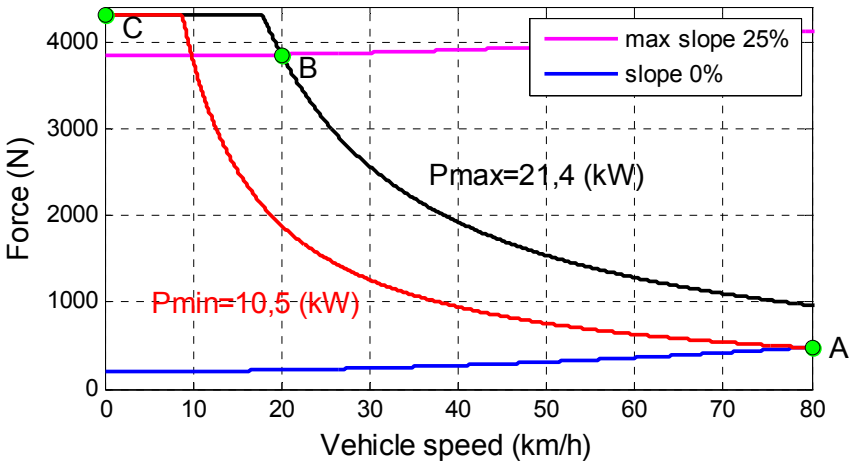

Figure 60: Vehicle traction force and resistance force for slopes of 0% and 25%

In Figure 60 the resistance force curves for a slope 0 and 25% are shown. Specification 1a (max speed at horizontal drive) identifies point A on the graph, that is characterized by a power of 10,5 kW, so it is possible to draw the constant power curve (in red colour). This operative point is fundamental to sizing the Primary Converter,

because the Fuel Cell System has to feed the Electric Drive without using the Rechargeable Energy Storage System.
Specification 2a (max speed at max slope) identifies point B, characterizing the max traction power for the propulsion system (about 21,4 kW).
Finally, specification 2b (start-up acceleration) defines point C and so the maximum traction force. So the Electric Drive can be completely defined considering operative points B and C.
The Rechargeable Energy Storage System has been sized considering the power surplus with respect to the one generated by the Fuel Cell System in order to respect specification 2b.
The amount of H_2 storage is determined considering specification 1c (vehicle range). The main results of the system sizing are listed in Table 9.

Table 9: Preliminary sizing of the considered vehicle

Vehicle mass (kg) *empty* *full loaded*	 1095 1535
Electric motor power (kW)	22
FCS power (kW)	13
Energy stored (kWh)	4,8
Reservoir size (kg H_2)	1,5

Some simulations of the vehicle were carried out in order to evaluate its performance. In particular the NEDC cycle, artificially limited to a max speed of 80 km/h, has been considered, and its reference speed profile is shown in Figure 61.

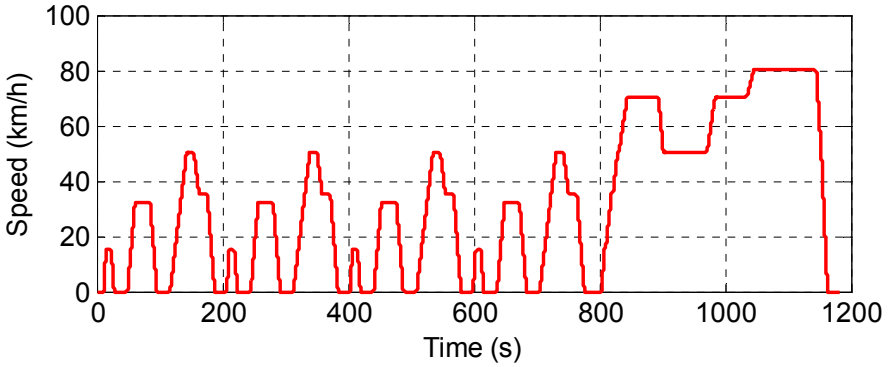

Figure 61: Vehicle speed for the NEDC cycle

Figure 62 (a) shows the simulated main drive train power fluxes (for the meaning of the quantities, see Figure 54), when the vehicle is performing the NEDC cycle. The RESS, FCS and ED power profiles are related by the balance equation, from where it is possible to infer that the hybridisation leads to Fuel Cell system downsizing: indeed its size depends on the mean power and not the peaks: so the presence of the RESS reduces considerably the FC system cost, weight and size. Other details are reported in [33].

The State of Charge (SOC) of the battery is shown in Figure 62 (b), in which is clearly seen that SOC value at the end of the simulation is roughly the same as at the beginning, since the control strategy keeps it in a small range around its reference (0,75 in the simulation).

The Hydrogen fuel rate consumption is shown in Figure 62 (c), computed considering stoichiometric correspondence between stack electrical current and hydrogen consumption.

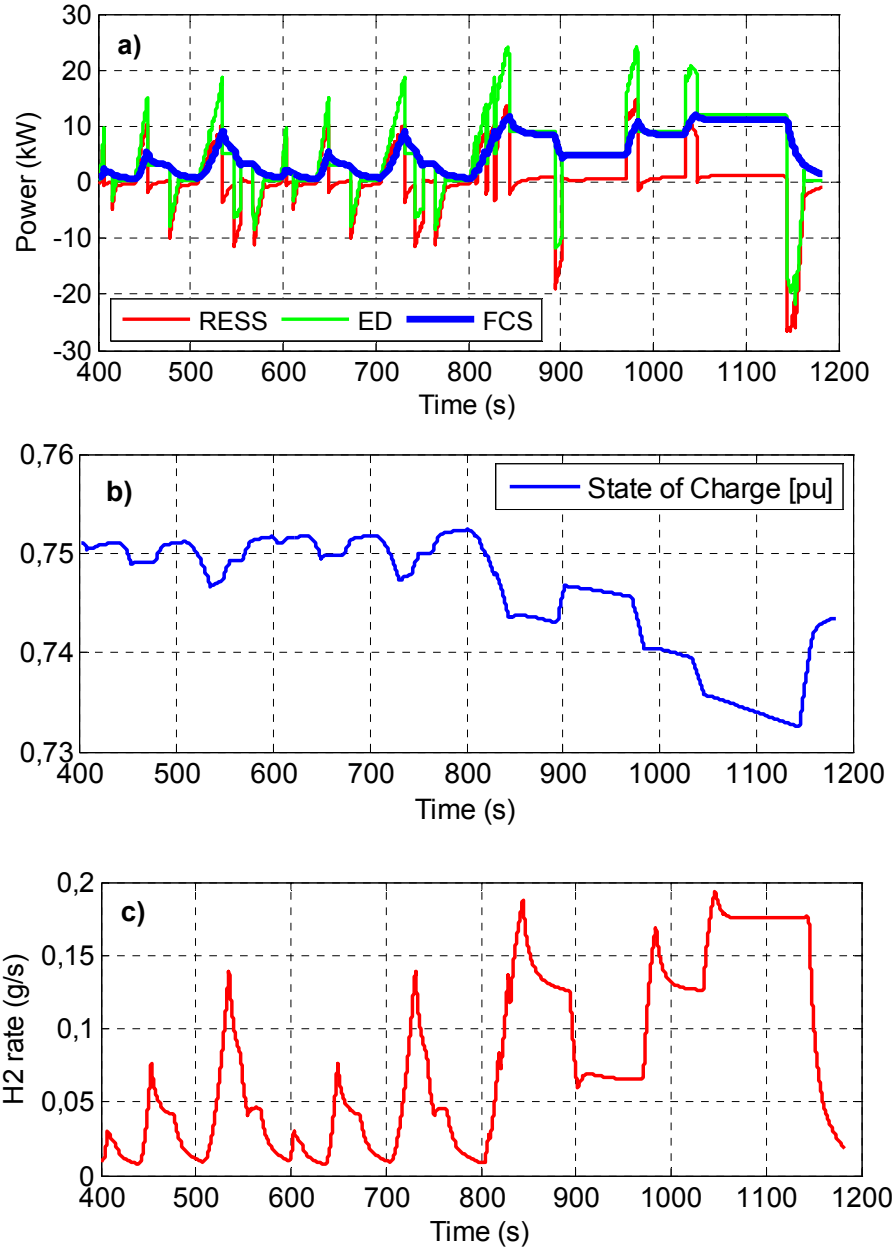

Figure 62: Simulation results of the considered FC based vehicle under the NEDC cycle

The vehicle performances are also summarized in Table 10. The acceleration test reports how much time the vehicle needs to reach the final speed for two operative conditions, empty and full loaded. The H_2 consumption has been calculated for modified NEDC (limited to 80 km/h) and at maximum constant speed.
It is interesting that the slope 25% requirements have involved a drive train power that is able to over-fulfil the acceleration requirement.

Table 10: Main performances of the hybrid vehicle VAN

Vehicle Load	empty	full
Max speed (km/h)	80	
Acceleration test (s)		
0 - 40 km/h	5,5	7
0 - 60 km/h	9,6	12,9
0 – 80 km/h	21	30
H_2 consumption (g/km)		
Modif. NEDC cycle	6	7,3
Constant max speed	7,4	8,8

3.3 Layout

The main requirement of the Project is the realisation of a vehicle flexible and usable as the conventional version. Indeed, in addition to the sizing of the different components, several layout studies have been carried on. Finally, all the components have been disposed without influence passenger and luggage compartments of the standard Piaggio Porter. Furthermore, the weight distribution has been optimised to improve stability of the vehicle. In particular, the FCS is positioned under the driver seat: a co-design activity with the manufacturer has been defined, to dispose all the auxiliaries under the stack module, to have a compact and regular shape for easy installation on existing vehicle frame. The battery pack and electronic converters are disposed on the sides of the vehicle frame. H_2 cylinders are disposed with transversal orientation: they allow to store 1,1 kg of hydrogen at 35 MPa; the initial range specification cannot be fulfilled with this tank, but with the possible future use of 70 MPa (not yet implemented because of limitation of the Italian law) it will be by large overcome. Figure 63 shows the first schematic layout supposed for the vehicle.

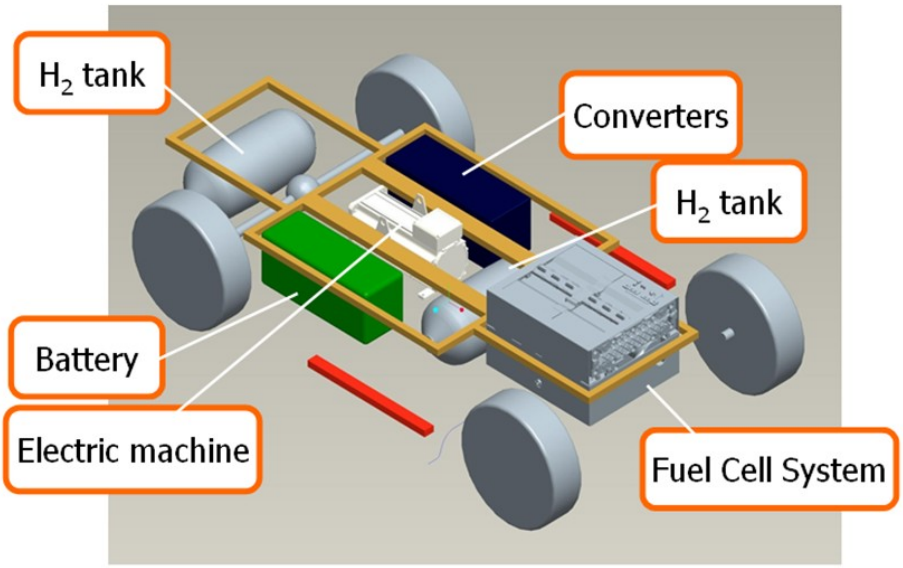

Figure 63: Schematic layout

Since the first schematic proposal, the company that works on the integration on-board[8], has defined the final disposition of all the components, starting from the CAD model of the Piaggio Porter vehicle. To realise the effective placement of the drive train components, the company designed and built the required mechanical supports. Moreover, the same company worked on the entire hydrogen piping, including valves and pressure regulators, that was designed and installed on-board as partially visible in Figure 64 and in Figure 65.

[8] EDI Progetti sas

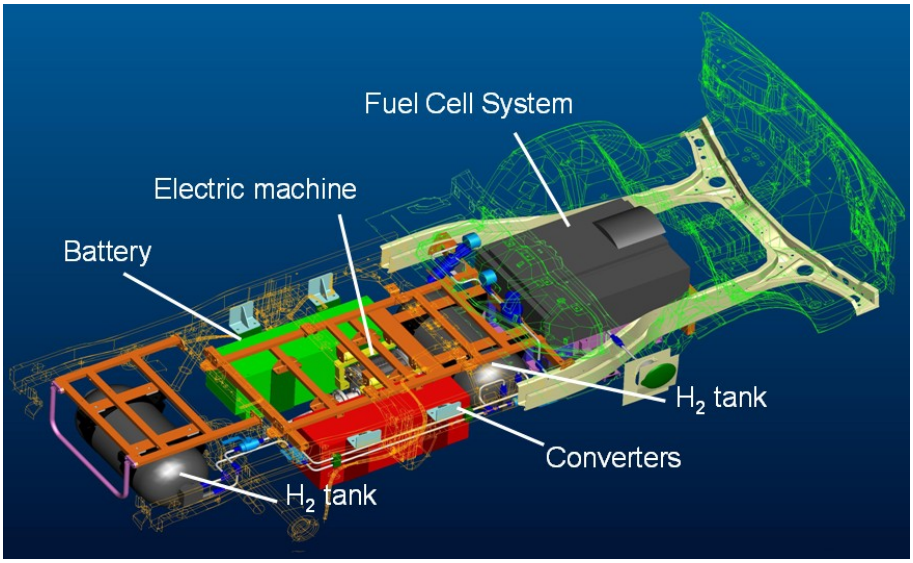

Figure 64: Final layout of the vehicle

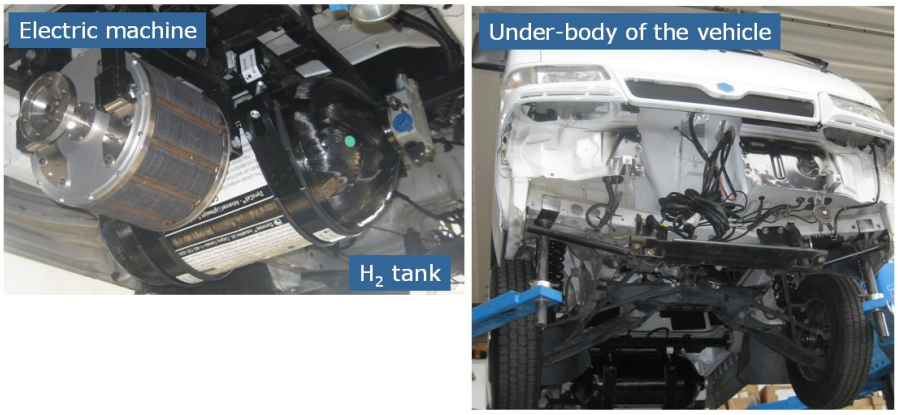

Figure 65: Under-body of the vehicle: in detail one of the two H_2 cylinders, and the electric machine

3.4 Experimental tests

3.4.1 Fuel-Cell System

The Fuel-Cell System, chosen in agreement with the vehicle performance specifications and simulation results, has been designed and realised by the manufacturer company[9]. It is well known for its realisation of Proton Exchange Membrane fuel cells, in which MEGA technology is used [45]. It allows to wrap into the same assembly the membrane/electrode and its gasket, for easy test and reparation procedures, both with reduction in cost. The general characteristics of the FCS installed on-board Piaggio Porter are directly reported in Table 11 and in Figure 66. The indicated nominal power does not include the electricity supply of the auxiliary devices. The reported mass includes stack and auxiliaries (blower, water pump, radiator).

Table 11. Fuel Cell System

Nominal power (kW)	13,2
Number of cells	144
Nominal voltage (V)	83,1
Nominal current (A)	159,6
Cell area (cm²)	210
Mass (kg)	60

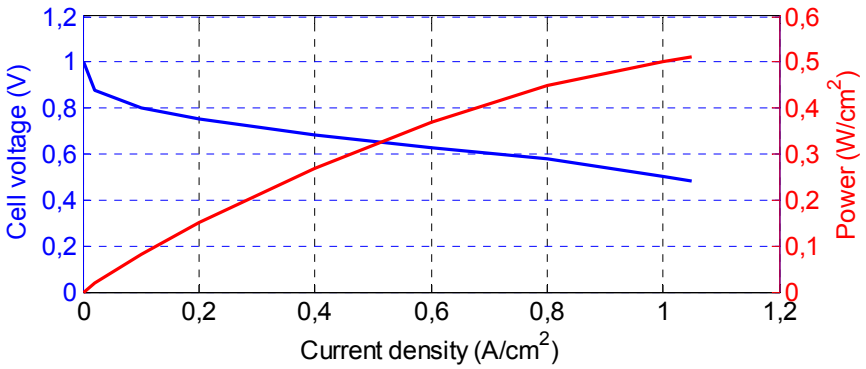

Figure 66: Characteristic curve V-I and Power curve of the FCS by manufacturer

[9] Morphic Exergy srl

Initially, tests on the FCS were related to verify the real performance of the system, trough the application of constant resistance loads. The Fuel Cell System under test is clearly shown in Figure 67. The FCS can be monitored by PC, connected with a CAN-USB interface, through a software realised by the manufacturer.

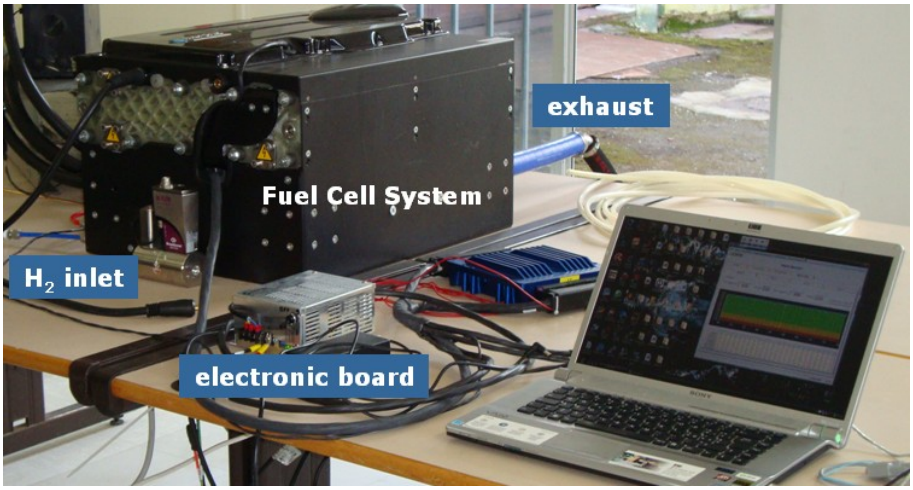

Figure 67: Fuel-Cell System under test

The voltage vs current corresponding to the different steps are shown in Figure 68. It must be said that at high powers, the correct balance of cell membrane humidification, and the air flow managed by the blower, might become critical aspects for the correct behaviour of the stack. For these reasons, a reduced number of cells may experience significant voltage drops, that can cause shut-down of the overall system. Because of this, the FCS under test cannot surpass 10,5 kW of power, respect to the 13,2 kW expected.

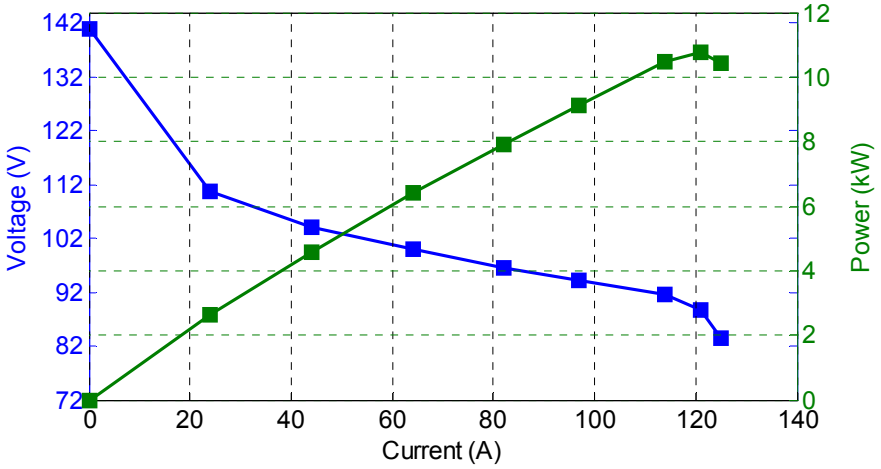

Figure 68: Characteristic curve V-I and Power curve obtained during tests

The second part of the activity was related to the FCS efficiency measure. A digital mass flow meter[10] was installed before the hydrogen inlet, to measure the effective mass flow required by the stack: the current output of the instrument was acquired by a multifunction acquisition board[11].

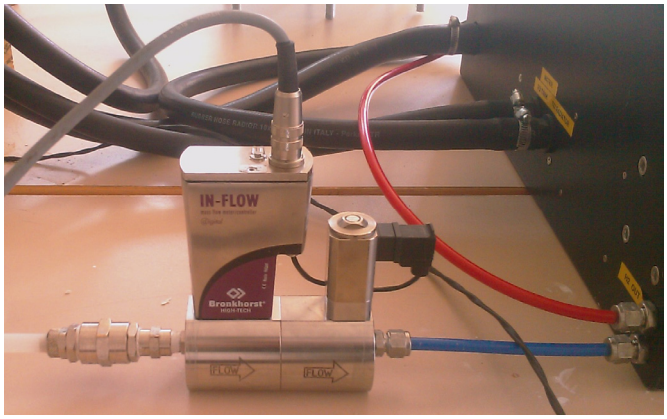

Figure 69: Mass flow meter installed before hydrogen inlet

[10] Bronkhorst High-Tech F-202AI-AGD-55-V-MFC
[11] National Instrument

The measured hydrogen flow for different load power values, obtained through constant resistance loads, is reported in Figure 70. Being the FCS considered of "dead-end" type, part of the fuel (the *Purge component* in figure) is normally employed for purge operation, respect to the one (the *Load component* in figure), that constantly feeds the cells.

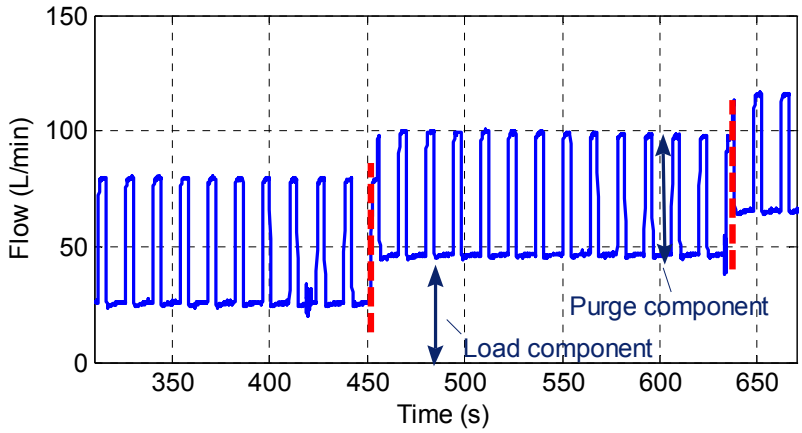

Figure 70: Example of hydrogen flow measured during tests

Efficiency was calculated referring to the following expression, that compares, for each value of load, the net electric energy E_{el} generated during the interval (t_1-t_2) by the FCS, respect to the energy E_{th} obtained through an equivalent hydrogen combustion process:

$$\eta = \frac{E_{el}}{E_{th}} = \frac{\int_{t_1}^{t_2} P_{net}\,dt}{\Delta H \int_{t_1}^{t_2} q\,dt} \qquad \text{(Eq. 45)}$$

where P_{net} is the electric net power obtained from FCS, (thus power adsorbed from auxiliaries, water pump, blower, electronic boards, is already subtracted from the gross stack output power), ΔH is the hydrogen Lower Heating Value (119,93 MJ/kg), q is the hydrogen mass flow measured during test.
The results are presented in Table 12 in presence or in lack of purge

operations, that influence significantly the final values of the efficiency calculated.
Since purging cause hydrogen (and efficiency) loss the purge operation considered in the numbers reported in the rightmost column of Table 12 are minimal; by contrast, the purges shown in Figure 70, because those measures were taken before purging optimisation.

Table 12: FCS Efficiency

FCS net power (W)	**η without purge**	**η with purge**
2105	0,46	0,42
3962	0,48	0,44
5443	0,47	0,44
5598	0,46	0,43
6790	0,46	0,43

3.4.2 Rechargeable Energy Storage System

The typology of the RESS chosen was defined through experimental tests, in which performance of high power lithium batteries and super-capacitors were evaluated. As mentioned in chapter 2, energy storage systems for hybrid vehicles are required to deliver or absorb electric power in short intervals of time, typically a few seconds or tens of seconds; therefore they need to have different characteristics from batteries for pure-electric vehicles, that are discharged in tens of minutes or hours.
Furthermore, to make a fair comparison of different storage systems for hybrid vehicles, they must be subjected to the same stress; in particular, their specific power must be assessed using the same discharge duration. Experimental results show that SCs can sustain high specific powers (up to, say, 5 kW/kg) only for very short times, in the order one second. For discharge durations in the order of tens of seconds, required for vehicle propulsion, high power lithium batteries and SCs can be both considered as competitive solutions [46]. Whenever the considered vehicle stress implies discharge in the order of one minute (like drive in slope condition, in which both FC System and RESS deliver a constant power), SCs alone cannot compete because of their low specific energy. These results can be easily

analysed in Ragone plots, already mentioned in Figure 43 (chapter 2), in which specific energy value vs specific power, for different discharge times, are reported for each device considered.
In conclusion, a battery pack composed by power oriented lithium cells[12] [31] was chosen, resulting in a total stored energy of 4,8 kWh. General characteristics of the battery pack chosen are summarized in Table 13.

Table 13: lithium battery

Number of cells	42
Nominal voltage (V)	155,4
Nominal capacity (Ah)	31,0
Energy stored (kWh)	4,8
Mass (kg)	43,4

Experimental tests on the RESS were initially related to the characterisation of lithium high-power cell, in terms of efficiency evaluation. Several tests were carried out, reproducing charge-discharge cycles shown in Figure 71. These tests are able to identify general characteristics of storage devices examined, both with the possibility to evaluate the SOC level.

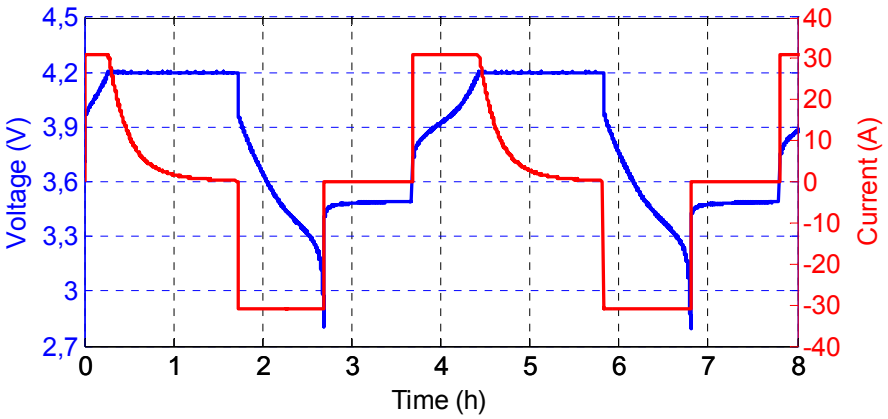

Figure 71: Voltage and current during charge-discharge cycles

The coulombic efficiency was computed using the following expression, where Q_c and Q_e are the absorbed and extracted charge,

[12] KOKAM SLPB-78216216H

respectively.

$$\eta_Q = \frac{Q_e}{Q_c} = \frac{\int i_d(t)dt}{\int i_c(t)dt} \qquad \text{(Eq. 46)}$$

Analysis of the experimental results has shown the coulombic efficiency of the considered cell to be as high as 0,99. Moreover, the battery state-of-charge (SOC) knowledge is also very important, to evaluate the management strategy of the vehicle. The technique already used in chapter 2 and described in [34] was used. From where it is possible to evaluate the SOC of the battery, obtaining the extracted charge Q_e starting from a known state, and numerically integrating the current exiting from the positive pin of the battery. An effective way to perform the error compensation caused by the integration of the current, can be the use of a correlation SOC and Open Circuit Voltage (OCV). The correlation OCV-SOC obtained for high power cell (31 Ah) is showed in Figure 72.

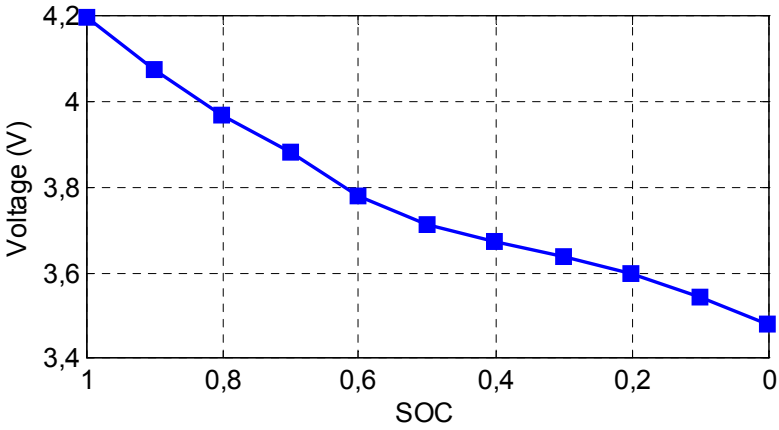

Figure 72: OCV-SOC correlation

Therefore in actual vehicle operation the battery SOC can be continuously evaluated based on numerical integration of the battery current, then corrected at any time the vehicle rests. Other experimental tests were conducted on the complete battery pack, to verify performance and characteristics declared in Table 13.

3.4.3 Electric drive

The Electric Drive was designed through a co-design activity with the manufacturer company[13]. The Electric Drive is composed by two DC/DC converters, the inverter, the electric machine and the DSP control unit. From analysis of performance and layout the sizing of the overall components have been defined. All the components are of air cooling type. The general architecture of the ED is reported in Figure 73.

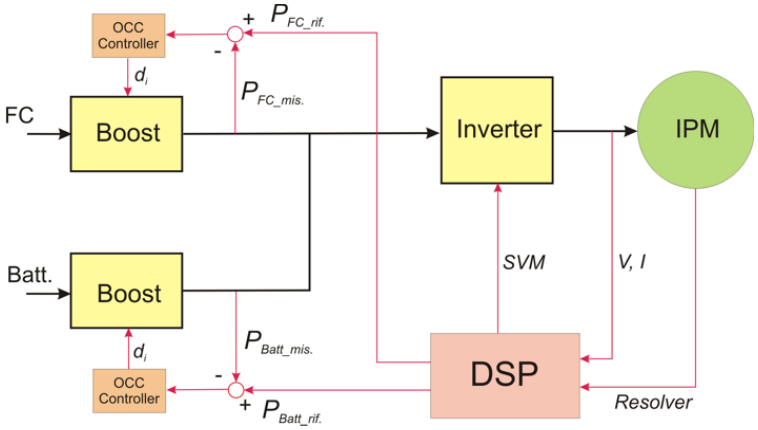

Figure 73: architecture of the Electric Drive

Both FCS and RESS are connected to the DC bus through a step-up DC/DC converter (boost). This solution allows to operate with a higher voltage (400 V), to reduce currents and losses for the inverter and the electric machine. The DC/DC converter employed for the FCS is of unidirectional type, while the DC/DC converter used for the RESS allows to implement the regenerative braking. About the inverter, the DSP unit implements a control technique based on Space Vector Modulation (SVM) strategy, also described in [47]. The average efficiency for each converter was about 98%. The total weight, included case, was about 15 kg.

The electric motor employed is of the Internal Permanent Magnet Brushless type. It allows a wide operating speed range and high torque

[13] EES Company

density. General specification obtained from simulation results are reported in Table 14.

Table 14: Electric Machine specification

Bus Voltage (V)	400
Nominal Torque (Nm)	200
Max Torque (Nm)	350
Nominal speed (rpm)	900
Max speed (rpm)	4500
Nominal power (kW)	20
Max power (kW)	40

Several transient FEM simulations have been performed, to define its thermal and mechanical characteristic [48]. The average value of efficiency, also visible in Figure 74, was about 95%. The motor mass was about 60 kg.

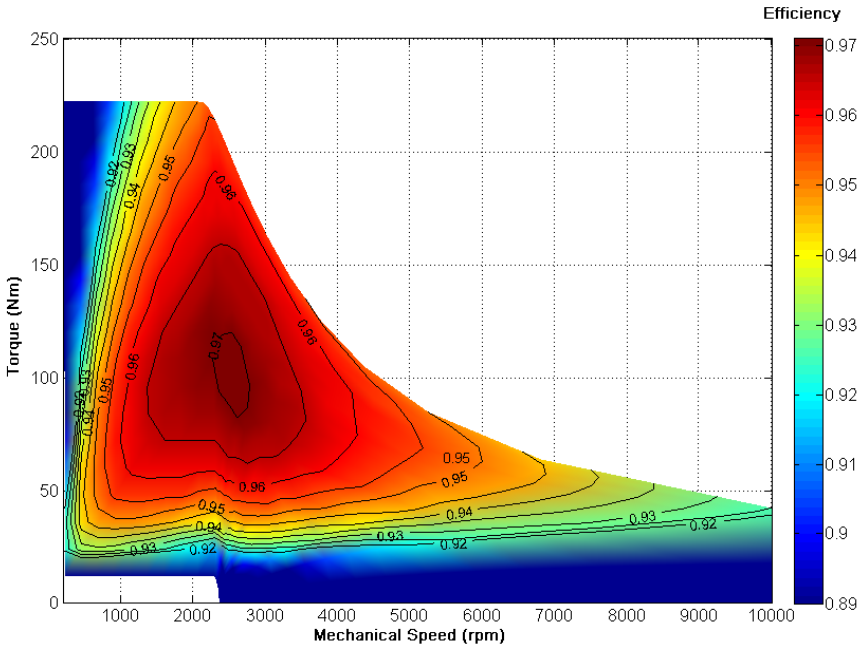

Figure 74: Efficiency map of the electric motor

3.5 Cost Analysis

Although the vehicle could be considered at prototype level, an industrial cost analysis for all the components of the power-train has been carried out, with reference to the current year and production of about 10 vehicles, and to the year 2020 and production of about 1000 vehicles. The results of the analysis were reported in Table 15, that shows that, as far as the purchase cost is concerned, the FC vehicle should be, by year 2020, much nearer than today to a real purchase cost competitiveness.

Table 15: Cost analysis

Component	Year 2010 10 vehicles (k€)	Year 2020 1000 vehicles (k€)
Fuel cell system	65	5,2
RESS	6	2
Electric drive	13	7,7
H_2 tank	20	10
Total	104	24,9

3.6 Electric version

After sizing the FC-based hybrid vehicle, it can be interesting to make a comparison with an equivalent electric version, to evaluate different characteristics of the two propulsion systems in terms of mass, volume, efficiency. The model can be realised staring from the same Electric Drive (ED), fed not by FCS and RESS, but only by the RESS. Also in this case, all subsystems were modelled weighting the accuracy and complexity for the purpose considered. In particular, since the fastest transients useful to globally size the drive train have constant times of the order of 100 ms, much faster phenomena, such as valve switching inside electronic converters, were considered to be algebraic. The main subsystems are:

- Rechargeable Energy Storage System (RESS): the RESS was modelled with a lithium battery, whit the same equivalent electrical circuit used for the FC-based vehicle.
- Auxiliary electrical load (AUX) that could be lights, air conditioner etc;

- Electric Drive (ED), consisting of an electric motor and a power controller. The converter was considered as having an algebraic behaviour, while the electric machine was considered as generating an electromagnetic torque being an algebraic function of voltage and frequency at its terminals.
- The vehicle, which also contained subsystems for mechanical transmission and vehicle dynamics. The final drive consisted of a fixed gear ratio driven by the traction motor. Mechanical equation already showed describing the vehicle longitudinal behaviour was used.

As for the FC-based version, a *forward approach* for this model was used:

- A driving duty cycle (called mission profile) fed to the driver block.
- The driver block converted the reference speed into commands for the ED.

Naturally, the energy management strategies presented before cannot be used, because all the power needed for the traction and auxiliaries is taken directly from the RESS.

The propulsion system sizing was defined in accordance with the following boundary conditions, the same also considered for the FC-based vehicle, summarised below:

1. horizontal drive:
   a) max speed: 80 km/h
   b) acceleration 0-80 km/h: within 60 s
   c) max speed range: 150 km

2. slope 25%:
   a) max speed: 20 km/h
   b) start-up acceleration: 0,3 m/s²

Characteristics traction curves similar to these obtained for the FC-based version can be obtained, with similar values of the power needed at horizontal drive and with 25% gradient.

Conditions 2a) and 2b) identified the max tractive power and the max (starting) tractive effort for the propulsion system: therefore they completely defined the characteristics for the ED.

The RESS was sized considering only the condition 1c) and input voltage admitted by the ED. Current limits, because of the large capacitance of the energy-oriented cells used, are always observed. General characteristics of the battery pack chosen are summarized in Table 16.

Table 16: EV Li-ion battery

Number of cells	100
Nominal voltage (V)	370
Nominal capacity (Ah)	70,0
Energy stored (kWh)	25,9
Mass (kg)	204,0
Volume (L)	94,0

It can be very interesting to make a comparison in terms of masses and volumes between FC-based and electric version, summarised in Table 17 Table 18. How can be noticed, the electric version presents a very short increment of mass, about 60 kg, and good reduction in volume, about 70 L.

Table 17: Volumes in comparison

	FC-HEV	**EV**
Fuel Cell System Volume (L)	85,0	-
Hydrogen tank Volume (L)	64,0	-
RESS Volume (L)	16,7	94,0
Total Volume (L)	**165,7**	**94,0**

Table 18: Masses in comparison

	FC-HEV	**EV**
Frame mass (kg)	750	750
Electric Drive mass (kg)	122	122
Fuel Cell System mass (kg)	60	-
Hydrogen tank mass (kg)	48	-
RESS mass (kg)	43	204
Load (kg)	550	550
Total mass (kg)	**1573**	**1626**

Finally the simulation results, all related to the fully loaded vehicle, are reported in the next table: the EV configuration is able to perform 16 km instead of 2 km during the drive in slope condition, because of

the bigger value of the RESS energy stored. Furthermore, during short acceleration tests (0-40 km/h), the EV configuration is not limited by the maximum discharge current limits, because of the bigger nominal capacitance of the RESS installed on-board, but only by the maximum power managed by the inverter. During long acceleration tests (0-80 km/h), the reduction in terms of mass makes faster the hybrid FC-based vehicle.

Table 19: General performance

	FC-HEV	**EV**
Max speed (km/h)	80	80
Range (km)	151	151
Fuel consumption (g/km) constant speed 80 km/h	8,7	-
Fuel consumption (g/km) NEDC cycle	7,3	-
Range, slope 25% (km)	2,4	16,0
Acceleration 0-40 km/h (s)	8,0	7,7
Acceleration 0-60 km/h (s)	13,7	13,7
Acceleration 0-80 km/h (s)	30,6	31,3

4. Design of electric and hybrid buses

With growing concern for environmental problems amongst governments and international policy formulation agencies, more stringent standards for fuel consumption and emissions have been developed. Electric vehicles (*EVs*) appear to be the best way out as they imply zero *in situ* emissions. However, factors such as high initial cost, short driving range, and long charging time are major limitations. Hybrid vehicles were developed to overcome the limitations of the conventional ICE-based vehicles and electric vehicles. This chapter presents the some issues related to development of a complete line of series-hybrid and electric versions of existing city buses for the Italian bus manufacturer Breda Menarini Bus (BMB) [49], involved in the Project Industria 2015, through the object-oriented modelling.

4.1 Propulsion system design

4.1.1 General architecture

As for the Fuel-Cell based Piaggio Porter, the series hybrid propulsion architecture, commonly chosen for hybridising buses, was adopted and shown in Figure 75, with the arrows along the power fluxes showing the actual directions when the numerical values are positive.

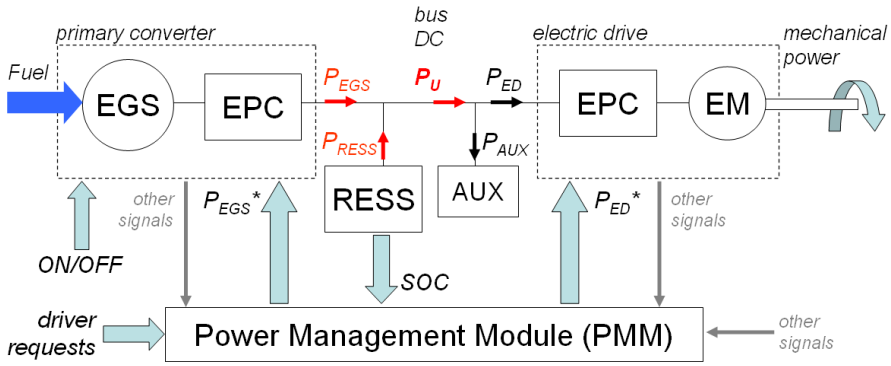

Figure 75: Principle scheme of a series-hybrid vehicle drive train

How reported in figure, the ICE is coupled to an electrical generator (EGS). The presence of a storage system (RESS) provides the vehicle flexibility in sharing the power required for propulsion. This management is carried out by the on-board Power Management Module (PMM), which continuously monitors the load requirement and decides how to share the power amongst the two sources according to predefined goals (typical goal is vehicle efficiency maximization).

4.1.2 Modelling activity

The series-hybrid buses models were defined through the object-oriented modelling: this is a relatively new modelling methodology based on object orientation and equations, characterised by:

- No need to define inputs and outputs at the model building stage.
- Ability of handling of large, complex multi-engineering models.
- Faster modelling by graphical model composition.

Therefore, modelling techniques needing manual conversion of equations to a block diagram, already reported by the authors in [50] and based on Matlab Simulink® package [51], also described in chapter 3, can be substituted by the usage of object-oriented modelling. The models were made using two commercial software packages, LMS Imagine.Lab AMESim® [52] and 3DS Dymola® [53]. AMESim stands for Advanced Modelling Environment for performing SIMulations of engineering systems: it allows object-oriented modelling, but basically requires the user to use closed built-in library models and proprietary methods for introducing new components. Dymola stands for Dynamic Modelling Laboratory: it allows model description by Modelica® modelling language, which allows users to create their own models and model libraries, or modify the ready made model libraries to better match their simulation needs.

All subsystems were modelled weighting the accuracy and complexity for the purpose considered. In particular, since the fastest transients useful to globally size the hybrid drive train have constant times of the order of 100 ms, much faster phenomena, such as combustion dynamics or valve switching inside electronic converters, were considered to be algebraic. Figure 76 depicts the simulation scheme in Dymola. The main subsystems were:

- Primary Converter, the main source for the vehicle energy propulsion, composed by the internal combustion engine coupled to the electricity generation system (EGS), that generates electricity available for propulsion. The model for the ICE used the BSFC maps. The model can emulate the engine torque and fuel flow, dependent on throttle position and engine speed. It contains inertia load and a start-up logic, useful when ON/OFF strategy need to be considered. The model for electric generator uses an asynchronous induction machine with integrated inverter and field oriented control, including voltage and current limitation as well as flux weakening.

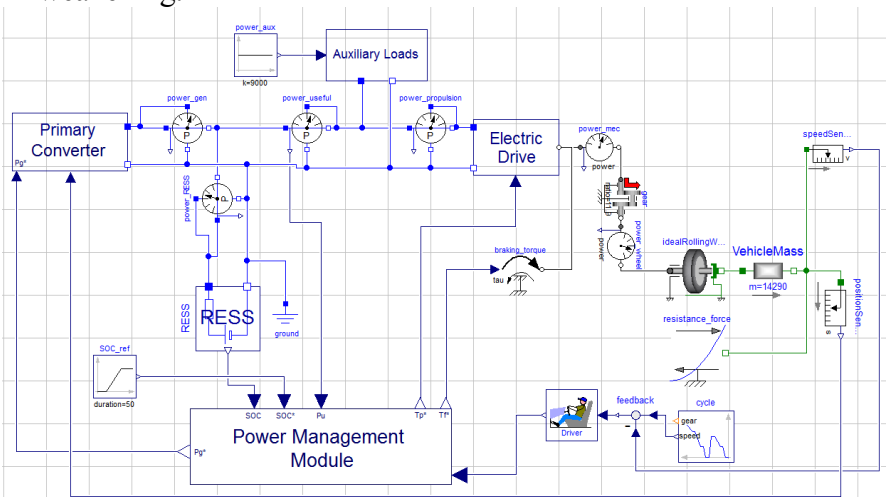

Figure 76: Series-Hybrid bus model in Dymola

- Rechargeable energy storage system (RESS) that could be composed of devices such as electrochemical batteries, supercapacitors, fly-wheels etc. The RESS was modelled with a lithium ion battery, considering its good performance in terms of power density and energy density.
- Auxiliary electrical load (AUX) that could be lights, the control system, the air-conditioner etc;
- Electric Drive (ED), to provide power and torque to the wheels and also to produce regenerative power, consisting of an electric motor and a power controller. The drive is constituted by an inverter-fed

induction machine controlled by a field oriented technique, similar to the one used for the electric generator.

- The vehicle, which also contained sub-systems for mechanical transmission and vehicle dynamics. The final drive consisted of a fixed gear ratio driven by the traction motor. Mechanical equations describing the vehicle longitudinal behaviour was used.
- The Power Management Module (PMM) is the most critical element in the model. It has the fundamental role to interpret driver's commands and determine, according to all the available information, the optimal way to share the power requested by auxiliaries and propulsion between the two energy sources of the vehicle.

Each sub-model was carefully constructed to be able to accurately emulate experimental results (for example, the model for the electric motor/generator needed parameters in a file defining the lost power vs the torque and the rotary velocity). The model of the battery needed data files listing the internal resistance vs. the depth of discharge. Similarly, the complete BSFC maps were fed to the ICE sub-model, and the model can determine the most efficient operating line, for the each level of power demanded. Efforts were made to model realistic sub-systems, building in parameters for efficiencies. The authors employed the *forward approach* for this model, which was:

- a driving duty cycle (called *mission profile* in the program) fed to the driver block.
- the driver block converted the reference speed into commands for the PMM.
- the PMM determined the most optimal strategy based on the instantaneous power demand levels, and feedback from key parameters of the EGS, RESS and ED. PMM outputs are reference signals for the Electric Drive and Primary Converter.

4.1.3 Energy management strategy

The energy management strategies already presented in chapter 3 can be used also for the primary sizing of the series-hybrid buses. Being the same architecture, the sum of energies of the two power sources is usually depicted as a DC bus. Power needed for the traction and auxiliaries is taken from this DC bus.

The fundamental role of the PMM is naturally to interpret driver's commands, and accordingly determine which part of the requested *useful* power would be delivered by the EGS and which by the RESS. In other words, to determine how to decompose the quantity $P_U(t)$, formed by $P_{ED}(t)$ and $P_{AUX}(t)$, into $P_{EGS}(t)$ and $P_{RESS}(t)$:

$$P_U(t) = P_{ED}(t) + P_{AUX}(t) = P_{EGS}(t) + P_{RESS}(t) \quad \text{(Eq. 47)}$$

This degree of freedom could be used to:

- Define the optimal SOC range in which the RESS has to be operated, to have maximum efficiency during small charge-discharge cycles.
- Define the optimal point of work in terms of power and rotary velocity, corresponding to the minimum fuel consumption.

On the other hand, experimental results also presented in [43] and in chapter 3 show that efficiency profile is quite flat for lithium ion battery. Indeed, the general optimisation problem becomes a sub-optimisation problem for the only primary converter.

The last relationship is also guaranteed by the physics of drive train. The possible control strategy used, the same already presented for the FC hybrid vehicle and reported in chapter 3, could be:

- $P_{ED}(t)$ is determined to answer the driver's commands as closely as possible. It could be considered a direct consequence of trip characteristics, vehicle mass and power losses in the ED.
- $P_{AUX}(t)$ is determined by the evaluation of auxiliary loads.
- $P_{EGS}(t)$ is determined by PMM according to some optimization rule (that will be discussed later).
- $P_{RESS}(t)$ is automatically determined by difference.

The user load P_U draws the main focus in this control strategy, while the power generation from fuel; P_{EGS}; is given a supporting role. The *useful* power that goes into the load $P_U(t)$ could be imagined to be constituted by an average value and a ripple. Equation is thus modified as follows:

$$P_U(t) = P_{Ua}(t) + r(t) \quad \text{(Eq. 48)}$$

It is possible to control the system such that the quantity $r(t)$ is delivered by P_{RESS} (t), and does not form part of the primary converter:

$$P_{RESS}(t) = P_{RESSa}(t) + r(t), \therefore P_{EGS}(t) = P_{Ua}(t) - P_{RESSa}(t) \qquad \text{(Eq. 49)}$$

Hence, the EGS delivers only average powers: it works at fixed or slowly variable points. The RESS manages the ripple component $r(t)$ of the needed useful power (shallow charging-discharging micro-cycles), with the addition of the average power $P_{RESSa}(t)$, to maintain the SOC balanced during normal driving condition, or when extended charge or discharge phases are required (ICE ON-OFF strategy).
Also this strategy presented above requires the consideration (even approximate) of the future system load, i.e. the future behaviour of the power demand $P_U(t)$, which is a function of the driver's request for torque and the vehicle duty cycle. The approximate level of power needed by the vehicle in future could be obtained by multiplying the past history of $P_U(t)$ with a simple filter:

- $P_{Ua}(t)$ is the output of a filter having as input $P_U(t)$ and as a transfer function $1/(1+s\tau)$.
- $P_{Ua}(t) = \frac{1}{T}\int_{t-T}^{t} P_U(\tau)d\tau$

In both cases a suitable value for τ needs to be chosen. In Figure 77, the general scheme of the logic implemented into the PMM.

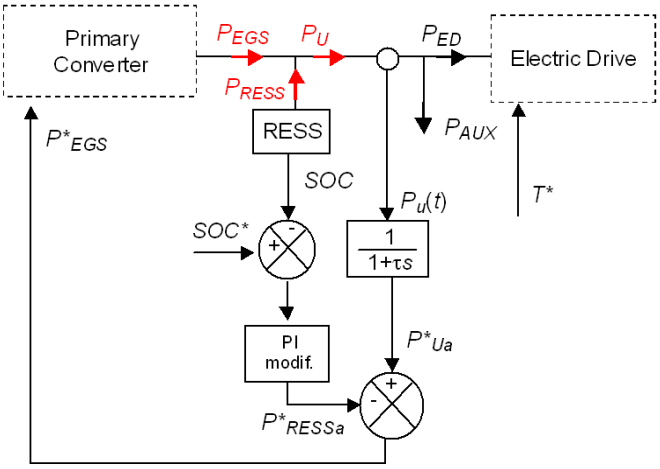

Figure 77: Energy management strategy implemented in the PMM

How reported in the previous section, the start-up logic has been introduced for the primary converter, to simulate the ON-OFF strategy. This strategy can be used when the average power P_{Ua} is lower than power generated by the primary converter P_{EGS}: during OFF states the battery is discharged ($P_{RESSa}< 0$), and re-charged by EGS during ON states ($P_{RESSa}>0$). ON-OFF strategy can be applied in two different ways:

- Programmed mode: at bus stops, or in ZEV mode, to avoid noise pollution and pollutant emissions.
- Non programmed mode: during traffic congestions, to avoid poor efficiency zones for the primary converter.

The power delivered from the EGS corrected by the presence of the ON-OFF strategy can be preliminary evaluated through the following energy balance equation.

$$P_{EGS}(t) = \frac{P_{Ua}(t_2 - t_0)}{(t_1 - t_0)} \qquad \text{(Eq. 50)}$$

where P_{EGS} is the power generated by the primary converter during ON-states, P_{Ua} is the average power requested from propulsion, $(t_1\text{-}t_0)$ the length of the ON-state, $(t_2\text{-}t_0)$ the overall length of the interval considered (also indicated in Figure 78).

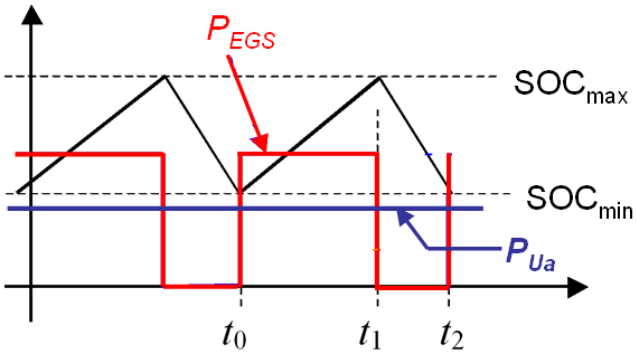

Figure 78: Meaning of the quantities used for describing ICE ON-OFF strategy correction

After determining $P_{EGS}(t)$, an internal algorithm was used to choose the optimal values of the ICE rotary velocity (indicated in Figure 79),

corresponding to the minimum fuel consumption. More details on possible hybrid vehicle energy management strategies can be found in [32], [44], [54]-[56].

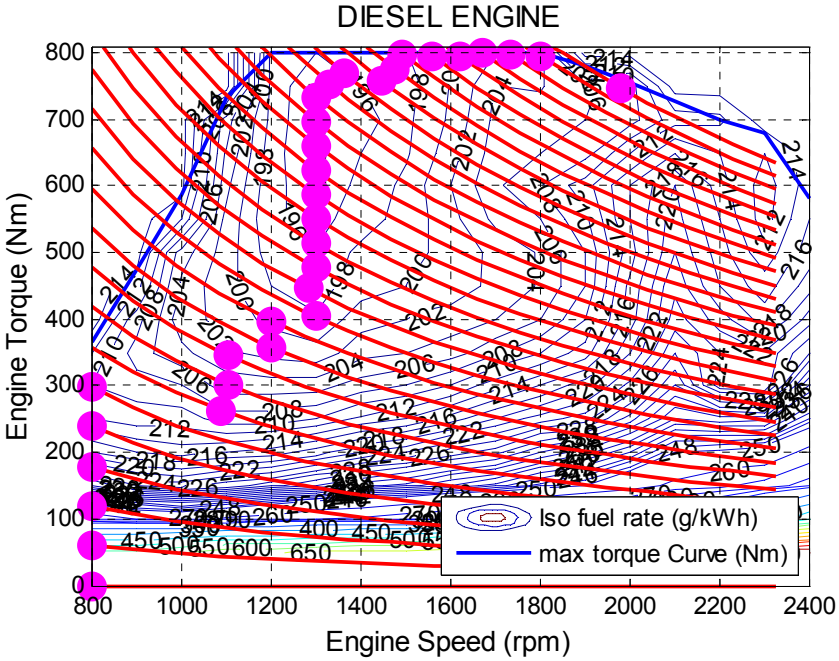

Figure 79: Output of the internal optimisation algorithm: the optimal values of the ICE angular velocity are reported directly on the engine map

4.2 Simulation results

The propulsion system sizing was sized in accordance with the following boundary conditions.

1. Level road

a) max speed: 80 km/h

b) max speed without discharge the RESS: 50 km/h

c) programmed ON/OFF

- vehicle running SORT1 cycle, ICE OFF at bus stops considering stops duration of 20 s every 300 m.
- vehicle running SORT1 cycle, considering drive as zero emission vehicle (ZEV) for 22% of the total time: it means, considering a bus terminals distance of about 8 km, 1,6 km in ZEV mode.

2. Road with 16% gradient

a) max speed: 10 km/h (range 0,5 km)

b) start-up acceleration: 0,3 m/s²

In Figure 80 the resistance force curves at level gradient or 16% slope are shown. The specification 1a and 1b (max speed at level road) identify points A and B on the graph, characterised by a requested power, respectively, of 68,5 kW and 32,2 kW. Specification 2a and 2b identify, respectively, points D and F.

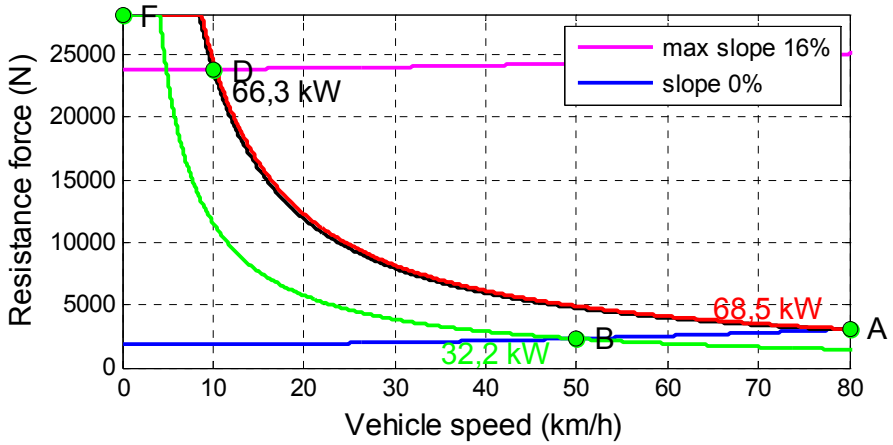

Figure 80: Traction characteristic of the vehicle

Conditions 2a) and 2b) identified the max tractive power and the max (starting) tractive effort for the propulsion system: therefore they completely defined characteristics for the ED.

The RESS was sized considering condition 1c) (pure electric mode on level gradient), according to the specified range and maximum current limits for the Li-ion battery, evaluated in the real urban cycle and in the SORT1 cycle.

The sizing of the ICE could be evaluated with reference to the *maximum power*, i.e., the max power needed by the ICE, or the *efficient power*, i.e., the power at which the engine efficiency is highest.

Due to the power management algorithms selected, the *efficient power* would also be the average useful power evaluated by considering the ON/OFF strategy for the primary converter. In fact, the two different sizing criteria could be summarised as:

- constant speed drive at 50 km/h, ICE ON, bus fully loaded: the constant ICE power obtained is the *maximum power* required;
- Vehicle running SORT1 cycle on level gradient, with programmed ON/OFF strategy, bus partially loaded: when the vehicle is stationary at bus stops or in ZEV mode, ICE is switched OFF. The ICE power obtained during the ON states is the *efficient power* required.

The main characteristics of the sizing are listed in Table 20.

Table 20: Sizing of the considered hybrid buses

	Bus Models		
	Vivacity M	***Avancity L***	***Avancity S***
Length (m)	9	12	18
Weight (full load) (t)	13,95	17,96	26,67
Weight (partial load) (t)	11,3	14,3	21,1
Auxiliaries (kW)	6	9	12
ICE max power (kW)	48	61	84
ICE efficient power (kW)	36	48	69
RESS Energy (kWh)	31,1	38,9	51,8
ED power (kW)	2 x 60	2 x 90	4 x 60

Figure 81 shows the results of the simulation for the power fluxes (definitions of quantities in Figure 75) in the model for the *Avancity L* bus on the SORT1 cycle. It clearly shows the distribution of the power from the two sources.

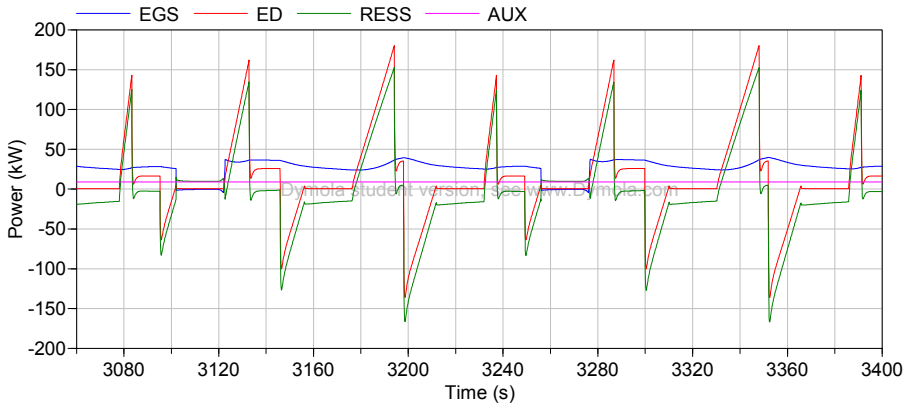

Figure 81: Simulation of the Series-Hybrid Avancity L bus model on SORT1 cycle: power fluxes of the drive train

Similar such simulations were carried out for all the different bus models and on all the possible city driving cycles where the buses are finally targeted. Figure 82 and Figure 83 are related to the simulation on a real profile of urban cycle, measured by BMB during normal operation of buses in Bologna city.

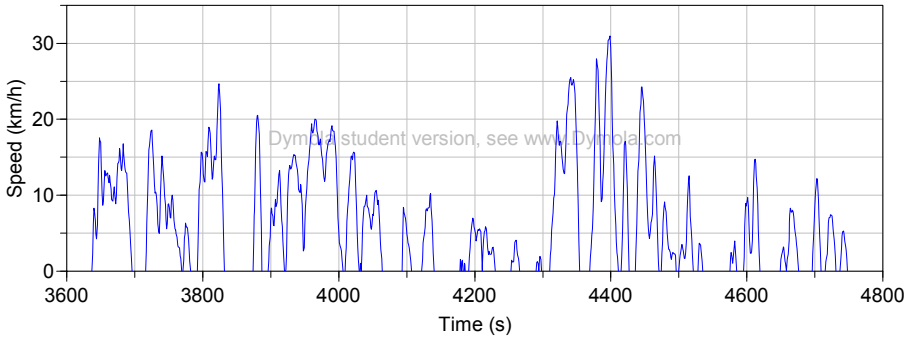

Figure 82: Bologna1 cycle: speed profile

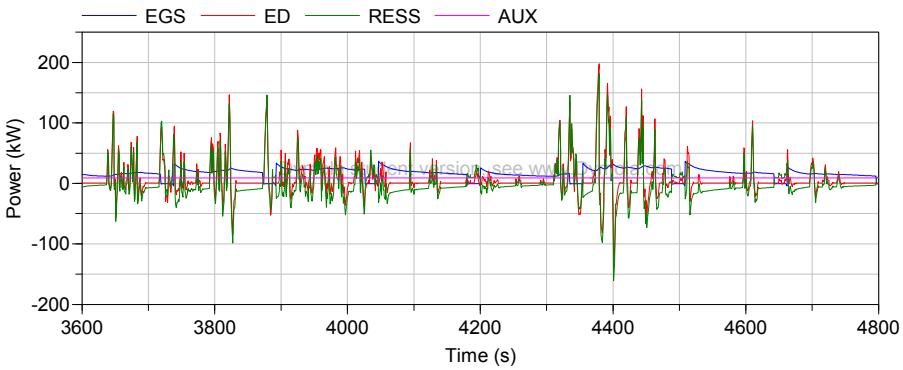

Figure 83: Simulation of the Series-Hybrid Avancity L bus model on Bologna1 cycle: power fluxes of the drive train

From the main results it was interesting to note that the size of the ICE needed reduced significantly from the one in the conventional bus. Because of the impossibility to have access to specific fuel consumption maps for smaller engines, and hence, to evaluate the fuel consumptions, the model was downscaled starting from the existing BSFC maps. The engine was downsized with reference to the torque, keeping the same BSFC values as the bigger engine for the smaller, thus avoiding, the poor efficiency zones of the original engine. This, however, was only an ad-hoc solution, but the results obtained through this approach would also be similar.

Fuel consumptions are summarised in, related to the Avancity L (12 m version), comparing performance of the hybrid bus, to the conventional one. In particular, different working condition have been evaluated for the hybrid bus, reported below:

- ICE always ON.
- Programmed ON-OFF strategy activated during bus stops.
- Programmed ON-OFF strategy activated during bus stops and ZEV mode.

Both the hybrid and the conventional vehicles were evaluated not only during normal driving condition, but considering the addition of a possible traffic congestion, with the vehicle stationary and the only auxiliary devices activated (9 kW for the Avancity L), for a duration of 500 s. For the hybrid version, drive as ZEV mode after the traffic congestion can be neglected, to avoid further long discharge of the battery, also visible in Figure 84.

Table 21: Fuel consumption

	Avancity L		
	ON	***ON-OFF bus stops***	***ON-OFF bus stops ZEV***
HEV (full load) SORT1 cycle (L/km)	0,579	0,567	0,617
HEV (full load) SORT1 cycle traffic congestion (L/km)	0,634	0,624	-
Conv.(full load) SORT1 cycle (L/km)	0,759	-	-
Conv.(full load) SORT1 cycle traffic congestion (L/km)	0,839	-	-

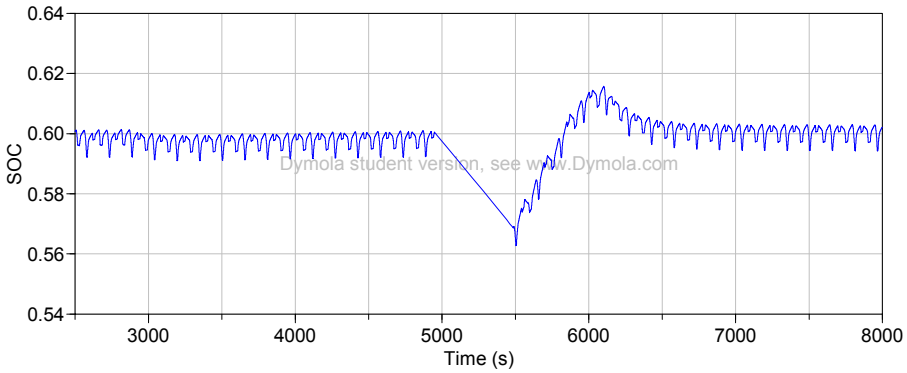

Figure 84: Simulation of the Series-Hybrid Avancity L bus model on SORT1 cycle: SOC

From the simulation results summarised in Table 21, the following conclusion can be presented:

- the series hybrid driveline showed a reduction of about 24% in fuel consumption compared to the conventional one.
- the effect of the ON-OFF strategy at bus stops can give an additional fuel consumption reduction of about 2%.
- however, long time OFF periods, e. g. for covering a significant part of the trip in pure electric mode can result in no consumption reduction, or even in some increase because after the OFF period

the ICE is operated to rapidly recover energy in the battery, working at full power. Some enhancement on the ICE management (non yet implemented) might in principle avoid or attenuate this issue.

- If traffic congestion is taken into account, the fuel consumption reduction between hybrid and conventional rises to 26%.

Figure 85, where instantaneous fuel consumption is reported, depicts some details of the ON-OFF strategy implemented: some graphical difference between absence or presence of ON-OFF strategy can be observed up to 5000 s. In addition, as reported before, it can be noticed that fuel consumption rises up strongly after the traffic congestion, during which the engine works at full power.

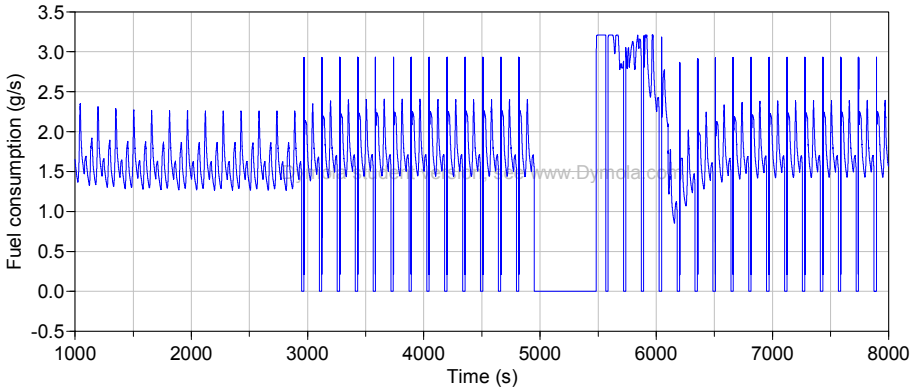

Figure 85: Simulation of the Series-Hybrid Avancity L bus model on SORT1 cycle: instantaneous fuel consumption

4.3 Cost Analysis

Although the vehicle could be considered at prototype level, an industrial cost analysis for all the components of the power-train has been carried out, with reference to the conventional version. The following criteria have been used:

- For the ICE, a cost of 250 €/kW was considered in reference to the conventional bus, while a cost of 100 €/kW was used for the hybrid vehicles, because of the choice of a smaller engine.
- About the RESS, a cost of 800 €/kWh was considered for the actual hybrid, while a reduction up to 500 €/kWh has been evaluated for the year 2020.
- About the ED and EG, a development cost of 100 k€ has been considered. In addition, the hardware components were evaluated in 200 €/kW for the electric machines and 50 €/kW for the converters.
- For the usage cost, a standard scenario in which the buses remain in service for a total duration of 15 years and 750 000 km (50 000 km/y) has been taken into account. The fuel consumptions were obtained from simulation results (Table 21), and the fuel cost equal to 1,5 €/L.
- The maintenance provided for hybrid vehicles consist in the complete substitution of the ICE (for which an additional replacement cost of 2000 € was considered) after 250 000 km and the replacement of the battery pack after 8 years, considering a cost of 500 €/kWh for the 2010 hybrid, and of 400 €/kWh for the 2020 hybrid.

Table 22: Cost analysis

	Year 2010 conventional	**Year 2010 10 HEVs**	**Year 2020 1000 HEVs**
Components cost			
ICE (k€)	40	6	6
EG (k€)	-	25	15
RESS (k€)	-	31	19
ED (k€)	-	55	45
Transmission (k€)	5	-	-
Total (k€)	**45**	**117**	**85**
Usage cost			
Fuel (k€/y)	56,9	42,5	42,5
Maintenance (k€)	0	35	32

Starting from data reported in Table 22, VAN, Payback Time and TIR were evaluated considering two different cases, related to the comparison between hybrid and conventional starting from 2010 and 2020, and an interest rate equal to 4 %.

Table 23: Cost analysis

	Year 2010 conv/HEV	**Year 2020 conv/HEV**
VAN (k€)	59,5	93,1
TIR (%)	15	32
Payback time (y)	6,5	3

The results of the analysis are reported in Table 23, that shows that, even if the higher cost of the components, considering also the usage cost, the hybrid vehicles show a real cost competitiveness.

4.4 Electric version

The electric versions of the buses can be obtained simply starting from the same Electric Drive (ED), fed not by the two different sources, EGS and RESS, but only by the RESS. All subsystems were modelled weighting the accuracy and complexity for the purpose considered. In particular, since the fastest transients useful to globally size the drive train have constant times of the order of 100 ms, much faster phenomena, such as valve switching inside electronic converters, were considered to be algebraic. Figure 86 depicts the simulation scheme in Dymola. The main subsystems were:

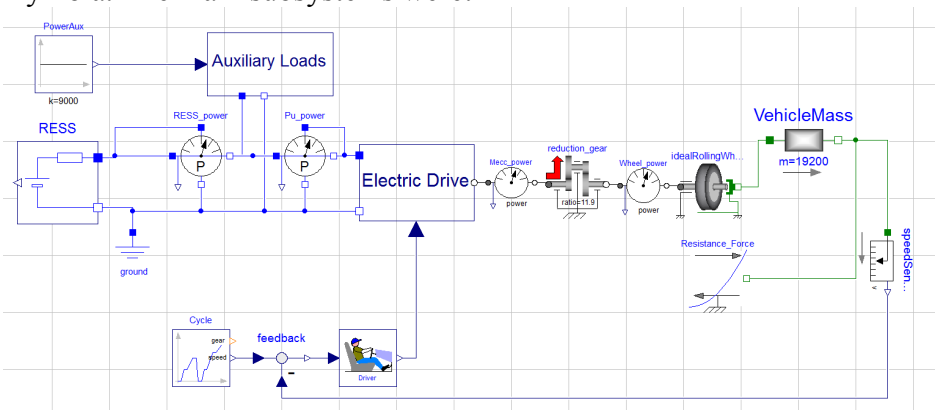

Figure 86: Electric bus model in Dymola

- Rechargeable energy storage system (RESS) that could be composed of devices such as electrochemical batteries, supercapacitors, fly-wheels etc. The RESS was modelled with a lithium ion battery, considering its good performance in terms of power density and energy density.
- Auxiliary electrical load (AUX) that could be lights, the control system, the air-conditioner etc;
- Electric Drive (ED), to provide power and torque to the wheels and also to produce regenerative power, consisting of an electric motor and a power controller. The drive is constituted by an inverter-fed induction machine controlled by a field oriented technique, similar to the one used for the electric generator.

- The vehicle, which also contained sub-systems for mechanical transmission and vehicle dynamics. The final drive consisted of a fixed gear ratio driven by the traction motor. Mechanical equations describing the vehicle longitudinal behaviour was used.

Each sub-model was carefully constructed to be able to accurately emulate experimental results. e.g. the model for the electric motor/generator needed parameters in a file defining the lost power vs. the torque and the rotary velocity. The model of the battery needed data files listing the internal resistance vs. the depth of discharge. The authors employed the *forward approach* for this model, which was:

- a driving duty cycle (called *mission profile* in the program) fed to the driver block.
- the driver block converted the reference speed into commands for the ED.

Naturally, the energy management strategies presented before cannot be used, because all the power needed for the traction and auxiliaries is taken directly from the RESS. Indeed, the main balance equation can be modified as follows:

$$P_U(t) = P_{ED}(t) + P_{AUX}(t) = P_{RESS}(t) \qquad \text{(Eq. 51)}$$

The propulsion system sizing was sized in accordance with the following boundary conditions.

1. Level road

a) max speed: 80 km/h

b) vehicle running SORT1 cycle, for a max range of 200 km, fully loaded.

2. Road with 16% gradient

a) max speed: 10 km/h (range 0,5 km)

b) start-up acceleration: 0,3 m/s²

Characteristics traction curves similar to these obtained for the hybrid versions can be obtained, with similar values of the power needed at level road and road with 16% gradient.

Also for the hybrid versions, conditions 2a) and 2b) identified the max tractive power and the max (starting) tractive effort for the propulsion system: therefore they completely defined characteristics for the ED.

The RESS was sized considering only the condition 1b) according to the specified range and maximum input voltage admitted by the ED. Current limits, because of the large capacitance of the energy-oriented cells used, are always observed. The main characteristics of the sizing are listed in Table 24.

Table 24:Sizing of the considered electric buses

	Bus Models		
	Vivacity M	***Avancity L***	***Avancity S***
Length (m)	9	12	18
Weight (full load) (t)	16,00	19,20	28,85
Weight (partial load) (t)	11,33	14,27	22,71
Auxiliaries (kW)	6	9	12
RESS Capacitance (Ah)	480	650	960
RESS Energy (kWh)	337,4	457,0	674,9
ED power (kW)	2 x 60	2 x 90	4 x 60

Obviously, values of indicated capacitance can be obtained also with more cells connected in parallel. It can be noticed that the range considered in conventional cycle SORT1 is reduced when a real cycle, is considered, how reported in the table related to the simulation results.

These results must be considered adding some considerations about cycle life evaluation. In our case, considering full charge-discharge profiles, from characteristic curves provided by the manufacturer [31], the cycle life evaluation cannot overcame 1500 cycles. If a reduction in terms of range can be accepted, maintaining a residual SOC of about 20%, number of cycles can rises up to 7000-8000.

Table 25: Performance of the considered electric buses

Bus	**Cycle**	**Aux. cons.** (kWh/km)	**Prop. cons.** (kWh/km)	**Range**	**Residual SOC***
9m	Bologna	1,15	1,18	141,4	-
	SORT1	0,52	1,39	203,1	0,01
12m	Bologna	1,75	1,55	139,1	-
	SORT1	0,81	1,83	200,6	0
18m	Bologna	2,35	2,36	132,2	-
	SORT1	1,08	2,79	200,3	0

*SOC evaluated after 200 km, starting from RESS fully charged

5. Design and modelling techniques for hybrid vehicles

5.1 Modelling activity: comparison between different modelling packages

To develop electric, hybrid or Fuel-Cell based propulsion systems, it is important to have at disposal tools able to simulate the envisaged vehicle behaviour, since the sizing of the different parts strongly depend on the vehicle mission profile and, more important, on the selected onboard energy management strategy.
Several good general-purpose vehicle simulators are available and well-known, such as ADVISOR® [57] used especially to investigate the energy management strategies, the component type and sizing interactions and the performance and energy implications of several power-train architectures. Other simulation programs such as like PSAT® [58] instead, allow implementing actual controllers, offer support for hardware-in-the-loop and provide more in-depth analysis of events and transients. Finally, a lot of simulation programs, such as the Fuel-Cell based simulator presented in chapter 3, are written using the Matlab-Simulink® [51] environment.
Matlab-Simulink® is normally chosen because of the following main reasons:

- possibility to fully deploy the modelling know-how and capability to develop new models.
- maximum flexibility in defining the vehicle energy management and implementing actual controllers.
- building of man-machine interfaces adequate to the skill and attitude of its researchers.

In the last years other commercial simulation packages, based on object-oriented modelling (also called a-causal modelling), have been developed, with dedicated multi-domain models and libraries, in order to make faster simulations and reduce development costs with fewer prototypes. This is a relatively new modelling methodology based on object orientation and equations, characterised by:

- no need to define inputs and outputs at the model building stage.
- ability of handling of large, complex multi-engineering models.
- faster modelling by graphical model composition.

Therefore, modelling techniques needing manual conversion of equations to a block diagram, that is to a causal model, based on Matlab Simulink® package, can be substituted by the usage of object-oriented modelling. The models reported in chapter 4 were made using two commercial software packages, LMS Imagine.Lab AMESim® [52] (AMESim), and 3DS Dymola® [53] (Dymola). AMESim allows object-oriented modelling, but basically requires the user to use closed built-in library models and proprietary methods for introducing new components. Dymola allows model description by the Modelica® modelling language, which allows users to create their own models and model libraries, or modify the ready made model libraries to better match their simulation needs.
In conclusion, new object-oriented techniques allow to make faster modelling activities respect to the old casual-model composition. Flexibility and possibility to fully deploy the model can be guaranteed only by the usage of open-source languages as Modelica®, that offer to the user the possibility to open and modify every single equation presented in each sub-model. To achieve this possibility, it is strong recommended Modelica® based languages respect to the close object-oriented languages.

5.2 Sizing of the Rechargeable Energy Storage System: general criteria

From the sizing of the Fuel-Cell based small urban-van and of the hybrid bus, it must be notice that the RESS can be sized not only with reference to the global energy required, to satisfy a range performance specification (for example driving in slope condition for the Fuel-Cell based small urban-van, or in pure electric mode for the hybrid bus), but considering also the maximum admitted current limits during charge or discharge phases. These limits are normally indicated by the

battery manufacturer, but several experimental tests are required, to observe real stress occurred to the device.
In particular, during specific power and efficiency test presented in chapter 2 related to high-power batteries, a strong asymmetric condition for charging and discharging operation was mentioned and observed during tests, how indicated in Table 26, partially derived from Table 6, in which different colours are related to limitation occurred during test (red for the current limit, blue for the voltage limit).

Table 26: Specific powers for the battery
(considered mass refers to modules, including cases)

discharge duration (s)	lithium battery specific power (W/kg)	
	charge	discharge
5	330	2100
10	330	2070
20	330	2030
60	330	1910
240	330	1450
1000	330	518

Otherwise, further tests related to the reproduction of realistic stress for batteries used on-board vehicles have showed limited over-temperature for repeated partial charge charge/discharge cycles (derived from Table 8) and during reproduction of the current profile defined to accommodate the needs of a vehicle performing a NEDC cycle.

Table 27: Measured stable case over-temperature for partial charge/discharge cycles

I/C_n (A/Ah)	pulse duration (s)	measured stable case over-temperature (°C)
3	60	1,73
6	60	4,74
8	60	6,91
9	30	6,57

After that, a cycle life evaluation was performed: the battery has been subjected to 1000 NEDC cycles: a full charge-discharge cycle to verify effective capacity of the device has been imposed every 136 NEDC. At the end of the test, reduction in terms of capacity was about 1,8%, for a global expected life of about 100 000 km.
In conclusion, under the general hypothesis that the stress at which the RESS is subjected can be directly associated with over-temperature working condition, it must be notice that the assumption of symmetric current limits can be absolutely allowed.

This assumption was partially followed for the sizing of the RESS employed for the hybrid bus, for which a flexible evaluation of the current limits has been proposed, according to these criteria:

- RESS was sized according to the manufacturer limits when the vehicle is running partially loaded.
- Manufacturer limits can be slightly overcame when the vehicle is running fully loaded, being this condition rarely verified during normal operating condition.

These differences can be also analysed in Table 28, considering that limits suggested by the manufacturer for the battery employed were, respectively, 5 A/Ah during discharging operation and 2 A/Ah during charging operation. Maximum current limits were evaluated with reference to the standard conventional cycle (SORT1) and to the real cycle, experimentally measured inside the city of Bologna.

Table 28: RESS max currents, Avancity L (12m), evaluated at partial and full load

I/C_n (A/Ah) discharge charge	SORT1	SORT1 EV	Bologna1	Bologna1 EV
Partially loaded	3	4,5	4	5
	2,5	2	2,5	2
Fully loaded	4	6	4	5,5
	3	2	3	2,5

5.3 Usage of Fuel Cell System on-board vehicles

From the sizing presented in chapter 2 related to the hydrogen vehicle, it is possible to make some conclusions about the usage of the fuel cell systems. From test experiences made, it is possible to infer that:

- The correct balance of cell membrane humidification and operation of all the auxiliary devices can influence the correct behaviour of the stack: i.e. if the air flow mass is not adequate to feed the cell, some loss of power might happen (10,5 kW respect to the 14,4 kW expected).
- Efficiency measures are significantly far from values reported in bibliography [13] for PEM fuel-cells (about 40% respect to 55%-60% expected). This is because, being the FCS considered dead-end type, part of the fuel is employed for purge operation (water may back diffuse from the cathode to the anode), respect to the one that feeds the cells.

From the comparison between fuel-cell based vehicle and electric version, both sized for the same performance specification (i.e. range, max speed) whose characteristic data are reported in Table 29, partially derived from (Table 17 -Table 19), it is possible to observe that the electric version takes advantageous in terms of volume, and presents a short increment of mass.

Table 29: Main results of comparison

	FC-HEV	*EV*
Max speed (km/h)	80	80
Range (km)	151	151
Total Volume (L)	165,7	94,0
Total mass (kg)	1573	1626
Range, slope 25% (km)	2,4	16,0
Acceleration 0-40 km/h (s)	8,0	7,7
Acceleration 0-60 km/h (s)	13,7	13,7
Acceleration 0-80 km/h (s)	30,6	31,3

Obviously, mass and volumes are subjected to changes, if different range specification are taken into account, how clearly shown in below. For higher range, comparable with a conventional car, the

hydrogen solution might become preferable respect to the battery-fed solution, specially in term of mass. Indeed, how reported in Figure 87, break-even points are about 100 km in term of mass, and about 500 km in term of volumes.
If performance was considered, it must be said that the fed battery electric version, being the RESS sized for the range specification, presents a more extended range also during drive at slope condition. Furthermore, a battery pack of extended capacity is not subjected to restricted current limits respect to the small battery pack of the hydrogen version: in the first part of acceleration the electric version appears advantageous, slightly damaged only by the reduced increment of mass.

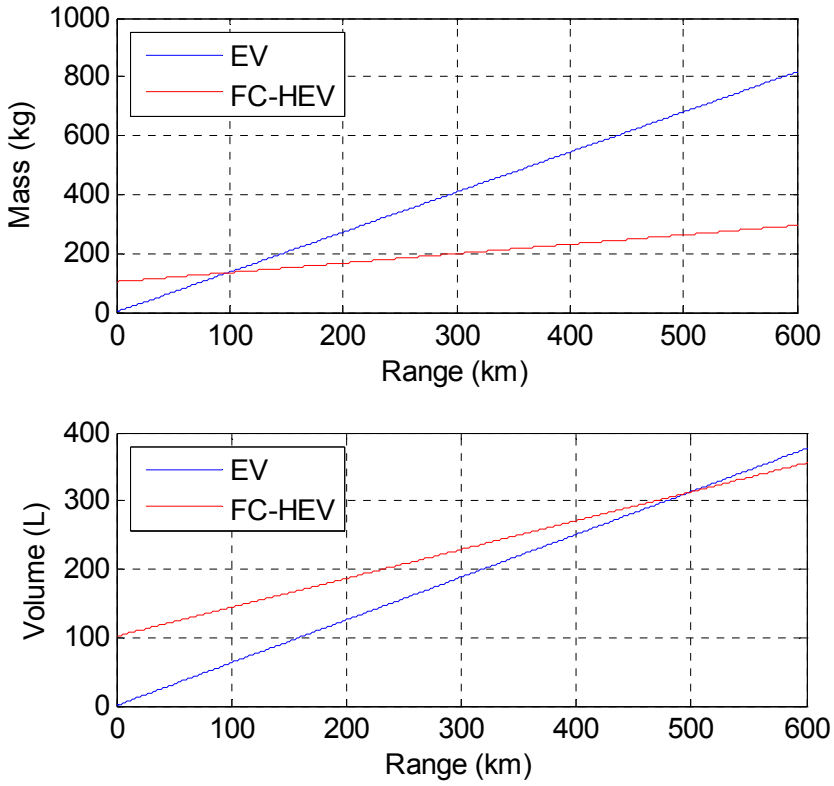

Figure 87: Comparison in term of mass and volume, related to the generation system

In conclusion, battery fed vehicles seem to be preferable respect to the fuel-cell version, basically for the possibility to obtain the same characteristics, in terms of performance and layout, with a significant reduction of cost: the cost analysis has showed that cost can be reduced considering the conversion from prototyping application to the series production. The results of the analysis reported in Table 15, show that the FC vehicle should be, by year 2020, much nearer than today to a real purchase cost competitiveness.

Conclusion

This thesis has shown the different issues concerning battery, hybrid and Fuel-Cell based propulsion systems for land vehicles, such as the efficiency evaluation and optimisation for all the different components, through the development of simulator packages and experimental tests specially on storage systems. The following main conclusions may be drawn:

The problem to optimise hybrid and Fuel-Cell based vehicles was analysed using an unified approach: in order to define a global optimisation, it is important to define the optimal SOC range in which the Rechargeable Energy Storage System has to be operate, and the optimal point of work for the Primary Converter: as far as the RESS, if lithium batteries are chosen, the efficiency profile is quite flat: the global optimisation problem indeed becomes a sub-optimisation problem for the Primary Converter, that delivers average powers working at fixed or slowly variable points, while the RESS manages the ripple components, with further strategies to maintain the SOC balanced during normal driving condition, or when extended charge or discharge phases are required.

The sizing of the batteries should be determined through experimental results presented in chapter 2, where extended tests considering the real performance of power oriented lithium batteries in comparison with super-capacitors have been performed: they suggest a more flexible use, specially during charging, respect to the limits imposed by manufacturer.

Design of hybrid drive trains require good simulation tools, to determine the sizing of different components and definition of opportune energy management strategies. Starting from the Matlab-Simulink® environment, alternative packages (as Dymola/Modelica® and LMS AMESim®) have been tested. They allow to make faster modelling activities respect to the casual-model composition, ensuring the same flexibility and possibility to fully deploy the models, specially in case of open-source languages as Modelica®, where the possibility to open or modify the existing models is absolutely guaranteed, allowing the complete control of the models.

Bibliography

[1] C.C. Chan, "The state of the art of electric and hybrid vehicles", Proceedings of the IEEE, vol 90, n.2.

[2] G. Paganelli, G. Ercole, A. Brahama, Y. Guezzenec, G. Rizzoni, "A general formulation for the instantaneous control of the power split in charge-sustaining hybrid electric vehicles", in Proc. 5th Int. Symp. Advanced Vehicle Control, Ann Arbor, MI, 2000.

[3] A. Brahama, , Y. Guezzennec, G. Rizzoni, "Dynamic optimisation of mechanical electrical power flow in parallel hybrid electric vehicles", 5th Int. Symp. Advanced Vehicle Control, Ann Arbor, MI, 2000.

[4] C. Lin, H. Peng, J. Grizzle, J. Kang: "Power management strategy for a parallel hybrid electric track", IEEE Transactions on control systems technology, Vol. 11, N. 6 Nov. 2003, pp. 839-849.

[5] X. He, M. Parten, T. Maxwell: "Energy management Strategies for a Hybrid Electric Vehicle", Symposium IEEE VPPC05, Chicago (USA), 7-9 September 2005, pp. 536-540.

[6] J. Moreno. J. Dixon, M. Ortuzar: "Energy management system for an electric vehicle, using ultracapacitors and neural networks", IEEE Transactions on Industrial Electronics, Volume 53, N. 2 , April 2006 pp 614-623.

[7] A. Soltis, X. Chen: "A new Control Strategy for Hybrid Electric Vehicles", IEEE Proceedings of the American Control Conference, Denver, Colorado, June 4-6 2003, Vol. 2, pp. 1398-1403.

[8] S. Barsali, M. Ceraolo, A. Possenti: "Techniques to Control the Electricity Generation in a Series Hybrid Electrical Vehicle, IEEE Transactions on Energy Conversion, Vol. 17, N. 2, June 2002, pages 260-266.

[9] M. Ceraolo, R. Giglioli, G. Pede, R. Cheli, E. Mingozzi: "Use of series-hybrid drive trains for railway traction", SPRTS – Ship Propulsion and Railway Traction Systems Conference, Bologna, Italy, 4-6 October 2005, pp. 258-265.

[10] M. Ceraolo, A. Caleo, P. Capozzella, M. Marcacci, L. Carmignani, A. Pallottini: "A Paralle-Hybrid Drive-Train for

Propulsion of a Small Scooter", IEEE Transactions on Power Electronics, Vol. 21, N. 3, May 2006, pp. 768-778.
[11] R. Cheli, G. Grande, R. Giglioli, R. Manigrasso, G. Pede: "Rail-car hybrid trains to reduce fuel consumption and emissions", 7th World Congress on Railway Research, Montreal, 4-8 June 2006.
[12] P. Pisu, G. Rizzoni: "A Comparative Study of Supervisory Control Strategies for Hybrid Electric Vehicles", IEEE Transactions on Control Systems Technology, Vol. 15, N. 3, May 2007, pp. 506-518.
[13] J. Larminie, A. Dicks, Fuel Cell Systems explained,Wiley, 2003.
[14] Smith, G., "Storage batteries", Pitman Advanced Publishing Program,
London, ISBN-13: 978-0273084167, 1980.
[15] Fan, D., White, R.E., "Mathematical Modeling of a Nickel-Cadmium Battery", J. Electrochem. Soc., 138(10): 2952-2959, 1991.
[16] Salameh, Z. M. , Casacca, M. A., Lynch, W. A., "A Mathematical Model for Lead-Acid Batteries", IEEE Trans. on Energy Conversion, 7(1):93-97, 1992.
[17] Valvo, M., Wicks, F. E., Robertson, D., Rudin, S., "Development and application of an improved equivalent circuit model of a lead acid battery," Proc. *Energy Conversion Eng. Conf.*, 2:1159–1163, 1996.
[18] Doyle, M., Meyers, J., Newman, J., "Computer Simulations of the Impedance Response of Lithium-Polymer and Lithium-Ion Rechargeable Batteries", *J. Electrochem. Soc.*, 147(1):99-110, 2000.
[19] Verbrugge, M. W., "Application of Simplified Model for the Analysis of a Novel Battery used in General Motors' Precept Hybrid Electric Vehicle," presented at 17th International Electric Vehicle Symposium (EVS-17), Canada, October 15-18, 2000.
[20] Ceraolo, M., "New Dynamical Models of Lead-Acid Batteries", *IEEE Trans. on Power Systems*, 15(4):1184-1190, 2000.
[21] Capel, A., "Mathematical model for the representation of the electrical behaviour of a lithium cell," presented at IEEE Power Electronics Specialists Conference 2001, Canada, June 21-21, 2001.

[22] Wu, B., Mohammed, M., Brigham, D. , Elder, R. , White, R. E., "A non-isothermal model of a nickel-metal hydride cell," *J. of Power Sources*, 101(2):149-157, 2001.
[23] Ceraolo, M. and Miulli, C., "A Dynamic Model of Nickel-Zinc Batteries", Electric Vehicle Symposium (EVS.19), Korea, October 19-23, 2002.
[24] Barsali, S., Ceraolo, M.,"Dynamical models of lead-acid batteries: Implementation issues," *IEEE Trans. Energy Conversion*, 17(1):16–23, 2002.
[25] Gomadam, P. M., Weidner, J. W., Dougal, R. A., White, R.E. "Mathematical modeling of lithium-ion and nickel battery systems," *J. of Power Sources*, 110(2):267–284, 2002.
[26] Dees, D. W., Battaglia, V. S., Belanger, A., "Electrochemical modeling of lithium polymer batteries," *J. of Power Sources*, 110(2):310-320, 2002.
[27] Buller, S., Thele, M., Doncker, R. W. D., Karden, E., "Impedance-based simulation models of supercapacitors and Li-ion batteries for power electronic applications," *IEEE Transact. on Industry Applications*, 41(3):742-747, 2005.
[28] Chen, M., Rincon-Mora, G. A., "Accurate electrical battery model capable of predicting Runtime and I_V Performance," *IEEE Transact. on Energy Conversion*, 21(2):504-511, 2006.
[29] Ceraolo, M., Lutzemberger and G., Marracci, M., "High power Lithium batteries usage in hybrid vehicles," presented at IEEE VPPC 2010, France, September 1-3, 2010.
[30] http://www.maxwell.com/ultracapacitors/products/modules/ bpak0020-15v.asp
[31] http://www.kokam.com/english/ product/ battery_main.html
[32] S. Barsali, M. Ceraolo, A. Possenti: "Techniques to Control the Electricity Generation in a Series Hybrid Electrical Vehicle, *IEEE Transactions on Energy Conversion*, Vol. 17, No 2, June 2002, pages 260-266.
[33] D. Poli, A: di Donato, G. Lutzemberger: "Modeling and simulation of hydrogen fuel-cell based propulsion systems", *9th International Conference on Engines and Vehicles (ICE2009)*, Capri, 13-18 September 2009.
[34] M. Ceraolo, T. Huria, G. Lutzemberger: "Experimentally determined models for high-power lithium batteries". *SAE 2011*

World Congress. Cobo Center Detroit, Michigan (USA), 12-14/4/2011.
[35] http://www.dieselnet.com/standards/cycles/ece_eudc.html.
[36] M. Ceraolo, C. Miulli, A. Pozio: "Modelling static and dynamic behaviour of proton exchange membrane fuel cells on the basis of electro-chemical description", Journal of Power Sources, Vol. 113, N. 1, Jan 2003, pp.131-144, ISSN: 0378-7753.
[37] T. Markel, A. Brooker, T. Hendricks, V. Johnson, K. Kelly, B. Kramer, M. O'Keefe, S. Sprok, K. Wipke : "ADVISOR: a system analysis tool for advanced vehicle modeling", *Journal of Power Sources* 110 pp 255-266, 2002.
[38] http://www.transportation.anl.gov/modeling_simulation/PSAT/index.html
[39] M. Ceraolo, C. Miulli, P. Cravini: "A Comparison of different fuel-cell based drive train typologies to be used on two-wheel vehicles", European Ele-drive Transportation Conference & Exhibition", Estoril (Portugal) 17-20 March 2004, paper n.°19_2004eet.pdf.
[40] M. Ceraolo, C. Miulli, P. Cravini: "Modelling of a PEFC-SC hybrid electric drive-train", *SPEEDAM 2004 June 16th - 18th, CAPRI (Italy).*
[41] R. Manigrasso, F.L. Mapelli: "Design and modelling of asyncronous Traction Drives Fed by Limited Power Source", Symposium IEEE VTS - VPPC '05, Chicago (USA), 6-8 October 2005.
[42] S. Barsali, M. Ceraolo: "Dynamical models of lead-acid batteries: implementation issues", *IEEE Transactions on Energy Conversion*, Vol. 17, N. 1, Mar 2002, Pages 16-23.
[43] M. Ceraolo, A. Di Donato, C. Miulli, G. Pede: "Microcycle-based Efficiency of Hybrid Vehicle Batteries", IEEE Vehicular Power and Propulsion Conference VPPC'05, Chicago (USA), 7-9 Sept. 2005.
[44] M. Ceraolo, A. di Donato, G. Franceschi: "A General Approach to Energy Optimization of Hybrid Electric Vehicles", IEEE Transactions on Vehicular Technology, May 2008, Vol. 57, N. 3, pp. 1433-1441.
[45] M. Ronchetti: "Celle a combustibile: Stato di sviluppo e prospettive della tecnologia", ENEA, 2008.

[46] M. Ceraolo, S. Barsali, G. Lutzemberger, M. Marracci: "Comparison of SC and high-power batteries for use in hybrid vehicles", 9th International Conference on Engines and Vehicles (ICE2009), Capri, 13-18 September 2009.
[47] N. Mohan, T. M. Undeland, W. P. Robbins: Power Electronics: Converters, Applications, and Design, Wiley Press, 2003.
[48] M. Ceraolo, G. Lutzemberger, F. Papini, L. Sani: "Il progetto filiera idrogeno: sviluppo di un mini-van ibrido-serie a celle a combustibile". ATA – Ingegneria dell'Autoveicolo, Vol. 63.
[49] http://www.bredamenarinibus.it/
[50] T. Huria, G. Lutzemberger, G. Pede, G. Sanna, Systematic development of series-hybrid bus through modelling, VPPC, Lille, 1-3 Semptember 2010.
[51] http://www.mathworks.com/
[52] http://www.amesim.com/
[53] http://www.dymola.com/
[54] K. T. Chau, Y. S. Wong, "Overview of power management in hybrid electric vehicles", *Energy Conversion and Management*, October 2002, Volume 43, Issue 15, Pages 1953-1968.
[55] M. Salman, M. Chang, J. Chen, "Predictive energy management strategies for hybrid vehicles", *IEEE Vehicular Power and Propulsion Conference VPPC'05*, 7-9 September 2005, Chicago (USA).
[56] A.I. Antoniou, A. Emadi, "Adaptive control strategy for hybrid electric vehicles," *Vehicle Power and Propulsion Conference, 2009. VPPC '09. IEEE* , vol., no., pp.242-246, 7-10 Sept. 2009.
[57] T. Markel, A. Brooker, T. Hendricks, V. Johnson, K. Kelly, B. Kramer, M. O'Keefe, S. Sprok, K. Wipke : "ADVISOR: a system analysis tool for advanced vehicle modeling", *Journal of Power Sources* 110 pp 255-266, 2002.
[58] http://www.transportation.anl.gov/modeling_simulation/PSAT/index.html